MODAL ANALYSIS OF DEEPWATER MOORING LINES BASED ON A VARIATIONAL FORMULATION

A Thesis

by

JOSE ALBERTO MARTINEZ FARFAN

Submitted to the Office of Graduate Studies of
Texas A&M University
in partial fulfillment of the requirements for the degree of

MASTER OF SCIENCE

Approved by:

Chair of Committee,	Richard Mercier
Committee Members,	Jun Zhang
	Achim Stössel
Head of Department,	John Niedzwecki

May 2013

Major Subject: Ocean Engineering

ABSTRACT

Previous work on modal analysis of mooring lines has been performed from different theoretical formulations. Most studies have focused on mooring lines of a single homogeneous material, and the effect of added mass and damping produced by the water has not been examined deeply.

The variational formulation approach, employed in this research to perform a modal analysis, has been useful to study the behavior of several realistic mooring lines. The cases presented are composed from segments of materials with different mechanical characteristics, more similar to those in current offshore projects. In the newly proposed formulation, damping produced by transverse motion of the mooring line through the surrounding water has been added to the modal analysis.

The modal analysis formulation applied in this work has been verified with calculations from commercial software and the results are sufficiently accurate to understand the global behavior of the dynamics of mooring lines with the damping produced by the sea water.

Inclusion of linearized drag damping in the modal analysis showed that the modal periods of the mooring systems studied depend on the amplitude of the transverse motion of the mooring line. When more amplitude in the motion is expected more damping is obtained.

Two realistic designs of mooring lines were compared: one made up with a main insert of steel rope, called “Steel System”, and one composed by a main insert of

polyester, named “Polyester System”. Comparing the natural periods of both systems, the Steel System appears to be safer because its fundamental natural period is more distant from the wave excitation periods produced by storms. The same happens considering the wave excitation periods produced by prevailing seas. In this case the natural periods of the Polyester System are nearer to the wave excitation periods causing fatigue loads.

The transverse mode shapes for lateral motions of the mooring lines are observed to be continuous and smooth across material transitions, such as transitions between chain and wire rope and transitions between chain and polyester rope. This behavior is not always observed in the tangential mode shapes for the Polyester System where significant differences in dynamic tension seem to be present in the specific cases studied.

DEDICATION

To Miriam and Niza, for their love and time.

ACKNOWLEDGEMENTS

This work was supported by the Instituto Mexicano del Petróleo and the CONACYT-SENER Fund. I am honored for this support.

I also would like to convey my gratitude to Dr. Richard Mercier for his patience and guidance during the development of this work.

I reserve special thanks to Dr. Jun Zhang and Dr. Achim Stössel for serving on my graduate committee.

The encouragement and friendship of my family and friends were essentials in my life throughout the fulfillment of this work, thank you.

TABLE OF CONTENTS

Page

ABSTRACT ii

DEDICATION iv

ACKNOWLEDGEMENTS v

TABLE OF CONTENTS vi

LIST OF FIGURES viii

LIST OF TABLES xi

1. INTRODUCTION 1

1.1 Motivation and objectives 6
1.2 Outline of thesis 7

2. LITERATURE SURVEY 9

3. STATIC ANALYSIS 12

3.1 Methodology 12
3.2 Definition of structural parameters 13
3.2.1 The catenary 14
3.2.2 Energy functional 19
3.2.3 Independent variable 20
3.2.4 Discretization 21
3.2.5 Shape functions 21
3.3 Numerical implementation 23
3.3.1 Definition of the system of reference 23
3.3.2 Initial configuration 24
3.3.3 Iterative process 25
3.3.4 Flowchart 27
3.3.5 Comparison of results 28
3.3.6 Configuration of a polyester system 31

4. MODAL ANALYSIS 34

4.1 Shape functions in three dimensional space 34
4.2 Equation of motion without damping included 35

4.2.1 Comparison of results with Orcaflex....38
4.3 Equation of motion with damping included....43

5. ANALYSIS OF DIFFERENT MOORING SYSTEMS....51

5.1 Description of the systems assessed....51
5.1.1 Steel Rope System....51
5.1.2 Steel System....53
5.1.3 Polyester System....55
5.2 Results of modal analysis....57
5.2.1 Behavior of the Steel Rope System....60
5.2.2 Damped natural periods for the Steel Rope System....70
5.2.3 Behavior of the Steel System....72
5.2.4 Damped natural periods for the Steel System....82
5.2.5 Behavior of the Polyester System....83
5.2.6 Damped natural periods for the Polyester System....93
5.2.7 Comparison of systems....94

6. SUMMARY AND CONCLUSIONS....98

REFERENCES....103

APPENDIX A....105

LIST OF FIGURES

Page

Figure 1 Schematic top view of a spread mooring stationkeeping system. 1

Figure 2 Schematic section of a spiral strand rope (left), and schematic section of a multistrand rope (right). 3

Figure 3 Schematic drawings of steel links. 3

Figure 4 Combination system of chain, fiber rope and chain. 4

Figure 5 Components of tension force in the cable. 14

Figure 6 Cable with tension in specific points. 15

Figure 7 Independent and dependent variables in the calculus of variations for this study. 20

Figure 8 Discretization of mooring line in slices. 21

Figure 9 Different views of the plane where the mooring line and its deformations are contained. 22

Figure 10 Definition of the origin of coordinates and the top tension location point. 23

Figure 11 Generation of nodes by splitting the mooring line. 25

Figure 12 Iterative process to find the final deformation of a cable resulting from the application of top tension. 27

Figure 13 Diagram that summarizes the iterative process to define the final configuration and forces of the cable. 28

Figure 14 Image of a cable to describe Irvine's model. 29

Figure 15 Comparison with DuBuque method. 31

Figure 16 Deformed configuration of a Polyester System. 33

Figure 17 Natural coordinates. 35

Figure 18 Comparison between the first four modal shapes in the plane generated by Orcaflex and the procedure followed in this study. 41

Figure 19 Comparison between the first four modal shapes out of plane generated by Orcaflex and the procedure followed. 42

Figure 20 Modal coordinates from the modal shape. 44

Figure 21 Static deformed configuration for the example tested without damping. 47

Figure 22 Modal shapes comparing the first four modes in plane. 48

Figure 23 Modal shapes comparing the first four modes out of plane. 49

Figure 24 Deformed configuration of the Steel Rope System. 53

Figure 25 Deformed configuration of the Steel System. 55

Figure 26 Deformed configuration of the Polyester System. 57

Figure 27 First two modal shapes for the Steel Rope System in air. 62

Figure 28 Third and fourth modal shapes for the Steel Rope System in air. 63

Figure 29 First two modal shapes for the Steel Rope System with submerged weight. 64

Figure 30 Third and fourth modal shapes for the Steel Rope System with submerged weight. 65

Figure 31 First two modal shapes for the Steel Rope System in water with added mass. 66

Figure 32 Third and fourth modal shapes for the Steel Rope System in water with added mass. 67

Figure 33 First two modal shapes for the Steel Rope System considering submerged weight, added mass, and damping. 68

Figure 34 Third and fourth modal shapes for the Steel Rope System, considering submerged weight, added mass, and damping. 69

Figure 35 First four damped natural periods for the Steel Rope System. 71

Figure 36 First two modal shapes for the Steel System in air. 73

Figure 37 Third and fourth modal shapes for the Steel System in air. 74

Figure 38 First two modal shapes for the Steel System with submerged weight. 75

Figure 39 Third and fourth modal shapes for the Steel System with submerged weight. 76

Figure 40 First two modal shapes for the Steel System in water with added mass. 77

Figure 41 Third and fourth modal shapes for the Steel System in water with added mass. 78

Figure 42 First two modal shapes for the Steel System considering submerged weight, added mass, and damping. 79

Figure 43 Third and fourth modal shapes for the Steel System, considering submerged weight, added mass, and damping. 80

Figure 44 First four damped natural periods for the Steel System. 83

Figure 45 First two modal shapes for the Polyester System in air. 85

Figure 46 Third and fourth modal shapes for the Polyester System in air. 86

Figure 47 First two modal shapes for the Polyester System with submerged weight. 87

Figure 48 Third and fourth modal shapes for the Polyester System with submerged weight. 88

Figure 49 First two modal shapes for the Polyester System in water with added mass. 89

Figure 50 Third and fourth modal shapes for the Polyester System in water with added mass. 90

Figure 51 First two modal shapes for the Polyester System considering submerged weight, added mass, and damping. 91

Figure 52 Third and fourth modal shapes for the Polyester System, considering submerged weight, added mass, and damping. 92

Figure 53 First four damped natural periods for the Polyester System. 94

Figure 54 Fundamental periods of free vibration for the three systems for three surrounding environments. 96

LIST OF TABLES

Page

Table 1 Data for validation example. 30

Table 2 Characteristics of a Polyester System 32

Table 3 Characteristics of mooring line for validation case with Orcaflex. 39

Table 4 Comparison of natural frequencies for Orcaflex validation case. 40

Table 5 Particulars of the mooring line tested with zero damping. 46

Table 6 Results of the mooring line tested with zero damping. 47

Table 7 Characteristics of the Steel Rope System. 52

Table 8 Characteristics of the Steel System. 54

Table 9 Characteristics of the Polyester System. 56

Table 10 Details of segments modeled in each system. 59

Table 11 First eight natural periods for Steel Rope System. 60

Table 12 First four damped natural periods for different normalized motion amplitudes in Steel Rope System. 61

Table 13 First eight natural periods for Steel System. 72

Table 14 First four damped natural periods for different normalized motion amplitudes in Steel System. 72

Table 15 First eight natural periods for Polyester System. 84

Table 16 First four damped natural periods for different values of normalized motion amplitude in Polyester System. 84

Table 17 Fundamental natural periods for each system. 95

Table 18 Fundamental damped natural periods and damping ratios for the three systems. 97

1. INTRODUCTION

A mooring line is a cable that anchors an offshore facility, from where it lies floating in the sea water level, to a specified point in the seabed, ending usually in an anchor. A floating marine platform installed in deep water, for instance, is held by several mooring lines in a specific array allowing the operation and safety of the platform. A typical stationkeeping system or mooring system is illustrated in Figure 1.

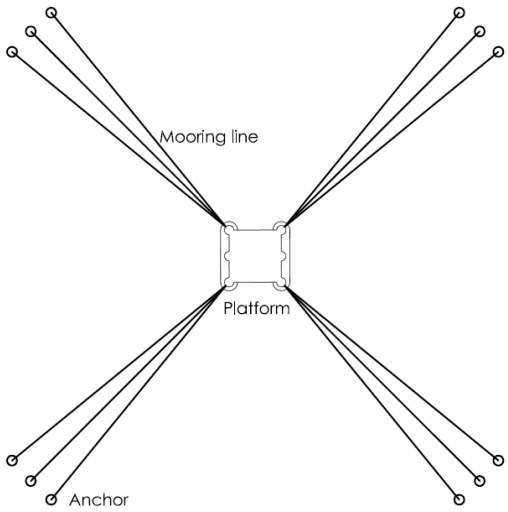

Figure 1 Schematic top view of a spread mooring stationkeeping system.

The use of mooring lines in the offshore industry is a consequence of the depth where the offshore facilities need to be installed. The use of fixed platforms in large depths is not economically feasible. Then, the concept of holding an offshore platform in place by mooring it with cables to the seabed immediately produces the problem of

eternal motion of the platform, and its components. Here, the study of mooring line dynamics becomes essential.

Studying a mooring line as a structural component is challenging because, unlike most of the structural components of an offshore facility, it is easily deformed, even from its own weight it gets an evident deformation. This deformation is highly non-linear, and the resistance against deformation produced by external loads depends in great part on these loads themselves. The behavior of cables is so unique that it was attractive for Navier in the 1820s, when he studied suspension bridges, and led him to conclude that "*The success is more assured when the challenge is bigger and looks bolder*" (Timoshenko (1953)).

The magnitude of the depth in which deepwater platforms must hold station demands lightness and high resistance in materials incorporated in mooring lines. These lines are basically made up of steel and synthetic materials, and even combinations of both in one mooring line. Steel is present in the form of wire rope and chain. Wire ropes are composed of strands or multistrands, see Figure 2. Steel chains are made up of links with stud or studless links, see Figure 3. According to API (2005), studless links have been more accepted by industry in recent years, because they are lighter than stud chains.

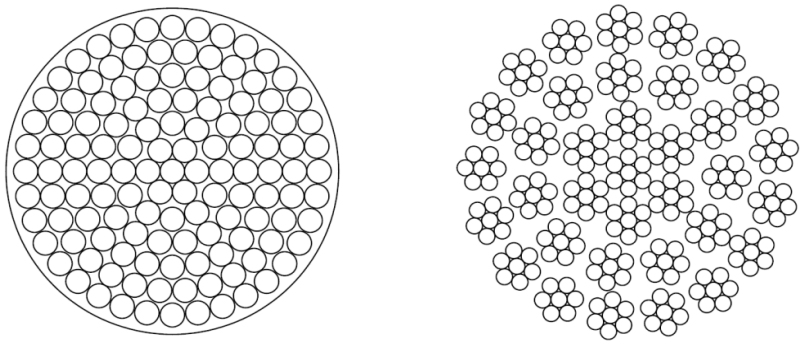

Figure 2 Schematic section of a spiral strand rope (left), and schematic section of a multistrand rope (right).

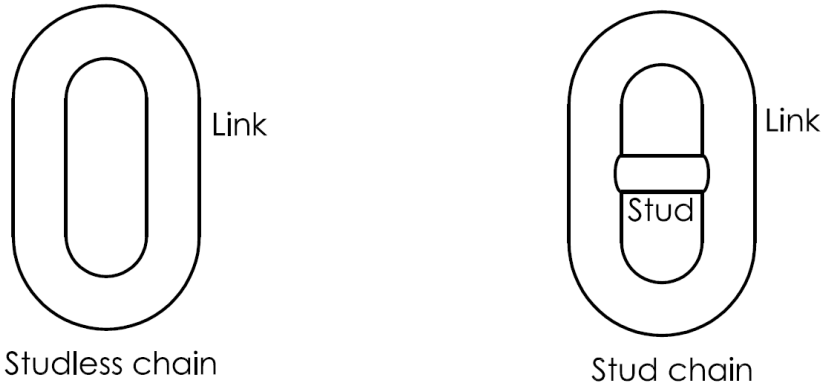

Figure 3 Schematic drawings of steel links.

Following the classification of API (2005), there are three kinds of mooring systems:

1. All Wire Rope System
2. All Chain System
3. Combination System

The All Wire Rope System refers to a mooring line completely manufactured in wire rope made up of strands of steel. The second system refers to mooring lines made up of links of steel, and the third refers to a mooring line made with the combination of chain, and wire rope or fiber rope, see Figure 4.

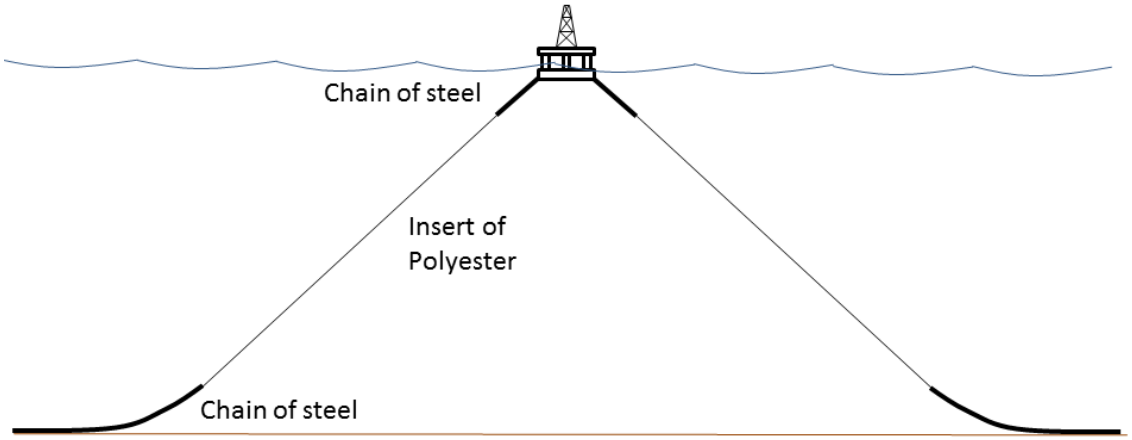

Figure 4 Combination system of chain, fiber rope and chain.

According to API (2005), fiber rope may be made up of

- Polyester (polyethylene terephthalate)
- Aramid (aromatic polyamide)
- HMPE (high modulus polyethylene)
- Nylon (polyamide)

Among those synthetic materials, polyester is the more commonly used. It has advantages like lightness and high extensibility, and although it does not have the

modulus of elasticity of steel, the range of its modulus of elasticity is suitable for the strength requirements, even in deep water depths. Moreover, unlike steel wire ropes these ropes are almost neutrally buoyant.

On the other hand, mooring lines made of steel have the main advantage of strength, as a result of high values of modulus of elasticity. Besides, in the form of chain, weight results in an advantage when catenary action is needed to anchor a floating system. Finally, the resistance to abrasion becomes ideal to deal with the friction produced with the seafloor in the lowest point of a catenary configuration.

Combination of both, steel and polyester, in mooring lines is a common practice. In these cases an insert, a middle part in the entire mooring line, is made of polyester, and the lower and upper ends are made of steel chain. In this way the advantages of both materials are applied.

In this work, one homogeneous system and two combination systems will be studied:

1. “Steel rope”
2. “Steel System”
3. “Polyester System”

The first one is made up entirely of a rope of steel, as referred to by its name; the second one has segments of chain, wire rope, and chain; and the third case has segments of chain, polyester rope, and chain.

1.1 Motivation and objectives

The study of dynamics of a mooring line is interesting because it cannot be addressed as a one degree of freedom system. Its mass distribution is continuous, thus it is necessary to represent it as a multi-degree of freedom system. On the other hand its ratio of cross-sectional area over length is very small. Its stronger stiffness is the axial stiffness, and basically it is in tension, with little resistance to relatively large displacements transverse to its longitudinal axis. Even if the tension load is large, the sag produced in the line is noticeable in most cases.

The previously mentioned geometrical characteristics of such cable systems have led to the study of its dynamics from different approaches. The fundamental theory related to the cable dynamics considers the cable as a continuous system, which is not necessarily suitable for modeling mooring lines with segments of very different mechanical characteristics, as in the case of steel wire rope and fiber rope.

Unlike cables in air, like those employed in suspension bridges, mooring lines are surrounded by water that provides buoyancy, added mass and damping to the motion of the line. The damping provided by the water and the effect of multi-segment lines with different materials have not been considered in many cases where the dynamics of mooring lines has been studied.

The inclusion of damping on the dynamics of the mooring line, considering the behavior of different materials in one mooring line, has led to the realization of this work. An equivalent linear viscous damping formulation produced by the relative

velocity drag of the water was added to the equation of motion for free vibrations of a mooring line in order to compare results with un-damped dynamic solutions.

Some realistic examples will be investigated in the model to obtain conclusions regarding the existence of different materials with different mechanical characteristics in one mooring line with the aim of studying their behavior.

1.2 Outline of thesis

The present work is divided into six sections. The present one describes the fundamental aspects, terminology and definitions of the mooring lines and their components. In this section motivations and objectives of the work are included as well.

The second section of this thesis is dedicated to reviewing the more important literature related with the dynamic analysis of mooring lines and cables.

Section number three of this work is devoted to showing how the static analysis, basic for the modal analysis in the mooring line, was performed. Some important derivations and definitions are made in order to emphasize the importance of specific variables and phenomena in the static and dynamic behavior of a mooring line. The way the method of analysis adopted was numerically implemented is described in this section as well.

The fourth section of this thesis describes the methodology for dynamic analysis of the mooring line. Important points of the formulation followed are shown in this part, and the computation algorithm is explained.

The fifth section is dedicated to analyzing realistic examples of three different mooring line systems and discussing the results. A mooring line, completely made up of steel rope, is the first example. The second example is a mooring line of steel with two segments of chain at its upper and lower ends, and a middle segment of rope. The last example is one with its end segments of steel chain, but with an insert of polyester as the middle segment. The comparison between them is made in the same conditions, the same surrounding environment, the same configuration in seawater, and the same top tension. The results of the parametric variations between cases are examined in their different modes to better understand the response of any mooring system.

Conclusions are placed in section six of this work. The assessment of the results is done from the perspective of the design of mooring lines. Further research is proposed based on the unresolved questions, like the effect of the bending stiffness in the basic formulation.

2. LITERATURE SURVEY

It is common to find fundamental theory related to vibration of cables in two main branches: first in the motion of horizontal cables, and second in inclined cables. Irvine (1978) follows this classification to develop the governing equations of the motion of horizontal cables, and then proposed the transformation of the approach to inclined cables by rotating the cable and its main global axis. With this purpose non-dimensional values are employed in geometrical variables. In both cases the elongation of the cables is considered, and the governing equations consider a homogenous material regarding its modulus of elasticity and cross-sectional area.

Triantafyllou and Bliek (1983) found that the lower part of a marine cable behaves as a chain with low frequencies, and the upper part behaves as a wire with higher frequencies, thereby producing hybrid modes with very close natural frequencies. Unlike horizontal cables, no crossover in modes is found in inclined cables. Besides, they established a relation between sag and elasticity, and sag and curvature in the cable. When sag decreases, elasticity becomes a more important variable, and when sag is large the curvature in the cable is more important.

Grinfogel (1984) developed asymptotic analytical expressions to find natural frequencies, modal shapes and dynamic tension in cables in which the ratio of weight to tension force is small. These equations are based on the linearized exact governing equations proposed by Triantafyllou and Bliek (1983), but through perturbation equations to get simple results. Here, the inclination is just one additional geometrical

variable that allows studying horizontal and inclined cables regardless of the slope of the cable.

The importance of the material elasticity of the cable in the dynamics of cables is shown by Burgess and Triantafyllou (1988). The distinction between transverse modes and elastic modes were defined because of the elasticity of the cable. Asymptotic solutions were developed for both horizontal and inclined cables.

Chucheepsakul and Srinil (2002) developed an approach to study free vibrations in marine cables based on the work-energy functional due to the strain generated by external forces such as top tension and hydrostatic forces. This methodology allows modeling the static configuration of the cable by the Galerkin finite element formulation, and then obtaining, by solving the eigenvalue problem, the modal shapes and natural frequencies.

Not many experimental works have been devoted to the vibration of cables. One of these works was performed by Rega et al. (2008). These authors reproduced experimentally key factors of the theory of dynamics of cables, such as frequency avoidance phenomenon, and associated hybrid modes. The inclination in the cable as an important factor in the avoidance, and the effects of the sag in the cable are highlighted.

An analytical solution based on the coupling of the linear differential equations that describe the motion in the plane of an inclined cable was developed by Zhou et al. (2011). By variable substitution the equation that describes the vertical motion is transformed to a Bessel equation, and the natural frequencies and modes in plane are

found by using non-dimensional parameters that represent ratios of geometrical to mechanical characteristics of the cable.

3. STATIC ANALYSIS

3.1 Methodology

In the statics of a mooring line, there are two principal variables important to know. One is the geometrical configuration resulting from the loads applied. The second one is how the internal loads are distributed along its length, mainly the axial force. Both variables mentioned are clearly related; a larger value of tension generates a straighter shape in the cable (i.e. one with less sag). This relation even produces a classification in the mooring lines as taut mooring line, when the geometrical configuration tends to be closer to a straight line, versus catenary mooring line, when the shape is similar to the configuration of a catenary.

The way to find the geometrical configuration resulting from the loads applied in most civil structures is by knowing the stiffness matrix of the structure, and dividing it by the static load vector that contains all the forces applied over the structure. In this way displacements are found and consequently internal forces. The stiffness matrix takes into account the rigidity produced by the elasticity of the material and the geometry of the components of the structure.

Chucheepsakul et al. (2003) developed a way to formulate a stiffness matrix of a mooring line, and a procedure to take into account the elasticity of the material of the cable, all this, to find the configuration of the cable in a similar way that is performed in

most civil structures. In this research this procedure was followed to form the stiffness matrix and define the final configuration of the mooring line.

The main advantages found in this method are:

- The possibility to model different sections in one mooring line.

  A mooring line comprised of different sections of materials needs to be represented taking into account these different properties. The method followed allows splitting the mooring line in several finite elements, each one with its own characteristics such as cross-sectional area and axial stiffness.

- The versatility to define movement in a tridimensional space.

  In the dynamic analysis it will be necessary to define motions in the plane of the mooring line, and out of the plane. Following this method, it is possible to define these configurations as a result of introducing specific degrees of freedom and shape functions.

3.2 Definition of structural parameters

In the procedure to be described it is important to define some concepts, shown in the next sections.

3.2.1 The catenary

For cables with high axial stiffness, the catenary equation can be used to find the configuration and forces without consideration of the elasticity of the material. Nevertheless, Irvine (1992) developed a formulation that considers the elasticity of the material and its cross-sectional area to account for the effect of the elongation in the cable. In both cases, the tension can be understood as the resultant of two components, one vertical, and other horizontal, see Figure 5.

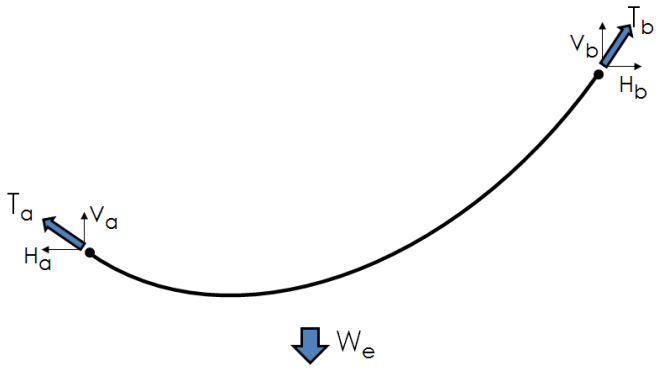

Figure 5 Components of tension force in the cable.

From the previous Figure 5 we can notice that by balancing forces:

$$\sum F_V = V_a + V_b - W_e = 0 \quad (1)$$

$$\sum F_H = H_b - H_a = 0 \quad (2)$$

Consequently

$$H_b = H_a \quad (3)$$

It can be seen that the horizontal component of the tension in the cable is constant.

From the derivation of the equation of the catenary made by Zill et al. (2012) we can follow the next formulation and conclude with another interesting key point. First, the lower end of the cable is placed such that its tangent is horizontal, as indicated in Figure 6.

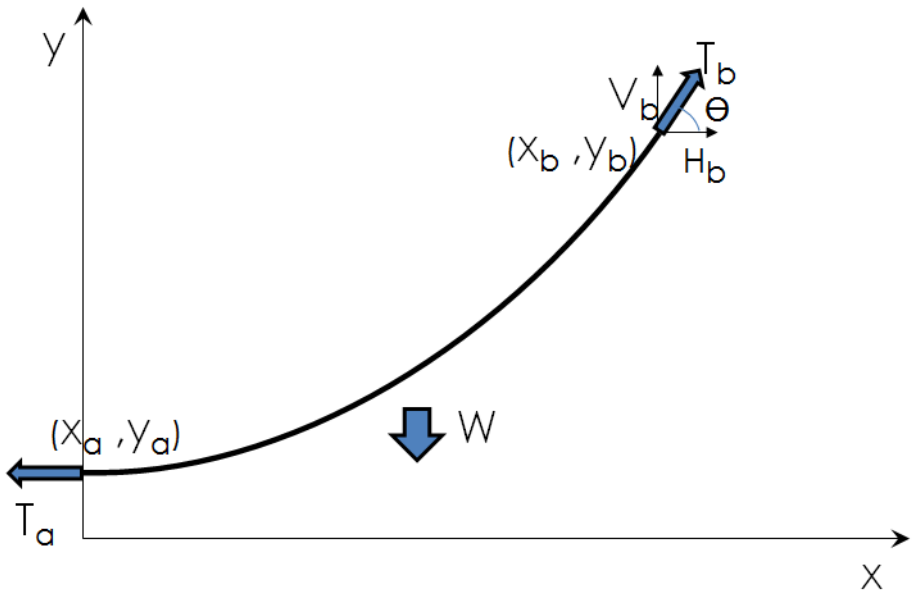

Figure 6 Cable with tension in specific points.

From Figure 6 it can be seen that

$$V_b = T_b \sin\theta \tag{4}$$

$$H_b = T_b \cos\theta \tag{5}$$

From equation (3)

$$T_a = T_b \cos\theta \tag{6}$$

By balance of forces in the vertical direction

$$W = T_b \sin\theta \tag{7}$$

The total weight W is

$$W = ws \tag{8}$$

where w is the weight per unit length, and s is the arc length of the cable. Then equation (7) becomes

$$ws = T_b \sin\theta \tag{9}$$

The arc length can be determined by

$$s = \int_0^{x_b} \sqrt{1 + \left(\frac{dy}{dx}\right)^2}\, dx \tag{10}$$

If equation (9) is divided by equation (6) then,

$$\frac{ws}{T_a} = \tan\theta \tag{11}$$

Consequently,

$$\frac{ws}{T_a} = \frac{dy}{dx} \tag{12}$$

If the derivative $\frac{ds}{dx}$ is performed, from equation (10)

$$\frac{ds}{dx} = \sqrt{1 + \left(\frac{dy}{dx}\right)^2} \tag{13}$$

But, if we differentiate again (12) with respect to x

$$\frac{d^2y}{dx^2} = \frac{w}{T_a}\frac{ds}{dx} \tag{14}$$

Replacing (13) in (14)

$$\frac{d^2y}{dx^2} = \frac{w}{T_a}\sqrt{1 + \left(\frac{dy}{dx}\right)^2} \tag{15}$$

Equation (15) is the governing differential equation of the catenary.

Making the next change of variable, and replacing (16) in (15), equation (17) is obtained. The $'$ symbol means derivative with respect to x in this derivation.

$$u = y' \tag{16}$$

$$\frac{du}{dx} = \frac{w}{T_a}\sqrt{1 + u^2} \tag{17}$$

Separating variables in equation (17)

$$\frac{du}{\sqrt{1 + u^2}} = \frac{w}{T_a}dx \tag{18}$$

Integrating (18):

$$\int \frac{du}{\sqrt{1 + u^2}} = \frac{w}{T_a}\int dx \tag{19}$$

$$\sinh^{-1} u = \frac{w}{T_a}x + C_1 \tag{20}$$

Applying the boundary conditions, it is given that *y'*(0) = 0, in other words:

$$u(0) = 0 \tag{21}$$

Then

$$0 = \frac{w}{T_a}(0) + C_1 \tag{22}$$

$$C_1 = 0 \tag{23}$$

Now, equation (20) becomes:

$$sinh^{-1} u = \frac{w}{T_a}x \tag{24}$$

From (24)

$$u = \sinh\left(\frac{w}{T_a}x\right) \tag{25}$$

Replacing (16) in (25), and integrating it,

$$\frac{dy}{dx} = \sinh\left(\frac{w}{T_a}x\right) \tag{26}$$

Integrating (26)

$$\int \frac{dy}{dx} = \int \sinh\left(\frac{w}{T_a}x\right) \tag{27}$$

$$y = \int \sinh\left(\frac{w}{T_a}x\right) + C_2 \tag{28}$$

$$y = \frac{T_a}{w}\cosh\left(\frac{w}{T_a}x\right) + C_2 \tag{29}$$

Applying boundary conditions, in equation (28)

$$y(0) = \frac{T_a}{w}\cosh(0) + C_2 \tag{30}$$

$$Y_a = \frac{T_a}{w} + C_2 \tag{31}$$

$$C_2 = Y_a - \frac{T_a}{w} \tag{32}$$

Now, equation (29) becomes:

$$y = \frac{T_a}{w}\cosh\left(\frac{w}{T_a}x\right) + Y_a - \frac{T_a}{w} \tag{33}$$

Recalling equation (3), and what it means: that the horizontal force is constant, if we call the horizontal tension as H_T, then,

$$y = \frac{H_T}{w}\cosh\left(\frac{w}{H_T}x\right) + Y_a - \frac{H_T}{w} \tag{34}$$

It can be seen from the previous expressions that, for cables with no uplift force at the bottom attachment point, if no elongation in the cable is considered, the static configuration of the cable is due to the ratio of the horizontal force to the self-weight, and no material characteristic is involved.

3.2.2 Energy functional

The energy functional represents the amount of energy, or work, developed by the tension force in the cable, with no consideration of drag forces. In this case, following Chucheepsakul et al. (2003), it is represented by the next expression:

$$\Pi = \int_0^H T\sqrt{1 + x'^2 + y'^2}dz \tag{35}$$

where T is the tension in the cable defined by:

$$T = T_H - \int_z^{Z_H} \frac{w}{1+\varepsilon}\, dz \tag{36}$$

In these equations w is the weight per unit of length of the cable, T_H is the top tension, ε is the strain, z is the elevation coordinate, and Z_H is the elevation of the point where the top tension is applied. The symbol x' is the derivative of x with respect to the z axis, and y'denotes the derivative of y with respect to z.

The stiffness is defined by Chucheepsakul et al. (2003) by twice differentiating the total energy Π with respect to the general coordinates, as indicated in equation (37).

$$K = \frac{\partial^2 \Pi}{\partial q_i \partial q_j} \tag{37}$$

The load vector, on the other hand, can be found by differentiating the total energy Π with respect to the general coordinates, equation (38).

$$R = \frac{\partial \Pi}{\partial q_i} \tag{38}$$

3.2.3 Independent variable

In the calculus of variations the independent variable does not participate in the process of variation (Lanczos, 1986). In this case, the independent variable is the vertical coordinate (z), consequently the variation of energy will be related with the displacement of coordinates in the horizontal plane; it means the variables x and y or their combination, see Figure 7.

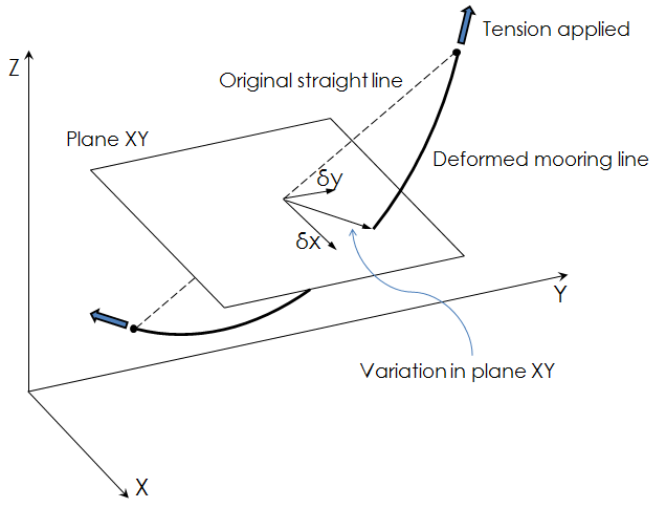

Figure 7 Independent and dependent variables in the calculus of variations for this study.

3.2.4 Discretization

Taking z as the independent variable, the cable will be discretized in several segments with equal value of height, in other words, the mooring line will be divided in several slices, see Figure 8. These values of height, and the associated vertical coordinates of the discretized elements, will never change throughout the whole procedure. Consequently it can be seen that the degrees of freedom of each coordinate in space will be those related to the coordinates x and y.

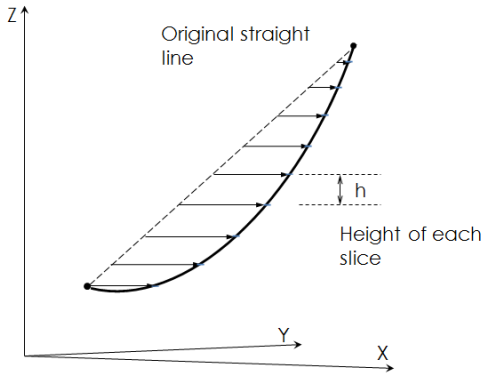

Figure 8 Discretization of mooring line in slices.

3.2.5 Shape functions

The shape functions are possible configurations that can define a deformed form of any structure. It is a consequence of the possible movements allowed in the structure by the degrees of freedom set. In this case of study, in the static solution, it is important to notice that the cable will always lie in a vertical plane, with no coordinates or points out of the plane mentioned, see Figure 9.

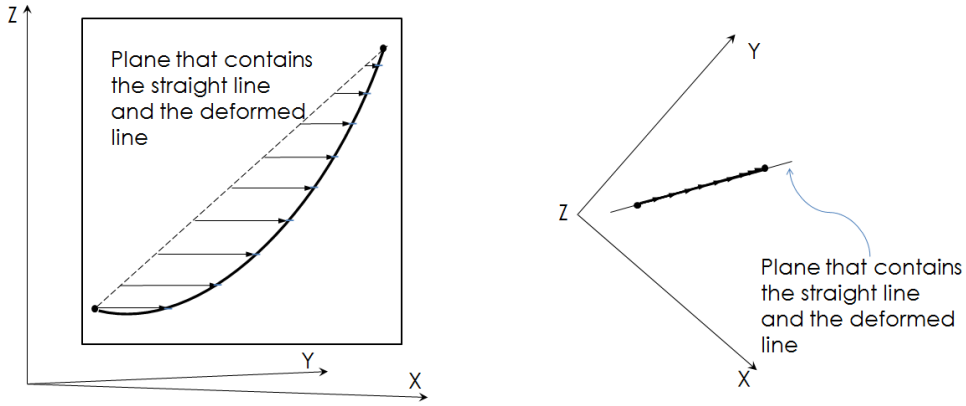

Figure 9 Different views of the plane where the mooring line and its deformations are contained.

The Hermitian interpolation, which allows the generation of the deformed shape in one plane, will be used in this static part of the study, and the shape functions can be represented as follows.

$$N_1 = 1 - 3\left(\frac{z^2}{h^2}\right) + 2\left(\frac{z^3}{h^3}\right) \tag{39}$$

$$N_2 = z - 2\left(\frac{z^2}{h}\right) + \frac{z^3}{h^2} \tag{40}$$

$$N_3 = 3\left(\frac{z^2}{h^2}\right) - 2\left(\frac{z^3}{h^3}\right) \tag{41}$$

$$N_4 = -\left(\frac{z^2}{h}\right) + \frac{z^3}{h^2} \tag{42}$$

3.3 Numerical implementation

The numerical implementation of the previous concepts in order to determine the displacements and forces of the mooring line, and consequently the final configuration after the application of tension in the cable, is presented below.

3.3.1 Definition of the system of reference

The method followed, proposed by Chucheepsakul et al. (2003), starts by setting a straight line that joins the extreme points. One point "touches" the seabed and is considered as the origin of the Cartesian system. The second extremity is the point where the top tension is applied, simulating the location where a floating system is connected to the line, see Figure 10.

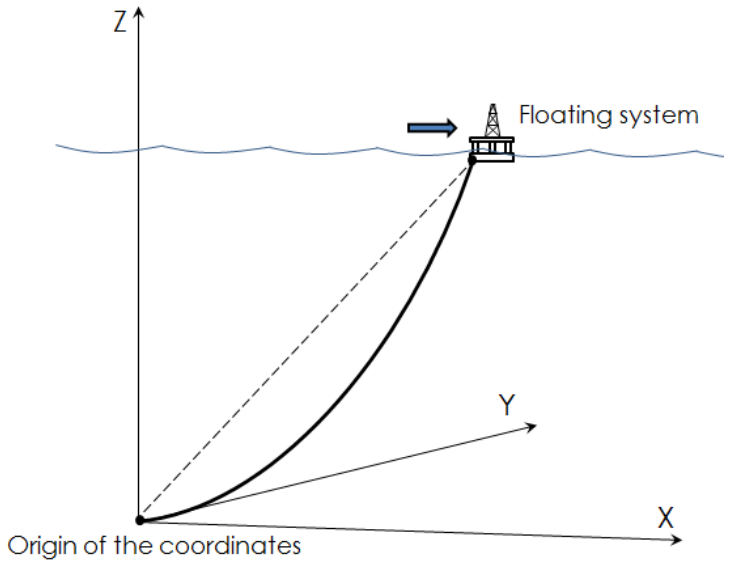

Figure 10 Definition of the origin of coordinates and the top tension location point.

3.3.2 Initial configuration

The initial configuration of the mooring line defines a stiffness matrix and a load vector produced by the initial straight geometry.

The equations (37) and (38) need to be expressed in matrix form, following Chucheepsakul et al. (2003), and without drag forces:

$$[K] = \left[\frac{\partial^2 \Pi}{\partial q_i \partial q_j}\right] = \int_0^h \frac{[N']^T T [N']}{(1 + x'^2 + y'^2)^{3/2}} dz \tag{43}$$

$$\{R\} = \left\{\frac{\partial \Pi}{\partial q_i}\right\} = \int_0^h \frac{[N']^T T}{(1 + x'^2 + y'^2)^{1/2}} \begin{Bmatrix} x' \\ y' \end{Bmatrix} dz \tag{44}$$

The matrix $[N]$ represents the shape functions in a matrix array, indicated as follows:

$$[N] = \begin{bmatrix} N_1 & N_2 & 0 & 0 & N_3 & N_4 & 0 & 0 \\ 0 & 0 & N_1 & N_2 & 0 & 0 & N_3 & N_4 \end{bmatrix} \tag{45}$$

The form of each shape function was defined in equations (39), (40), (41), and (42).

The matrix $[N']$ represents the derivative of the shape functions with respect to z. This is because the independent variable in this case is the vertical coordinate z. No changes in the vertical coordinates of each node will be developed because the slices in which the mooring line was discretized are constant. The vertical height of each slice is always “h = constant”.

The stiffness matrix and load vector of each element are merged by overlapping their common ends, see Figure 11.

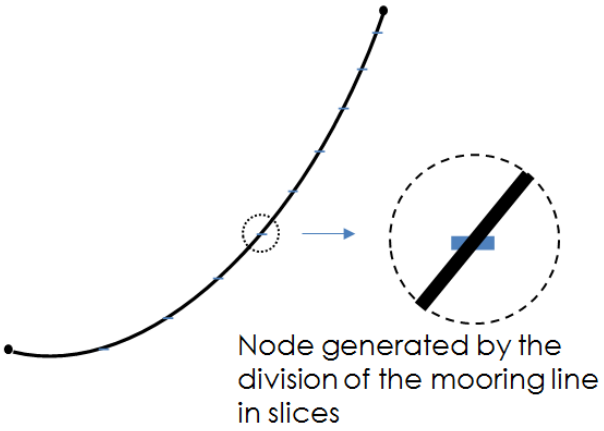

Figure 11 Generation of nodes by splitting the mooring line.

3.3.3 Iterative process

The initial straight line configuration is used to determine a set of associated horizontal displacements, which are added to the initial configuration of the cable producing a new configuration. The new configuration defines a new stiffness matrix and a new load vector, where it is possible to determine a new set of displacements and continue to iterate until a final configuration is found which satisfies the continuity and force equilibrium conditions.

In the iteration described, a process to include the elongation due to the elasticity of the cable is included. This process defines a value of strain that increases at each step of the iterative process by the Newton-Raphson method. The formulation is expressed as follows

$$\varepsilon^{n+1} = \varepsilon^{n} - \frac{f(\varepsilon^{n})}{f'(\varepsilon^{n})} \tag{46}$$

Following Chucheepsakul et al. (2003), the function $f(\varepsilon^{n})$ and its derivative are:

$$f(\varepsilon^n) = EA\varepsilon^n - T_H + \int_z^{Z_H} \frac{w}{1+\varepsilon} dz \tag{47}$$

$$f'(\varepsilon^n) = \frac{f(\varepsilon^n + \Delta) - f(\varepsilon^n)}{\Delta} \tag{48}$$

where *n* is the number of the iteration, and in the forward difference formula a value of $\Delta = 1\text{x}10^{-8}$ is proposed by Chucheepsakul et al. (2003).

The final configuration is found when the horizontal forces of each cable segment are approximately equal. One value of convergence is needed to be defined for numerical purposes. Since the horizontal force must be the same in any point of the cable, a maximum difference of horizontal force between the finite elements of the cable must be set. In the examples shown, a value of convergence of 0.01N was usual. Several iterations are carried out until this precision is reached.

Each step of the iterative process will generate a series of deformed lines where the first was a straight line, and the last one defines the final configuration of the cable taking into account all the considerations previously explained, see Figure 12. In this figure the initial configuration is indicated as a black dotted straight line, the successive intermediate configurations as blue straight lines, and the final configuration in black with cross points. In this last configuration, the cross points indicate the nodal points in which the whole line was discretized.

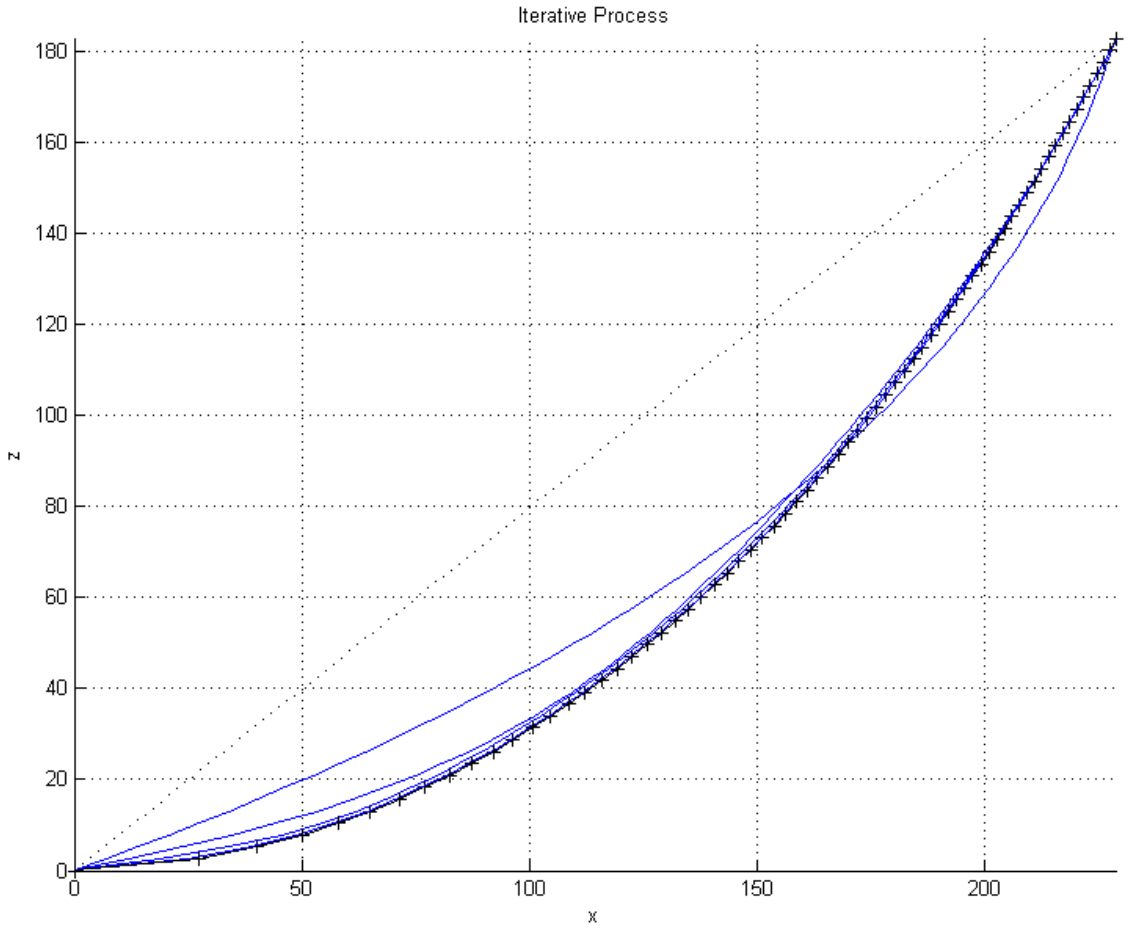

Figure 12 Iterative process to find the final deformation of a cable resulting from the application of top tension.

3.3.4 Flowchart

The essentials of the process previously explained can be summarized in Figure 13. It is important to note that the geometrical and mechanical characteristics determined by this process will be required for the dynamic solution.

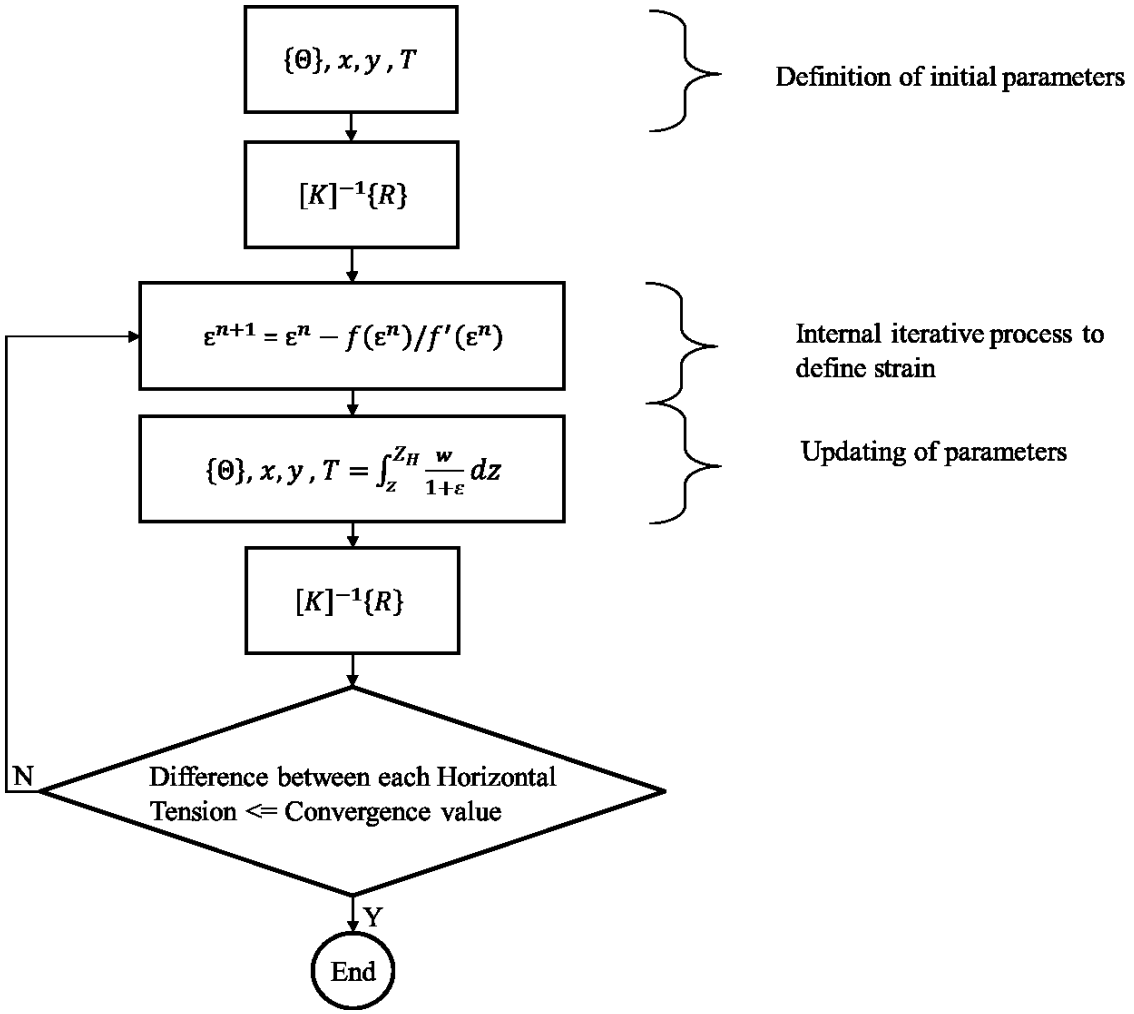

Figure 13 Diagram that summarizes the iterative process to define the final configuration and forces of the cable.

3.3.5 Comparison of results

The results produced by the model followed were compared with one example developed by DuBuque (2011) that was based on the elastic catenary of Irvine (1992). This formulation takes into account the elasticity of the material, and defines the

geometry in the plane for a cable subjected to a horizontal and vertical force at the top end of the cable (see Figure 14).

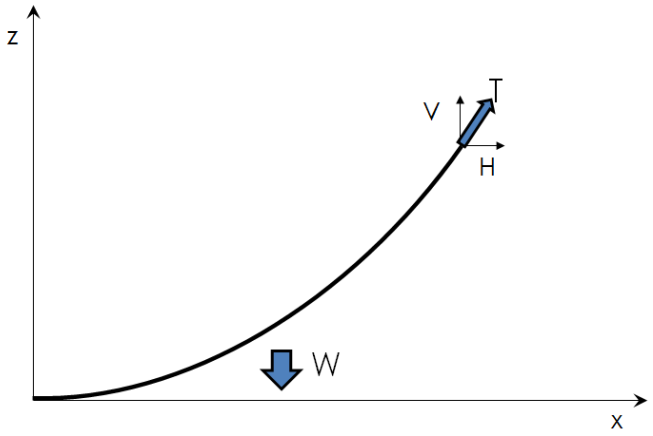

Figure 14 Image of a cable to describe Irvine's model.

The original formulation of Irvine (1992) is

$$x(s) = \frac{Hs}{EA_0} + \frac{HL_0}{W}\left[\sinh^{-1}\left(\frac{V}{H}\right) - \sinh^{-1}\left(\frac{V - Ws/L_0}{H}\right)\right] \tag{49}$$

$$z(s) = \frac{Ws}{EA_0}\left(\frac{V}{W} - \frac{s}{2L_0}\right) + \frac{HL_0}{W}\left[\sqrt{1 + \left(\frac{V}{H}\right)^2} - \sqrt{1 + \left(\frac{V - Ws/L_0}{H}\right)^2}\right] \tag{50}$$

In the above equations H and V are the horizontal and vertical components, respectively, of the tension applied at the upper end of the cable, W is the total weight of the cable, L_0 is the unstrained length, E is the modulus of elasticity, A_0 is the cross-sectional area of the cable, and s is the arc length at any specific point from the origin.

From equations (49) and (50) it is important to observe the effect of the axial stiffness (EA_0) on the deformed configuration of the cable, in contrast to the case of the inelastic catenary.

Based on this formulation DuBuque (2011) produced an example with the values shown in Table 1.

Table 1 Data for validation example.

Horizontal top force	$H = 50$ N
Vertical top force	$V = 75$ N
Total weight	$W = 70$ kg
Cross sectional area	$A_0 = 7.85\text{x}10^{-5}$ m^2
Modulus of elasticity	$E = 10\text{x}10^{8}$ Pa
Unstrained length	$L_0 = 10$ m

With these values, the static line configuration calculated using the method followed in this work was compared with that calculated by DuBuque. Figure 15 reveals a good agreement between the two models.

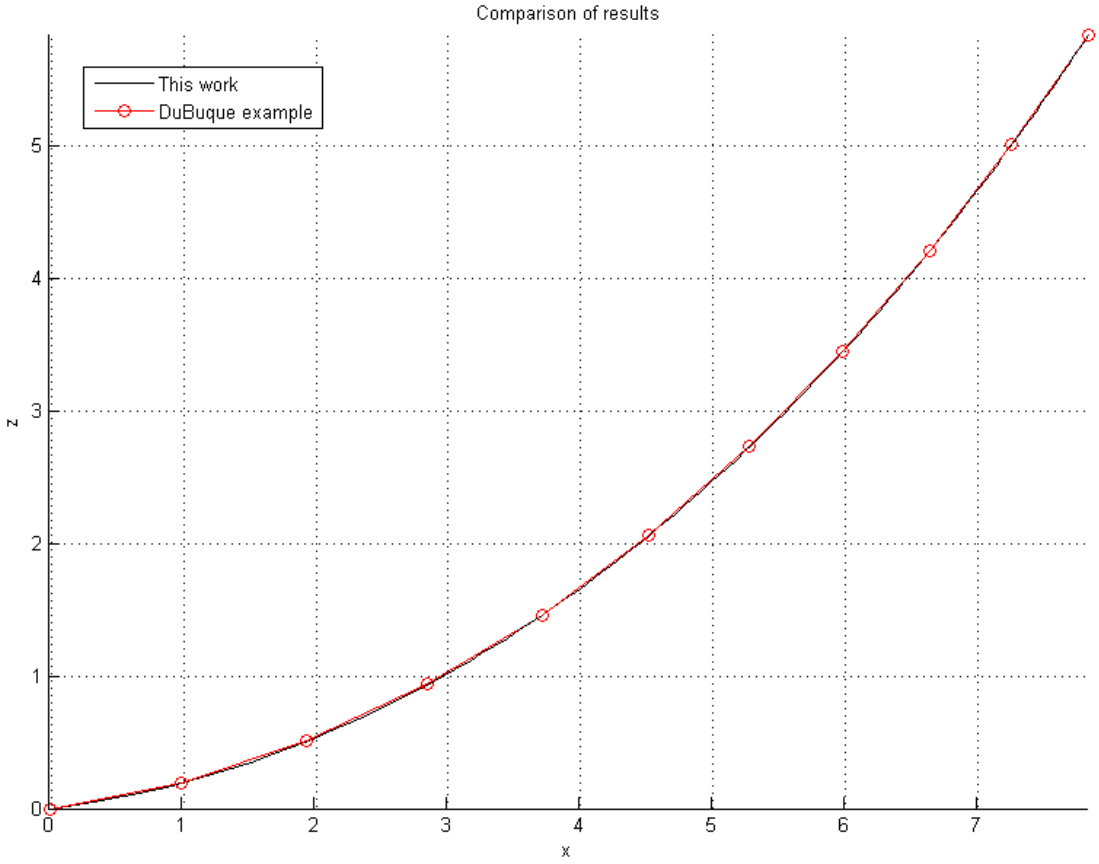

Figure 15 Comparison with DuBuque method.

3.3.6 Configuration of a polyester system

With the aim to analyze the deformed configuration of a Polyester System, a mooring line containing steel chain in the upper and lower part, and an insert of polyester in the middle of its entire length, is presented. The characteristic values of the system described are shown in Table 2.

Table 2 Characteristics of a Polyester System

Static Configuration in Seawater	
Water depth	1500 m
Anchor radius	2400 m
Top tension	1000 kN
Top Chain Properties	
Length	104.5
Stiffness (EA)	4.41 x 10^5kN
Submerged weight/length	913.213 N/m
Number of elements modeled	5
Polyester Rope Properties	
Length	1907.3
Stiffness (EA)	2.74 x 10^5kN
Submerged weight/length	71.613 N/m
Number of elements modeled	82
Bottom Chain Properties	
Length	904.7
Stiffness (EA)	4.41 x 10^5kN
Submerged weight/length	913.213 N/m
Number of elements modeled	13

It is interesting to observe the resultant configuration because the axial stiffness and weight of each material are very different. The elongation for steel is smaller than the elongation for the polyester under the same load, consequently the deformation in the

polyester produces almost a straight line as its converged configuration. On the other hand, the lower part of steel chain produces a catenary configuration, see Figure 16.

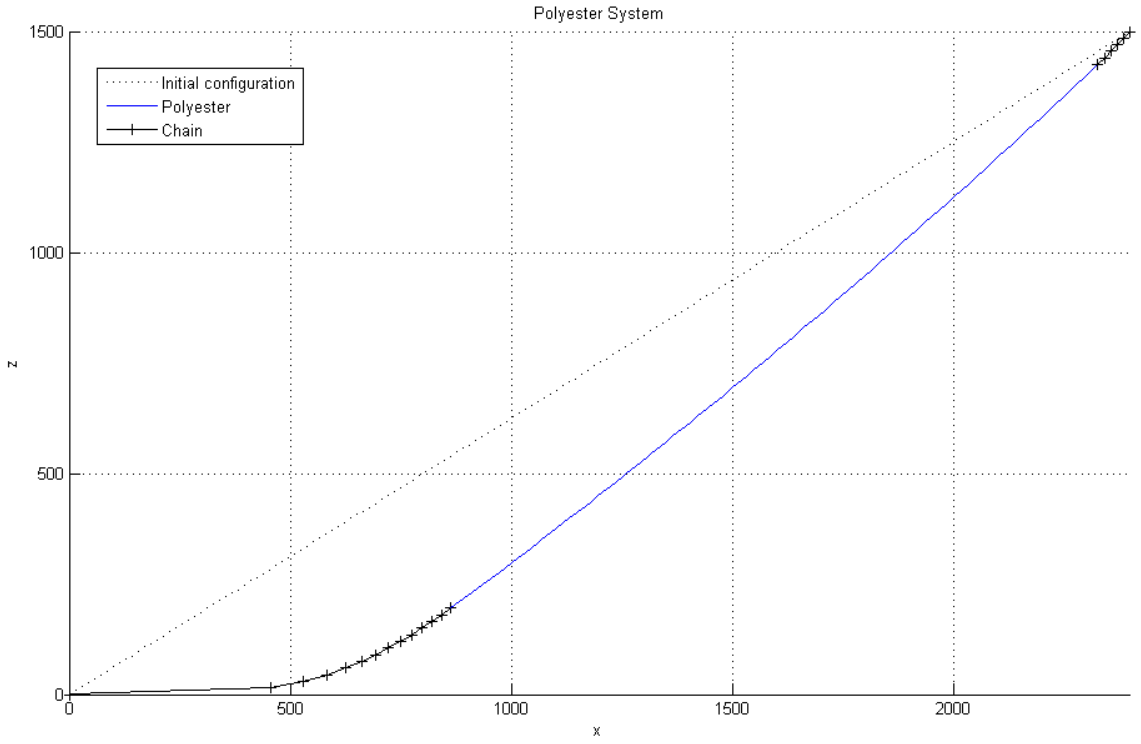

Figure 16 Deformed configuration of a Polyester System.

4. MODAL ANALYSIS

4.1 Shape functions in three dimensional space

From the static analysis, and following Chucheepsakul and Srinil (2002), the final (converged) deformed configuration and the axial tension in each finite element will be used for the modal analysis.

In the static analysis the deformed configuration of the cable lies in one plane, consequently the shape functions required were related to the degrees of freedom in only one plane.

In modal analysis motion of the cable in three dimensions is expected. This is one of the reasons why the shape functions are now related to the motions in the three dimensions of a Cartesian (X,Y,Z) coordinate system. In matrix form they can be represented as:

$$[N] = \begin{bmatrix} N_1 & N_2 & 0 & 0 & 0 & 0 & N_3 & N_4 & 0 & 0 & 0 & 0 \\ 0 & 0 & N_1 & N_2 & 0 & 0 & 0 & 0 & N_3 & N_4 & 0 & 0 \\ 0 & 0 & 0 & 0 & N_1 & N_2 & 0 & 0 & 0 & 0 & N_3 & N_4 \end{bmatrix} \tag{51}$$

In equation (51) each value of any shape function in the $[N]$ matrix is referred to equations (39) through (42).

On the other hand, natural coordinates were employed to define the motions of the cable in the development of the modal analysis of a marine cable. An explanation of this system of coordinates is shown in Figure 17.

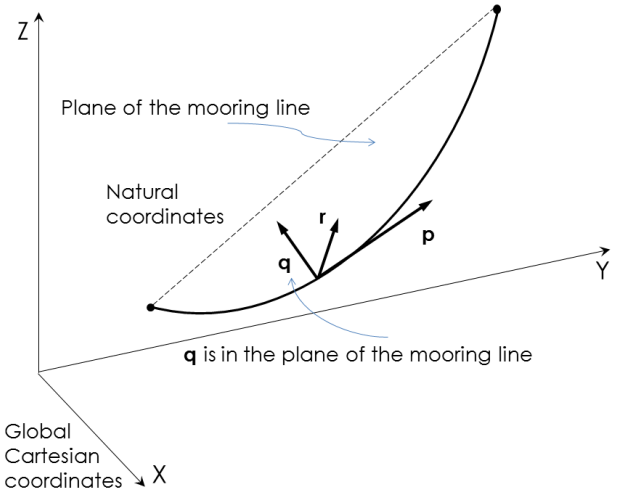

Figure 17 Natural coordinates.

In Figure 17 the (p) coordinate refers to tangential displacements, (q) refers to displacements perpendicular to tangential but in the plane of the mooring line, and (r) refers to coordinates perpendicular to the plane of the (p) and (q) coordinates.

A transformation matrix between the natural coordinates and the Cartesian coordinates was provided by Chucheepsakul and Srinil (2002).

4.2 Equation of motion without damping included

The equation of motion presented by Chucheepsakul and Srinil (2002) involves mass and stiffness. Following this procedure a modal analysis can be performed in the cable.

$$[M]\{\ddot{D}\} + [K]\{D\} = \{0\} \tag{52}$$

The matrix $[M]$ represents the mass, and $[K]$ represents the stiffness. The vector $\{D\}$ refers to a nodal displacement vector and the vector $\{\ddot{D}\}$ refers to an acceleration vector.

The values of mass and stiffness are calculated as indicated in equation (53) and (54).

$$[M] = \int_0^h [T]^T [N]^T [\bar{A}][N][T]dz \tag{53}$$

$$[K] = \int_0^h [T]^T [N']^T [\bar{B}][N'][T]dz \tag{54}$$

As in the static solution, the above quantities are computed for each finite element, and then merged for the entire mooring line. The matrix $[T]$ is a transformation matrix between the natural coordinates and Cartesian coordinates; this matrix is provided in appendix A.

The matrix $[N]$ represents the shape functions for the dynamic analysis, shown in equation (51). $[N']$ is the matrix with the derivatives of the shape functions with respect to the axis *Z*.

The matrix $[A]$ is the mass matrix, equation (55).

$$[A] = \begin{bmatrix} \widetilde{m} & 0 & 0 \\ 0 & \widetilde{m} & 0 \\ 0 & 0 & \widetilde{m} \end{bmatrix} \tag{55}$$

where $\widetilde{m}$ is calculated as in equation (56).

$$\widetilde{m} = \overline{m} + \rho A C_A s_0' \tag{56}$$

In the previous equation ρ is the density of water, A is the effective cross-sectional area of the mooring line and C_A is an added mass coefficient assumed equal to:

$$C_A = C_M - 1 \tag{57}$$

where C_M is a mass coefficient assumed equal to 2.

From equation (56) the mass per unit length of the cable $\overline{m}$ is:

$$\overline{m} = \left[\frac{w}{g(1+\varepsilon_0)}\right] s_0' \tag{58}$$

where s_0' is:

$$s_0' = \sqrt{1 + x_0'^2 + y_0'^2} \tag{59}$$

and ε_0 is the static strain in the cable obtained from the static analysis, g is the acceleration of gravity, and w is the weight per unit length of cable.

The $[\bar{B}]$ matrix is a matrix form of the stiffness, expressed in equation (60).

$$[\bar{B}] = \begin{bmatrix} \frac{T_a}{s_0'} + \frac{T_b x_0'^2}{s_0'^3} & 0 & \frac{T_b x_0'}{s_0'^3} \\ 0 & \frac{T_a}{s_0'} & 0 \\ \frac{T_b x_0'}{s_0'^3} & 0 & \frac{T_a}{s_0'} + \frac{T_b}{s_0'^3} \end{bmatrix} \tag{60}$$

where

$$T_a = EA\varepsilon_0 + 2\nu\rho g A_0 (Z_H - z_0) \tag{61}$$

$$T_b = EA - 2\nu\rho g A_0 (Z_H - z_0) \tag{62}$$

In equations (61) and (62) ν is the Poisson ratio, A_0 is the deformed cross-sectional area, Z_H is the total depth of water, and z_0 is the elevation coordinate for each node point of the cable in the static configuration.

The above expressions include the Poisson ratio in order to account for the tension produced by the hydrostatic pressure. However, in this work it will not to be taken into account, considering that the reduction in cable diameter is negligible. Moreover, the results of the dynamic analysis considering the value of tension T_b are not consistent. It was proven in the modal analysis that by neglecting this value the results are more accurate.

With equation (52) the eigenvalue problem shown in equation (63) is solved to find the frequencies and eigenvectors without damping.

$$([K] - \omega^2[M])\{D\} = \{0\} \tag{63}$$

The eigenvectors resulting from this equation are in natural coordinates (p), (q) and (r) due to the transformation performed in the definition of the stiffness matrix shown in equations (53) and (54).

4.2.1 Comparison of results with Orcaflex

The modal analysis was performed following the formulation proposed above, and programed in Matlab. For validation purposes a test case was investigated and the results were compared with the same analysis performed with Orcaflex. Orcaflex is commercially available software for the dynamic analysis of offshore marine systems. The data for the validation example performed are provided in Table 3.

Table 3 Characteristics of mooring line for validation case with Orcaflex.

Water depth	285.788 m
Anchor radius	165.000 m
Top tension	73.20 kN
Un-strained length	330.085 m
Stiffness (*EA*)	1.2854x 10^5 kN
Submerged weight/length	53.56 N/m

Table 4 compares the values of the first four natural frequencies obtained from the Matlab code developed in this work and from Orcaflex. Orcaflex did not compute results for the tangential modes. Interestingly, whereas the Matlab code calculated identical frequencies for the tangential, in-plane and out-of-plane components of each mode (as it should be), Orcaflex indicated similar but not equal frequencies for the in-plane and out-of-plane components.

Table 4 Comparison of natural frequencies for Orcaflex validation case.

Mode		Natural Frequency (rad/s)		% Difference
		Matlab	Orcaflex	
1	tangential	1.045	--	--
	in-plane	1.045	1.971	88.6%
	out-of-plane	1.045	1.039	-0.6%
2	tangential	2.089	--	--
	in-plane	2.089	2.130	2.0%
	out-of-plane	2.089	2.077	-0.6%
3	tangential	3.134	--	--
	in-plane	3.134	3.197	2.0%
	out-of-plane	3.134	3.109	-0.8%
4	tangential	4.179	--	--
	in-plane	4.179	4.134	-1.1%
	out-of-plane	4.179	4.134	-1.1%

Apart from the first in-plane mode where the difference in natural frequencies is substantial, the natural frequencies produced by the two analysis procedures are in good agreement.

The modal shapes from the numerical procedure developed in this work and the Orcaflex analysis were compared graphically and show good agreement. Figure 18 shows the modal shapes for the first 4 modes in the plane. In black is plotted the modal shape generated by Orcaflex, and in red by the procedure followed in this study. In blue is the line of the deformed configuration from the static analysis.

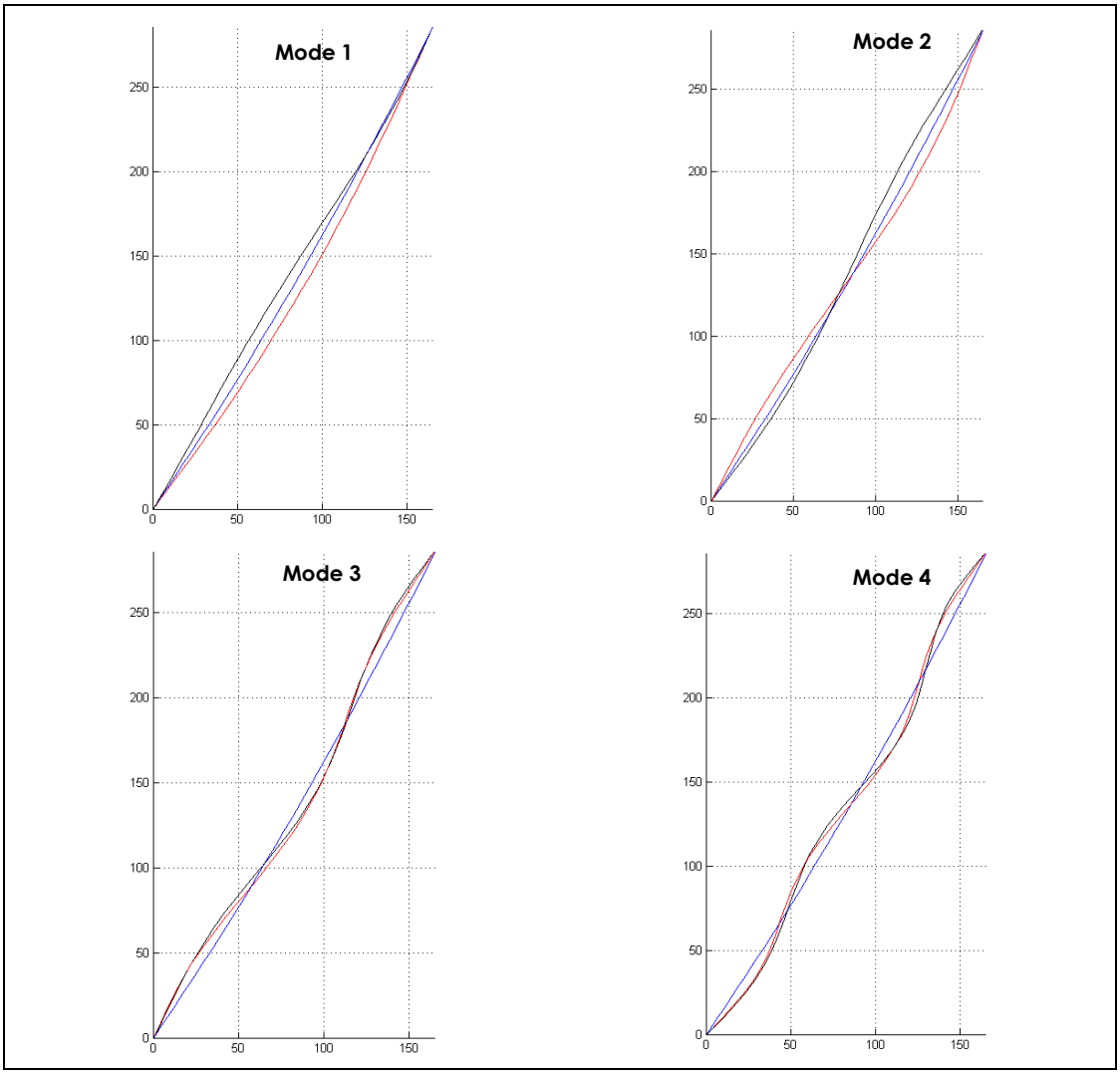

Figure 18 Comparison between the first four modal shapes in the plane generated by Orcaflex and the procedure followed in this study.

Figure 19 shows the modal shapes for the first 4 modes out of the plane. In black is plotted the modal shape generated by Orcaflex, and in red by the procedure followed.

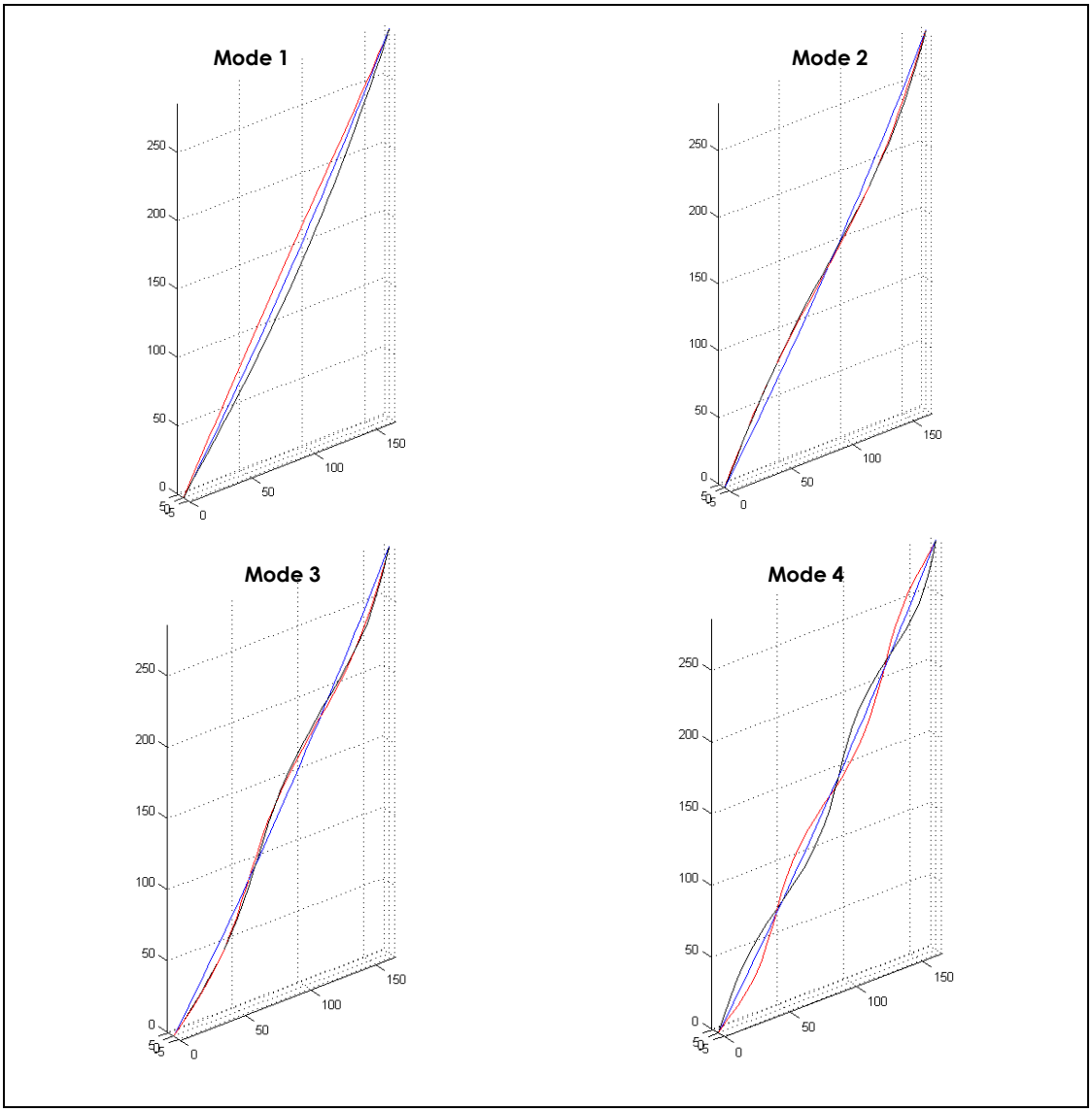

Figure 19 Comparison between the first four modal shapes out of plane generated by Orcaflex and the procedure followed.

4.3 Equation of motion with damping included

The addition of damping in the equation of motion is idealized from the Morison equation relative velocity drag term (64)

$$F = \frac{1}{2}\rho C_D A(u - \dot{x})|u - \dot{x}| \tag{64}$$

Here ρ is the density of water, C_D is the drag coefficient, A is the cross-sectional area of a slender element, and $u - \dot{x}$ represents the local relative velocity between the fluid and the structure in the direction normal to the axis of the slender member.

The Morison equation defines hydrodynamic inertia and drag forces in slender elements, such as a mooring line. The drag force is seen to be nonlinear, however, for the modal analysis we wish to model the drag damping as linear viscous; consequently a statistical linearization of the Morison drag force is required. The procedure is presented as follows.

Recognizing that in our case the mooring line is moving with harmonic motion in calm water (u = 0), the term representing the relative velocity is replaced as proposed in the next equations.

$$(u - \dot{x})|u - \dot{x}| = u_{eq}\dot{x} \tag{65}$$

$$u_{eq} = \sqrt{\frac{8}{\pi}}\sigma_{\dot{x}} \tag{66}$$

Here $\sigma_{\dot{x}}$ is the standard deviation of the body velocity from the modal analysis not including damping in the equation of motion. Since each mode represents sinusoidal

motion with frequency ω, the standard deviation of velocity at a particular node point where the amplitude of motion is D is calculated according to

$$\sigma_{\dot{x}} = \sqrt{\frac{1}{2} D^2 \omega^2} = \frac{D\omega}{\sqrt{2}} \tag{67}$$

The value u_{eq} is calculated for each node along the length of the mooring line for each value of natural frequency ω, defined by a modal analysis with no damping performed through the equation (63). The magnitude of the amplitude D is taken from the natural coordinates (q) and (r) obtained from the modal shapes of the analysis without damping included, see Figure 20.

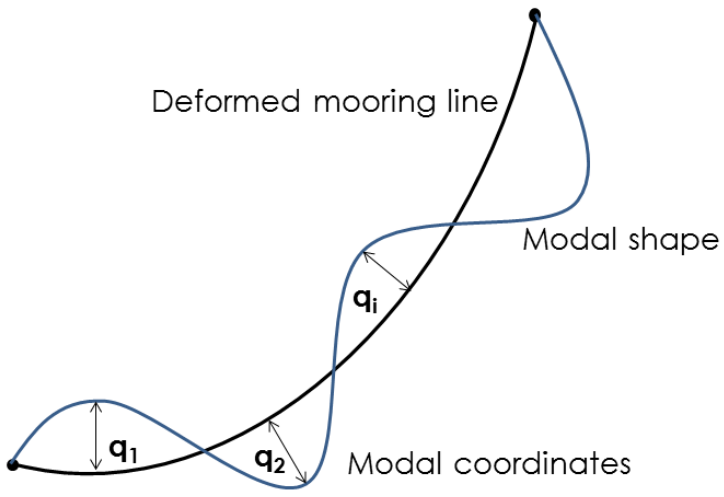

Figure 20 Modal coordinates from the modal shape.

The values of the natural modal coordinates (q) and (r) are normalized with respect to the maximum value of the sag of the cable determined from the static analysis. Equation (68) and (69) show the normalization for the natural coordinates (q) and (r).

$$q_{norm} = \delta \cdot sag\left(\frac{q}{\max(abs(q))}\right) \tag{68}$$

$$r_{norm} = \delta \cdot sag\left(\frac{r}{\max(abs(r))}\right) \tag{69}$$

where δ is a specified fraction between 0 and 1. In the modal analysis assumed values of δ equal to 0, 0.001, 0.01, 0.1, 0.5 and 1.0 were investigated.

These normalized values become the amplitudes in the equation (67), and with them, values of u_{eq} are obtained for each modal coordinate of the cable for each value of frequency in the modal analysis. The damping matrix $[C]$ is formed with each row representing the frequencies and the columns represent the degrees of freedom.

Following Rao (2007) the equation of motion (63) including the damping term is written as the following characteristic equation:

$$\lambda^2[M]\{D\} + \lambda[C]\{D\} + [K]\{D\} = \{0\} \tag{70}$$

By using the followed expression

$$\lambda = \omega^2 \tag{71}$$

and rewriting equation (70) we have:

$$\lambda^2\{D\} = -\lambda[M]^{-1}[C]\{D\} - [M]^{-1}[K]\{D\} \tag{72}$$

Defining a displacement vector

$$x = \begin{Bmatrix} D \\ \lambda D \end{Bmatrix} \tag{73}$$

we can rewrite equation (72) as

$$\lambda \begin{Bmatrix} D \\ \lambda D \end{Bmatrix} = \begin{bmatrix} 0 & 1 \\ -\frac{[K]}{[M]} & -\frac{[C]}{[M]} \end{bmatrix} \begin{Bmatrix} D \\ \lambda D \end{Bmatrix} \tag{74}$$

Complex frequencies and eigenvalues result by solving this new eigenvalue problem. The results are available in a double size matrix where they are expressed twice, and the frequencies are expressed as imaginary numbers.

In order to validate this methodology, one example was performed considering the $[C]$ matrix as a zero matrix. The results were compared with a corresponding example with the standard no damping formulation. The mooring line particulars for the example tested are shown in Table 5.

Table 5 Particulars of the mooring line tested with zero damping.

Static Configuration in Seawater	
Water depth	2000 m
Anchor radius	1925.19 m
Top tension	2946 kN
Seawater density	1025 kg/m^3
Wire Rope Properties	
Un-strained length	2794 m
Stiffness (*EA*)	1.1606 x 10^6 kN
Mass/length	69.9 kg/m
Submerged weight/length	540.4 N/m

A graphic that shows the static deformed configuration for this example under the previous characteristics is shown in Figure 21.

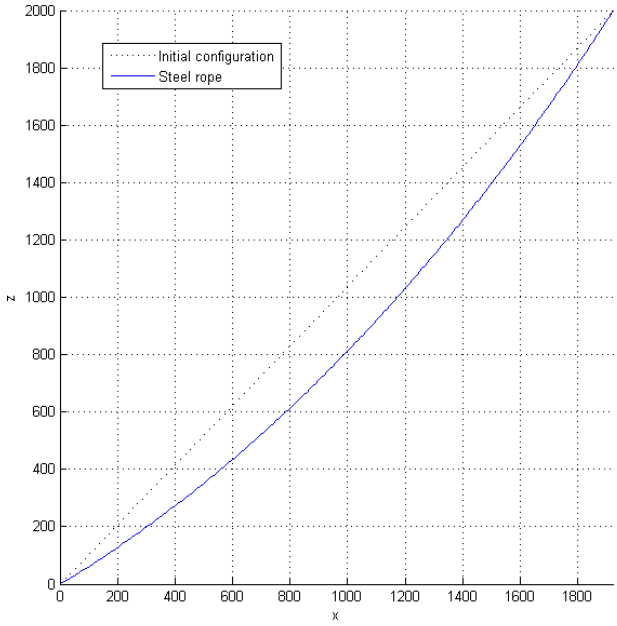

Figure 21 Static deformed configuration for the example tested without damping.

The results of the example with the damping matrix as a zero matrix, and the results with the same data under the procedure without damping, are shown in Table 6.

Table 6 Results of the mooring line tested with zero damping.

Example tested	1st frequency (rad/sec)	2nd frequency (rad/sec)	3rd frequency (rad/sec)	4th frequency (rad/sec)
Example tested in procedure without damping	0.2058	0.4110	0.6163	0.8217
Example tested in procedure with damping (damping = 0)	0.2058	0.4110	0.6163	0.8217

The modal shapes for the first four modes in plane are shown in Figure 22.

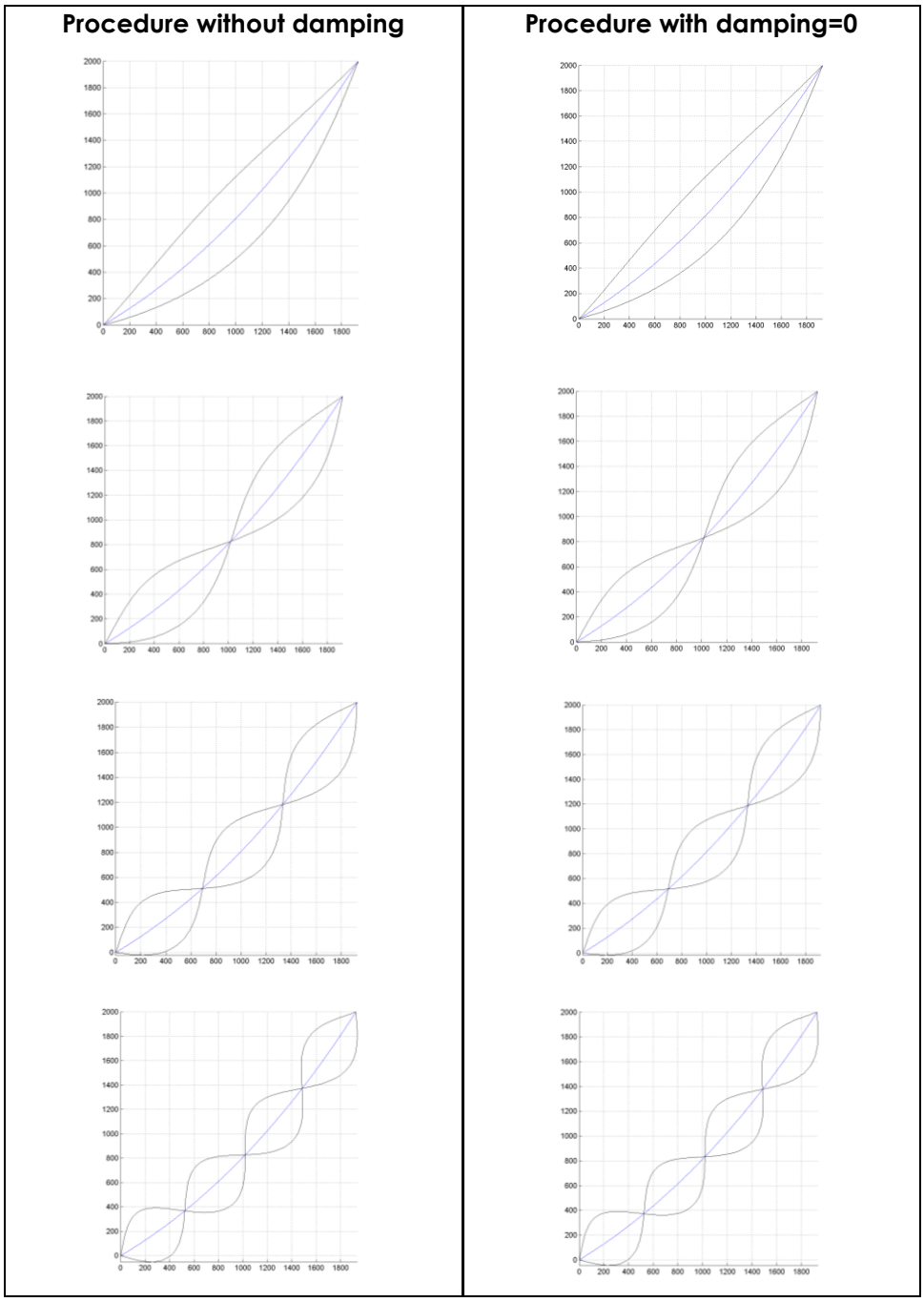

Figure 22 Modal shapes comparing the first four modes in plane.

The modal shapes for the first four modes out of plane are shown in Figure 23.

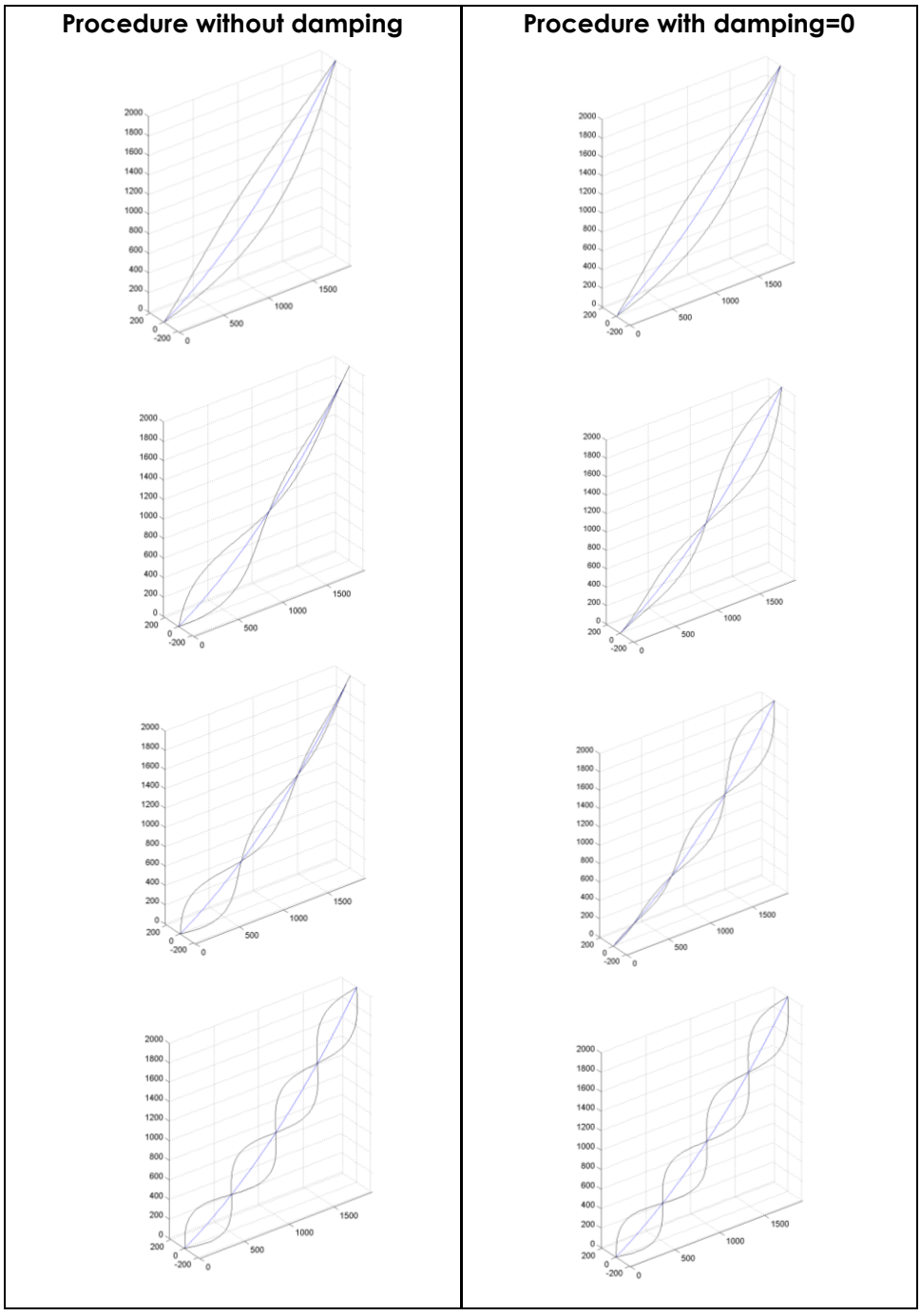

Figure 23 Modal shapes comparing the first four modes out of plane.

The values of the frequencies produced in the two methods explained previously are in precise agreement, and the global behavior of the in-plane modal shapes generated by both procedures has a good agreement over all. The out-of-plane mode shapes for the second and third modes show noticeable differences which cannot be explained, whereas the shapes for the first and fourth modes are in good agreement.

5. ANALYSIS OF DIFFERENT MOORING SYSTEMS

5.1 Description of the systems assessed

With the method of modal analysis presented previously, three mooring systems were examined. The names and characteristic of each one are described below.

5.1.1 Steel Rope System

The steel rope system is made up entirely of steel rope. The geometric and mechanical characteristics of this system are tabulated in Table 7. A drawing showing the deformed configuration of this system as if it were submerged in water can be seen in Figure 24.

Table 7 Characteristics of the Steel Rope System.

Static Configuration in Seawater	
Water depth	2000 m
Anchor radius	1925.19 m
Top tension	2946 kN
Seawater density	1025 kg/m^3
Wire Rope Properties	
Un-strained length	2794 m
Stiffness (*EA*)	1.1606 x 10^6 kN
Mass/length	69.9 kg/m
Submerged weight/length	540.4 N/m

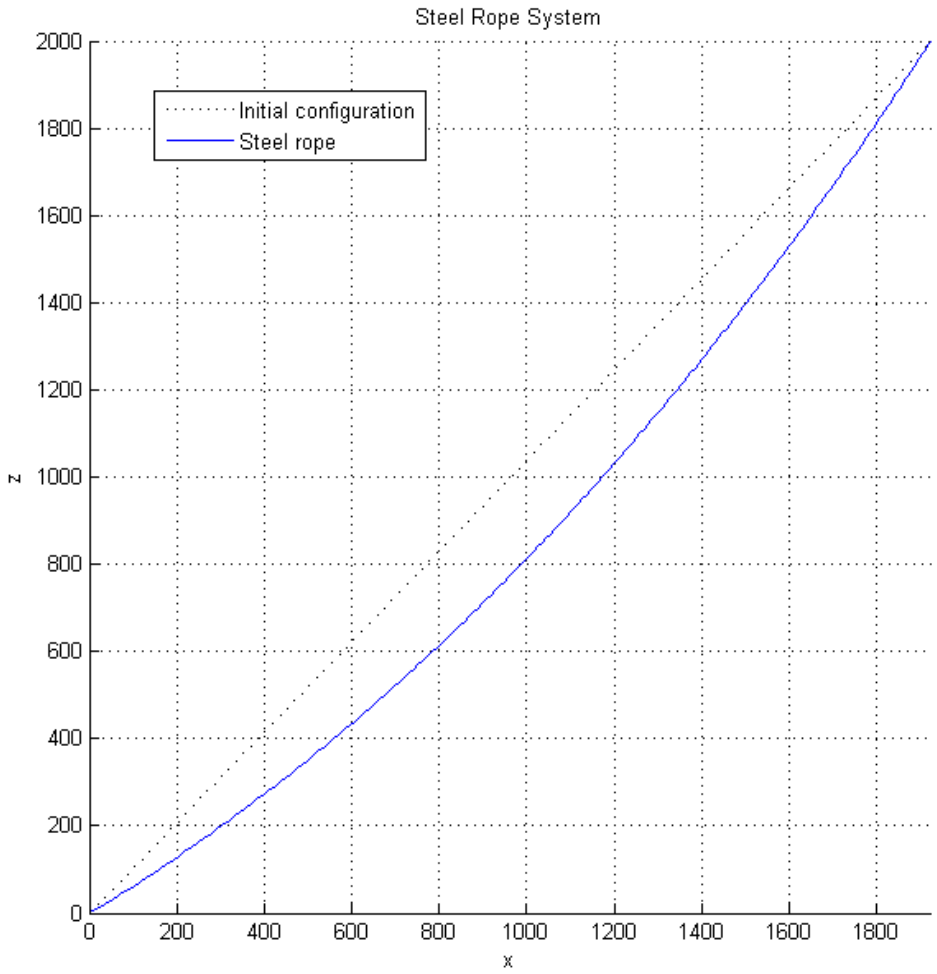

Figure 24 Deformed configuration of the Steel Rope System.

5.1.2 Steel System

The steel system is a mooring line with three segments, two of them of steel chain, and one in the middle, of steel rope. The characteristic values of this mooring line are shown in Table 8.

Table 8 Characteristics of the Steel System.

Static Configuration in Seawater	
Water depth	2000 m
Anchor radius	2330 m
Top tension	2946 kN
Top Chain Properties	
Un-strained length	76.2 m
Stiffness (*EA*)	1.2687×10^6 kN
Submerged weight/length	2611 N/m
Steel Rope Properties	
Un-strained length	2804.2 m
Stiffness (*EA*)	1.1606×10^6 kN
Submerged weight/length	540.4 N/m
Bottom Chain Properties	
Un-strained length	243.8 m
Stiffness (*EA*)	1.2687×10^6 kN
Submerged weight/length	2611 N/m

Figure 25 shows the deformed shape of the Steel System in proportional dimensions of depth and anchor radius.

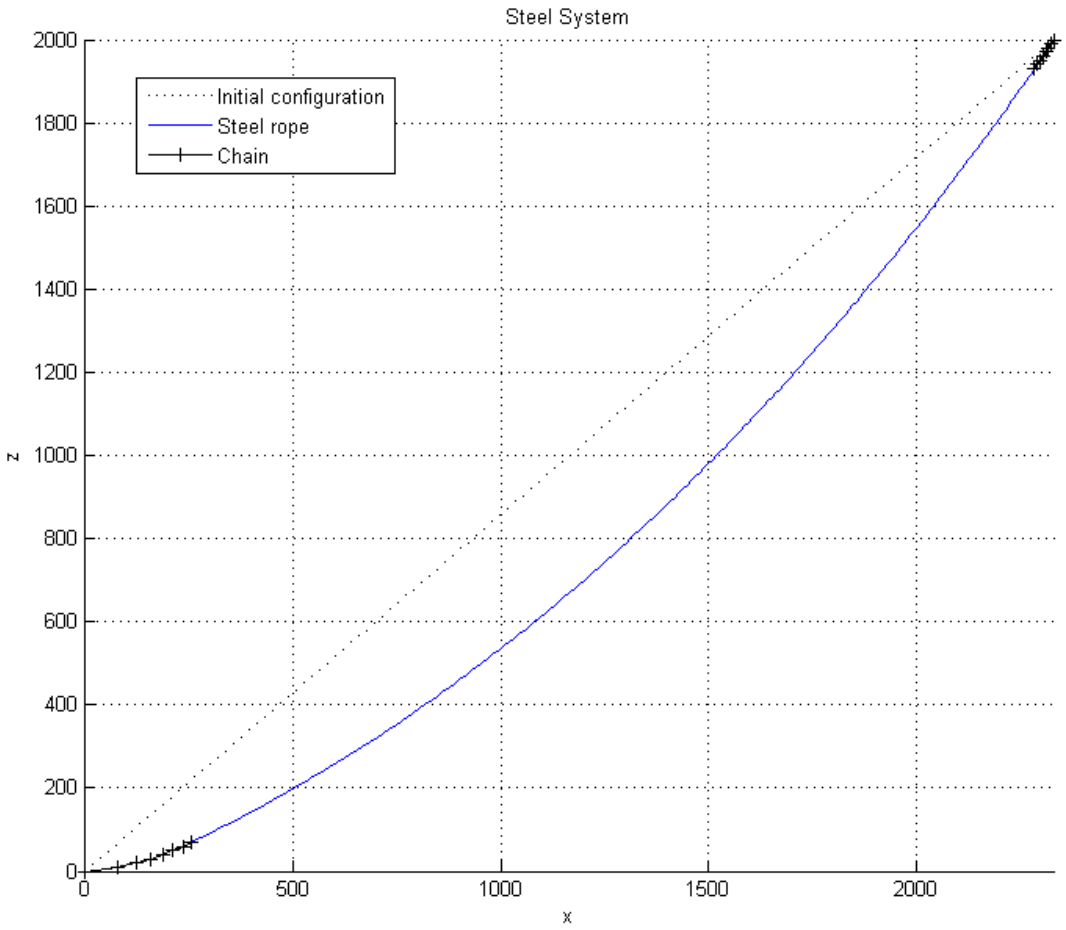

Figure 25 Deformed configuration of the Steel System.

5.1.3 Polyester System

The polyester system is a mooring line composed by three segments, two of steel chain and one insert of polyester. The particulars for this system are provided in Table 9.

Table 9 Characteristics of the Polyester System.

Static Configuration in Seawater	
Water depth	2000 m
Anchor radius	1527m
Top tension	2946 kN
Top Chain Properties	
Un-strained length	76.2 m
Stiffness (*EA*)	1.2687×10^6 kN
Submerged weight/length	2611 N/m
Polyester Rope Properties	
Unstrained length	2174.4 m
Stiffness (*EA*)	2.4554×10^5 kN
Submerged weight/length	122.7 N/m
Bottom Chain Properties	
Unstrained length	243.8 m
Stiffness (*EA*)	1.2687×10^6 kN
Submerged weight/length	2611 N/m

The plot of the static submerged configuration of the polyester system is shown in Figure 26.

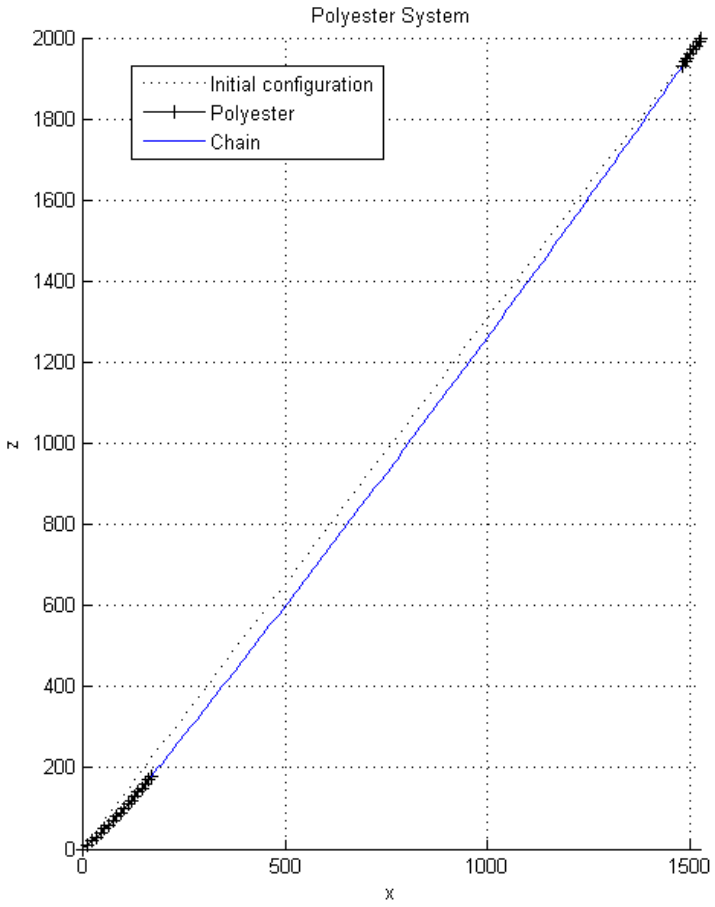

Figure 26 Deformed configuration of the Polyester System.

5.2 Results of modal analysis

Four cases with different surrounding environment where analyzed for each of the three mooring systems. A description of each one is presented next.

1) *Air*

   In this case the cable is modeled considering its weight as if it were in air. In other words, no buoyancy or added mass is considered. Although this is not a realistic case for mooring lines, the example is investigated with the aim of comparing with the submerged cases.

2) *Water, only submerged weight*

   In this case, the buoyancy of the cable produced by water is considered. Only the mass of the mooring line is considered. The added mass and damping associated with motion of the line through the water is not considered. No currents will be considered.

3) *Water, submerged weight, and added mass*

   Here, the buoyancy due to water is considered, and the added mass generated by the surrounding water to the cable is taken into account. The added mass was computed as the density of sea water (1025 kg/m^3) times the volume of the cable.

4) *Water, submerged weight, added mass, and damping*

   In this last case, the submerged weight, and added mass were considered. Moreover, the drag damping produced by the water was incorporated in the analysis.

The modeling details for each case are presented in Table 10.

Table 10 Details of segments modeled in each system.

Steel System						
Case	Number of elements			Length (m)		
	Lower segment	Middle segment	Upper segment	Lower segment	Middle segment	Upper segment
1) Air	7	186	7	257.8	2794.8	71.9
2) Weight submerged	7	186	7	258.9	2793.4	72.1
3) Weight submerged, added mass	7	186	7	258.9	2793.4	72.1
4) Weight submerged, added mass, damping	7	186	7	258.9	2793.4	72.1

Polyester System						
Case	Number of elements			Length (m)		
	Lower segment	Middle segment	Upper segment	Lower segment	Middle segment	Upper segment
1) Air	16	177	7	236.5	2176.7	81.0
2) Weight submerged	18	175	7	248.1	2162.6	84.0
3) Weight submerged, added mass	18	175	7	248.4	2162.4	83.9
4) Weight submerged, added mass, damping	18	175	7	248.4	2162.4	83.9

5.2.1 Behavior of the Steel Rope System

The first eight periods of free vibration for this system are shown in Table 11 for the first three cases which do not involve damping.

Table 11 First eight natural periods for Steel Rope System.

Case	First eight periods (s)							
	1	2	3	4	5	6	7	8
1) Air	27.5	13.8	9.2	6.9	5.5	4.6	3.9	3.4
2) Weight submerged	27.1	13.6	9.0	6.8	5.4	4.5	3.9	3.4
3) Weight submerged, added mass	30.5	15.3	10.2	7.6	6.1	5.1	4.4	3.8

As the magnitude of the linearized drag damping is dependent on the amplitude of vibration, modal analysis was performed for various assumed amplitude levels, expressed as a fraction of the static sag in the cable. Table 12 provides the damped natural periods and implied damping ratios ζ for the Steel Rope System.

Table 12 First four damped natural periods for different normalized motion amplitudes in Steel Rope System.

Case	First four periods (s) and damping ratio ζ (%)							
	1	ζ	2	ζ	3	ζ	4	ζ
1 Sag	40.3	65.4	20.5	66.6	15.0	73.3	11.8	76.5
0.5 Sag	35.4	50.8	17.7	50.3	10.7	30.2	8.7	48.7
0.1 Sag	31.5	25.0	15.6	19.5	10.4	19.5	7.7	16.1
0.01 Sag	30.6	8.1	15.3	0.0	10.2	0.0	7.6	0.0
0.001 Sag	30.5	0.0	15.3	0.0	10.2	0.0	7.6	0.0

The first two modal shapes for this system in air are shown in Figure 27.

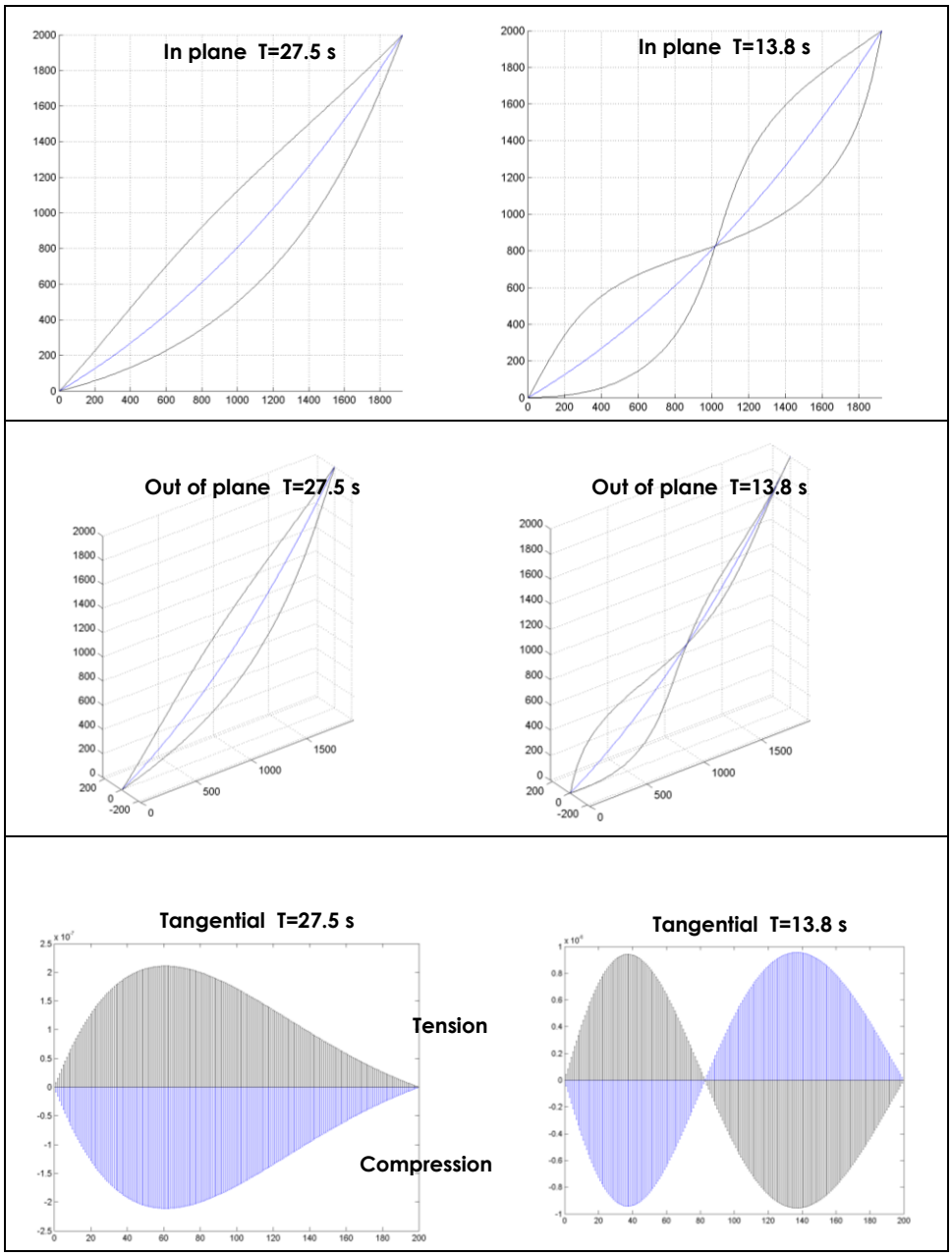

Figure 27 First two modal shapes for the Steel Rope System in air.

The 3rd and 4th modal shapes for this system in air are shown in Figure 28.

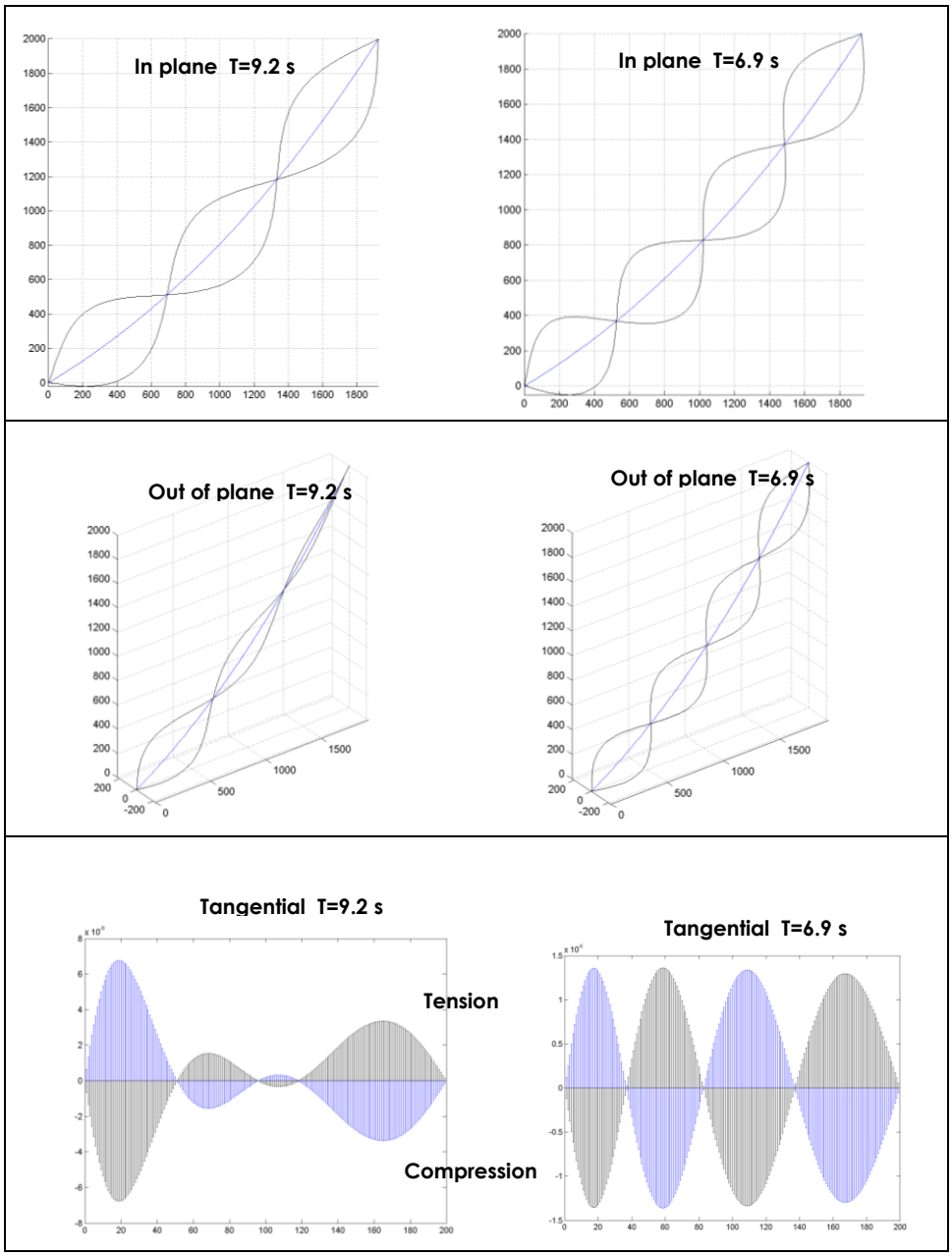

Figure 28 Third and fourth modal shapes for the Steel Rope System in air.

First two modal shapes for this system in the 2nd case are shown in Figure 29.

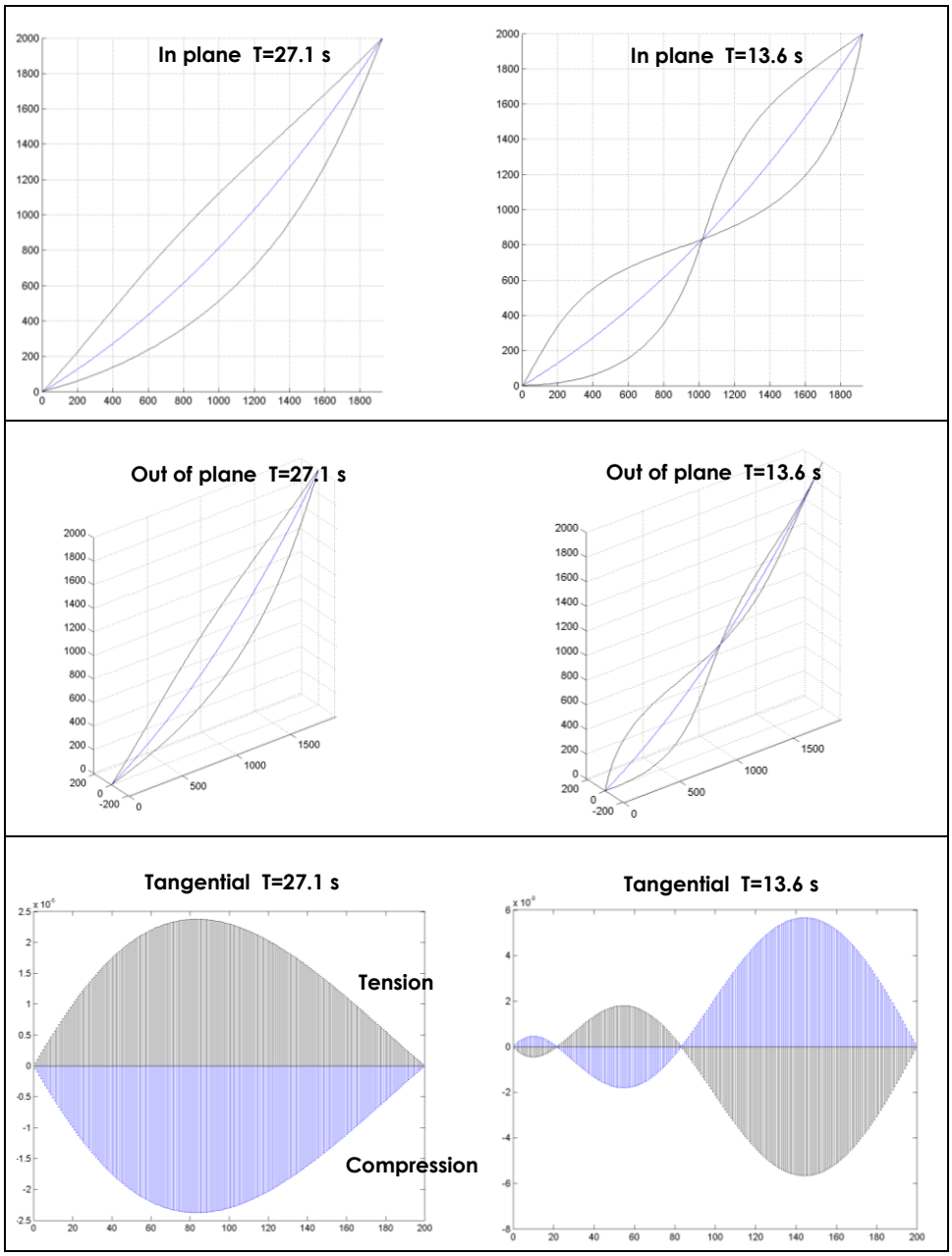

Figure 29 First two modal shapes for the Steel Rope System with submerged weight.

3rd and 4th modal shapes for this system in the 2nd case are shown in Figure 30.

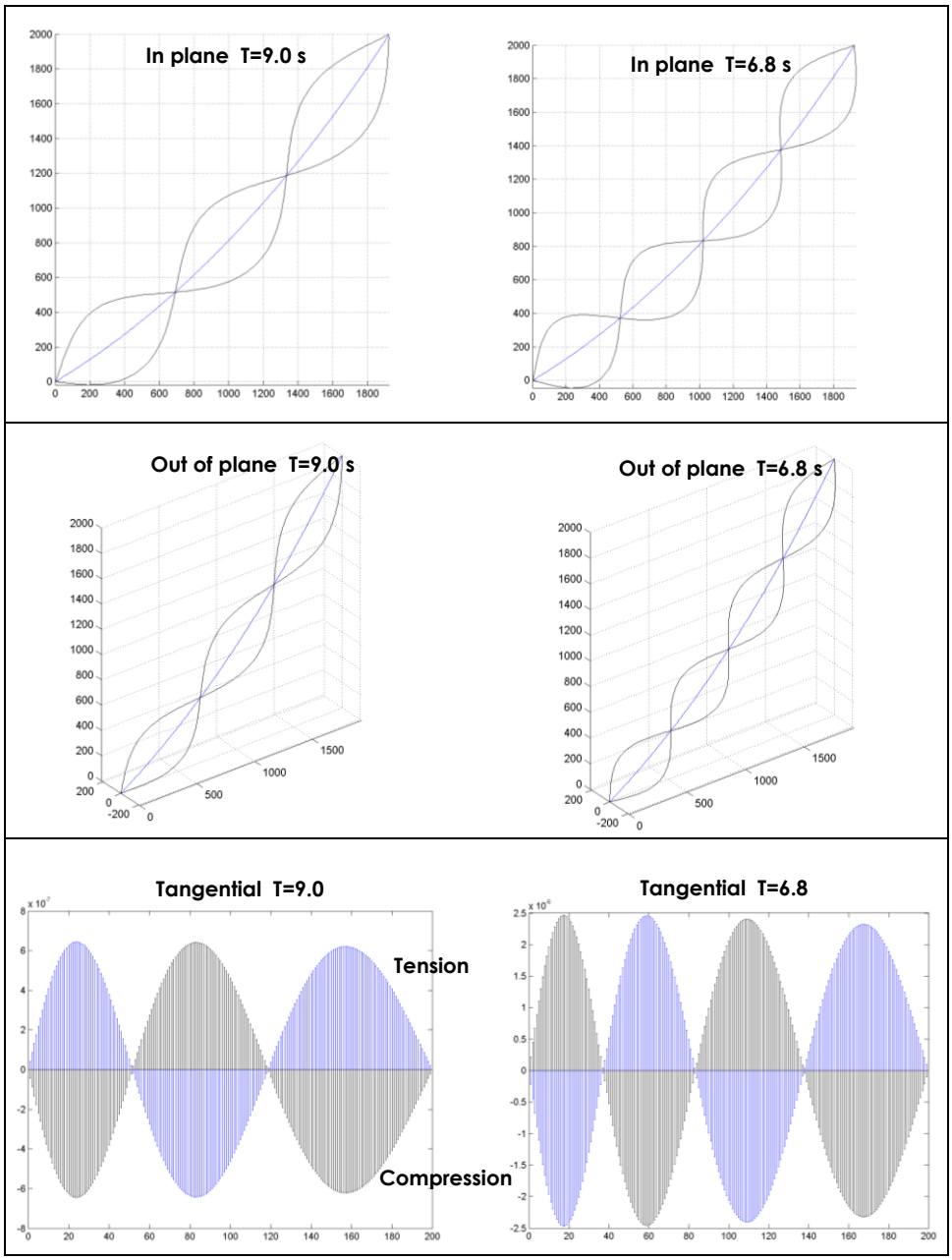

Figure 30 Third and fourth modal shapes for the Steel Rope System with submerged weight.

The first two modal shapes for the 3rd case are shown in Figure 31.

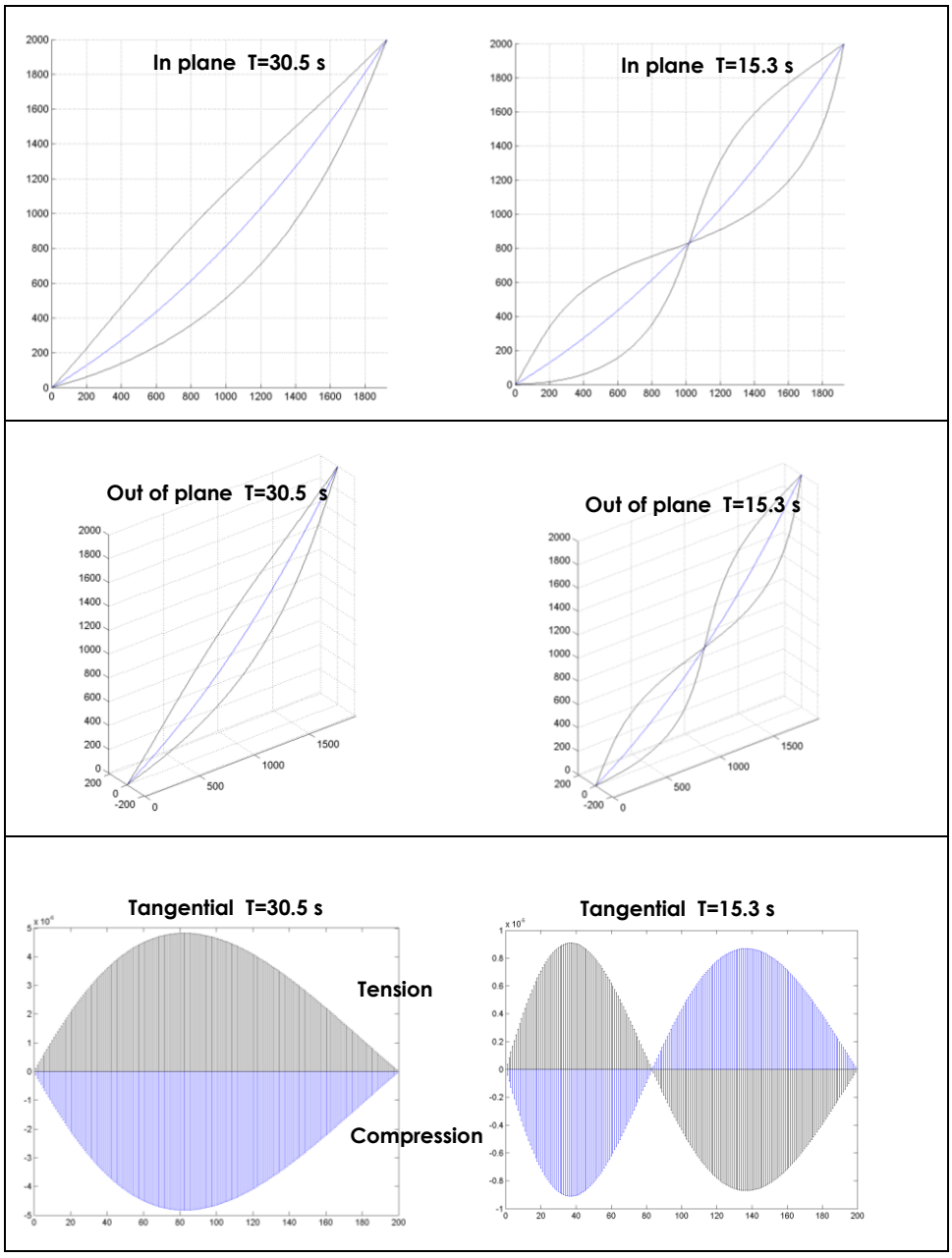

Figure 31 First two modal shapes for the Steel Rope System in water with added mass.

3rd and 4th modal shapes for this system in the 3rd case are shown in Figure 32.

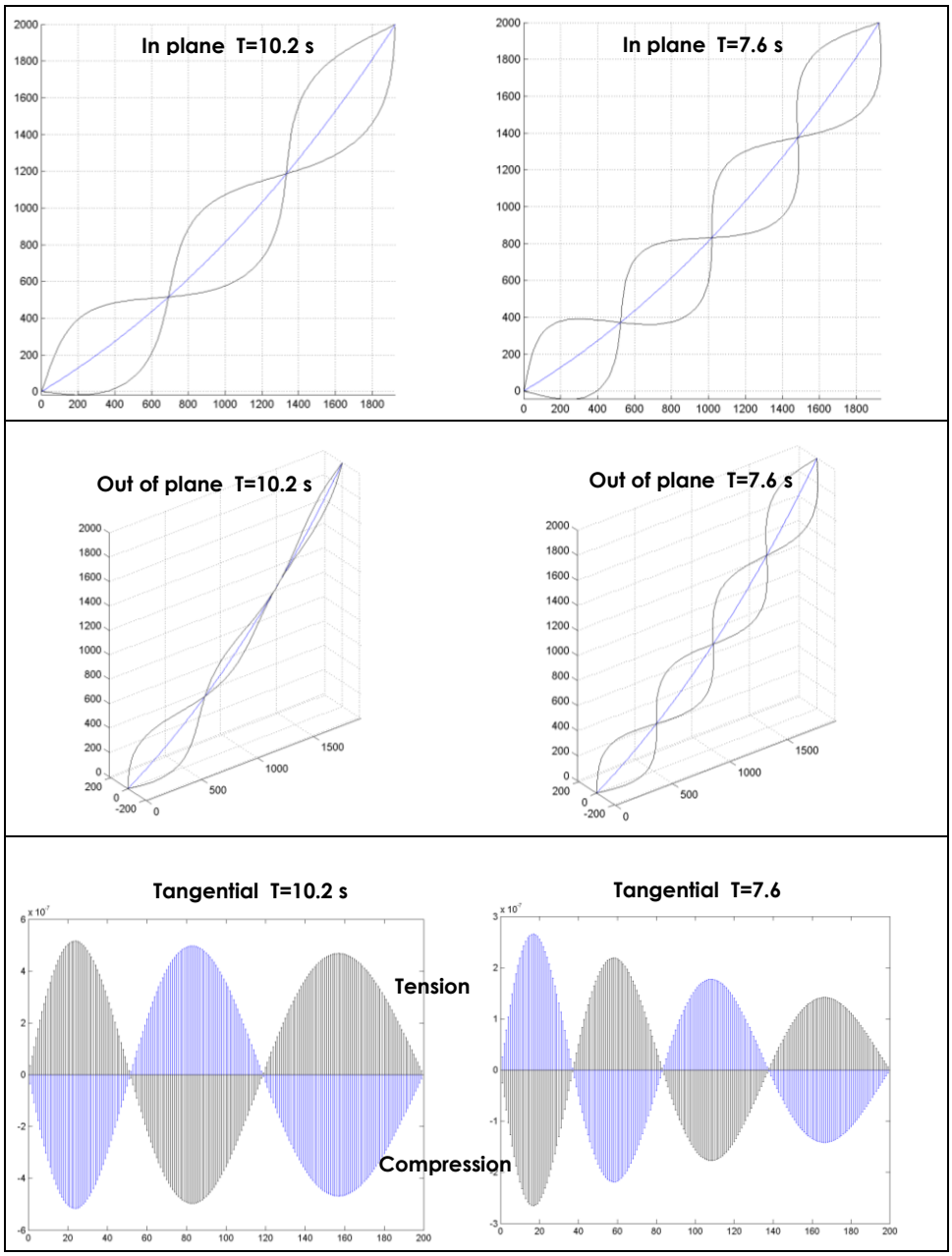

Figure 32 Third and fourth modal shapes for the Steel Rope System in water with added mass.

The first two modal shapes for the 4th case are shown in Figure 33.

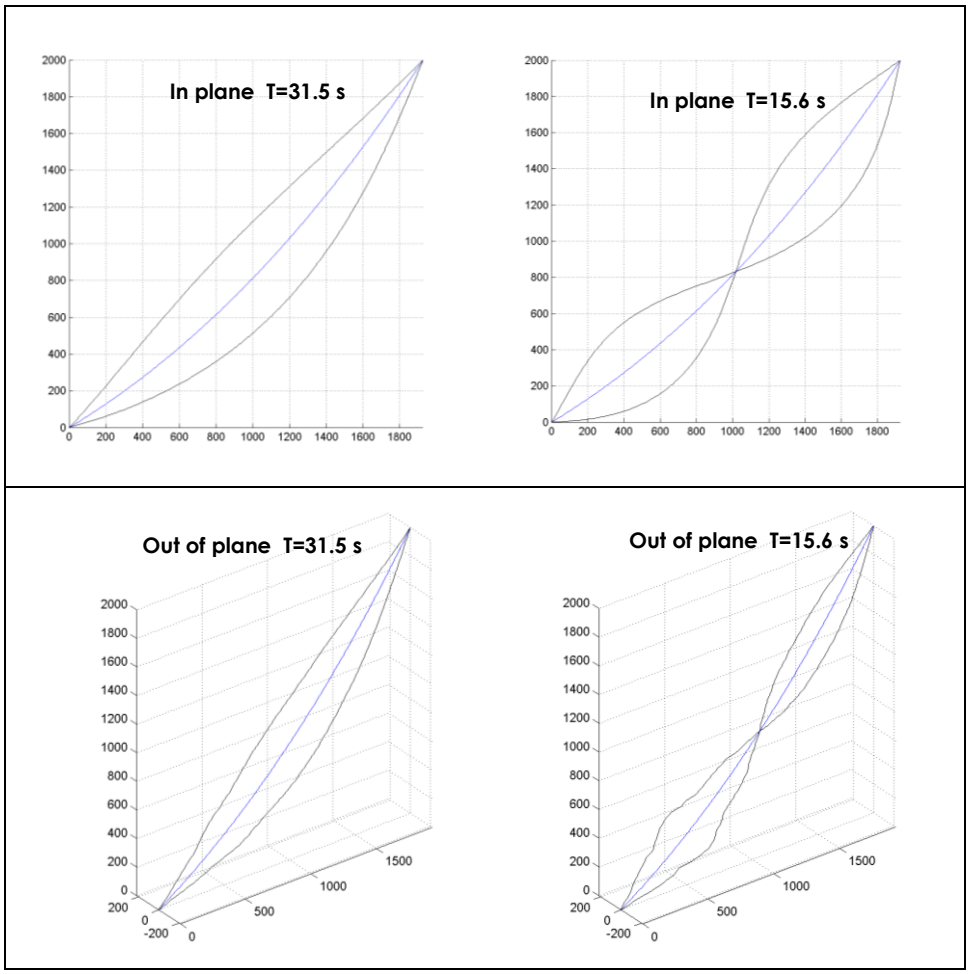

Figure 33 First two modal shapes for the Steel Rope System considering submerged weight, added mass, and damping.

The above shapes correspond to the 0.1 sag level of damping and are scaled.

3rd and 4th modal shapes for this system in the 4th case are shown in Figure 34.

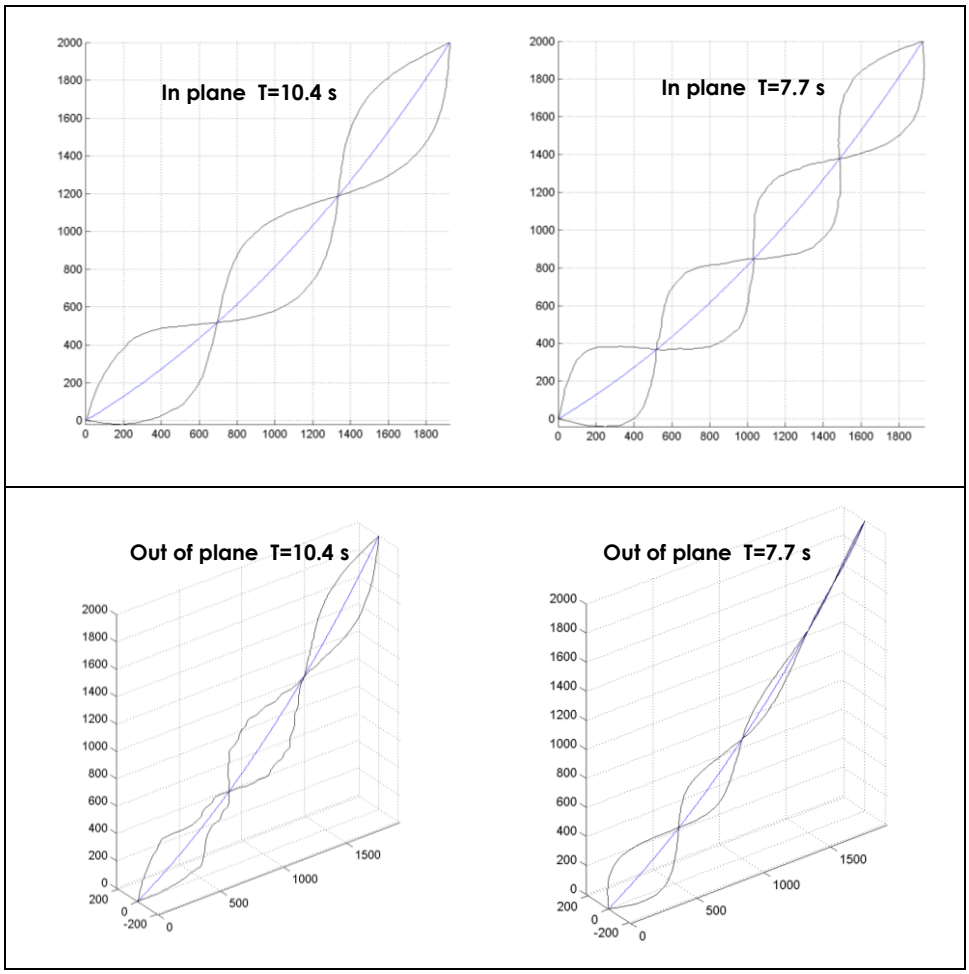

Figure 34 Third and fourth modal shapes for the Steel Rope System, considering submerged weight, added mass, and damping.

For this last surrounding case the tangential mode was not performed because no tangential components where included in the damping matrix. The above shapes correspond to the 0.1 sag level of damping, and are scaled

In all the surrounding cases, except for the damping case, the in-plane modes were very uniform in the distribution of their shape along the length of cable.

For the out-of-plane modal shapes there is not uniformity in the modal shapes for all the cases, especially for the second and third mode, where the modal shapes had more amplitude in the lowest part of the cable. This behavior was observed even in the case where the cable is in air.

For the tangential modes, different from the first mode, the modal shapes are not always regular in their shape along the length of the cable. In some cases there is not a correspondence between the number of the modal shape and the number of times the shape crosses the longitudinal axis of the cable (i.e the number of zero displacement node points in the modal shape).

In all the cases the first mode showed always uniformity in its modal shape regardless of the surrounding environment of the mooring line.

5.2.2 Damped natural periods for the Steel Rope System

The first four natural periods for the Steel Rope System in water without damping and with damping produced by several values of sag as the normalization parameter of modal shapes are presented in Figure 35. There the increment of damping due to the increment of the value for the normalization of the modal shape can be seen. In all cases the fundamental period was over 20 seconds, approximately the corresponding maximum period of waves produced by a storm (Tedesco et al. 1999).

The effect of modeling damping impacted significantly the natural periods of the mooring line if a large value of normalization of the modal shape is adopted.

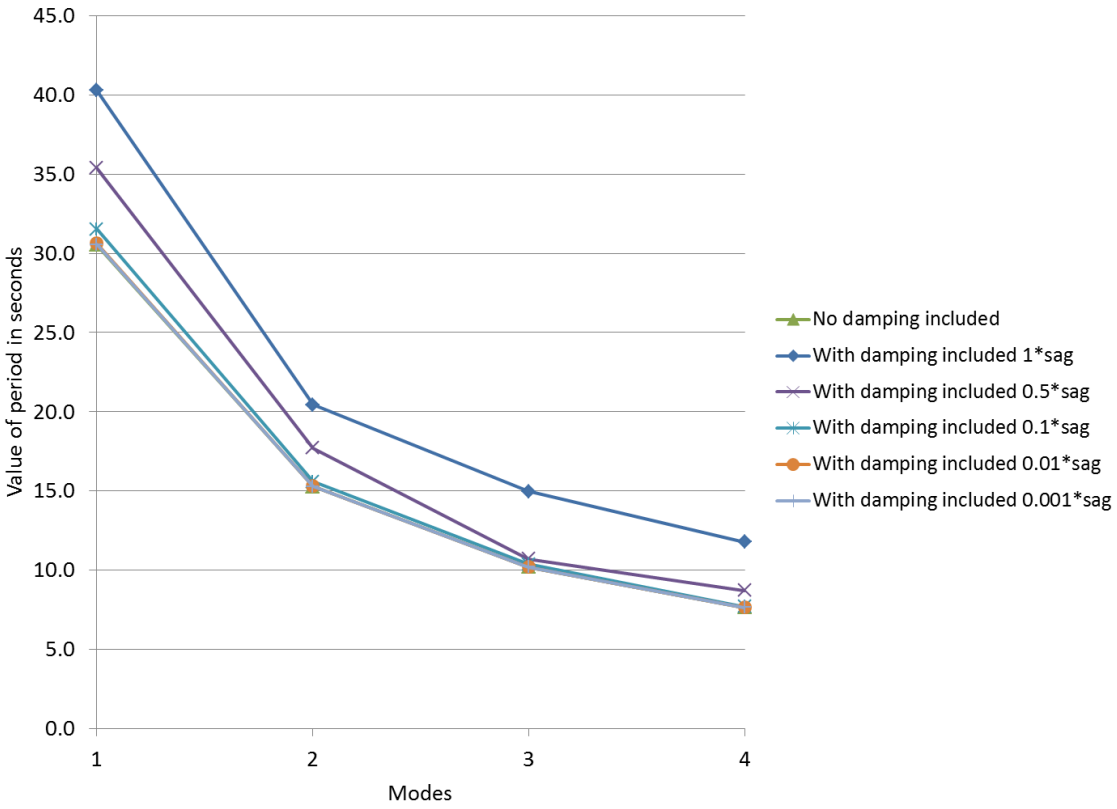

Figure 35 First four damped natural periods for the Steel Rope System.

5.2.3 Behavior of the Steel System

The first eight periods of free vibration for this system are shown in Table 13 for the first three cases which do not involve damping.

Table 13 First eight natural periods for Steel System.

Case	First eight periods (s)							
	1	2	3	4	5	6	7	8
1) Air	32.1	16.7	11.8	9.0	7.1	5.8	4.9	4.4
2) Weight submerged	31.7	16.6	11.8	9.0	7.1	5.8	4.9	4.3
3) Weight submerged, added mass	35.6	18.5	13.1	10.0	7.9	6.5	5.5	4.8

Modal shapes normalized with respect to different values of sag of the cable, in the static condition, produced the natural periods and the damping ratio (ζ) shown in Table 14 for the Steel System.

Table 14 First four damped natural periods for different normalized motion amplitudes in Steel System.

Case	First four periods (s) and damping ratio ζ (%)							
	1	ζ	2	ζ	3	ζ	4	ζ
1 Sag	39.5	43.3	31.5	80.9	28.0	88.4	23.1	90.1
0.5 Sag	36.3	19.5	22.2	55.3	17.7	67.2	13.5	67.2
0.1 Sag	35.7	7.5	18.7	14.6	13.3	17.3	10.2	19.7
0.01 Sag	35.6	0.0	18.5	0.0	13.1	0.0	10.0	0.0
0.001 Sag	35.6	0.0	18.5	0.0	13.1	0.0	10.0	0.0

First two modal shapes for this system in air are shown in Figure 36.

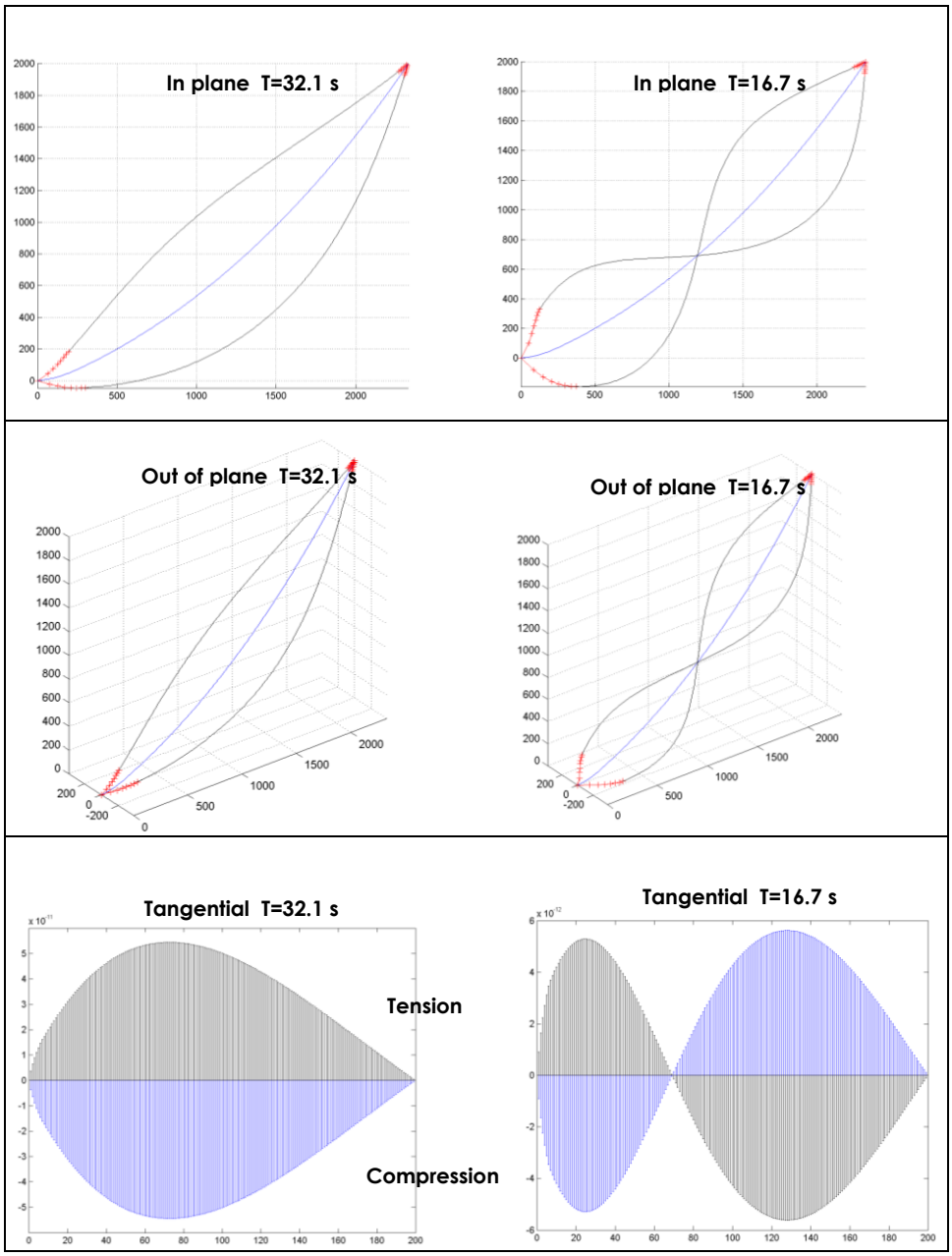

Figure 36 First two modal shapes for the Steel System in air.

3rd and 4th modal shapes for this system in air are shown in Figure 37.

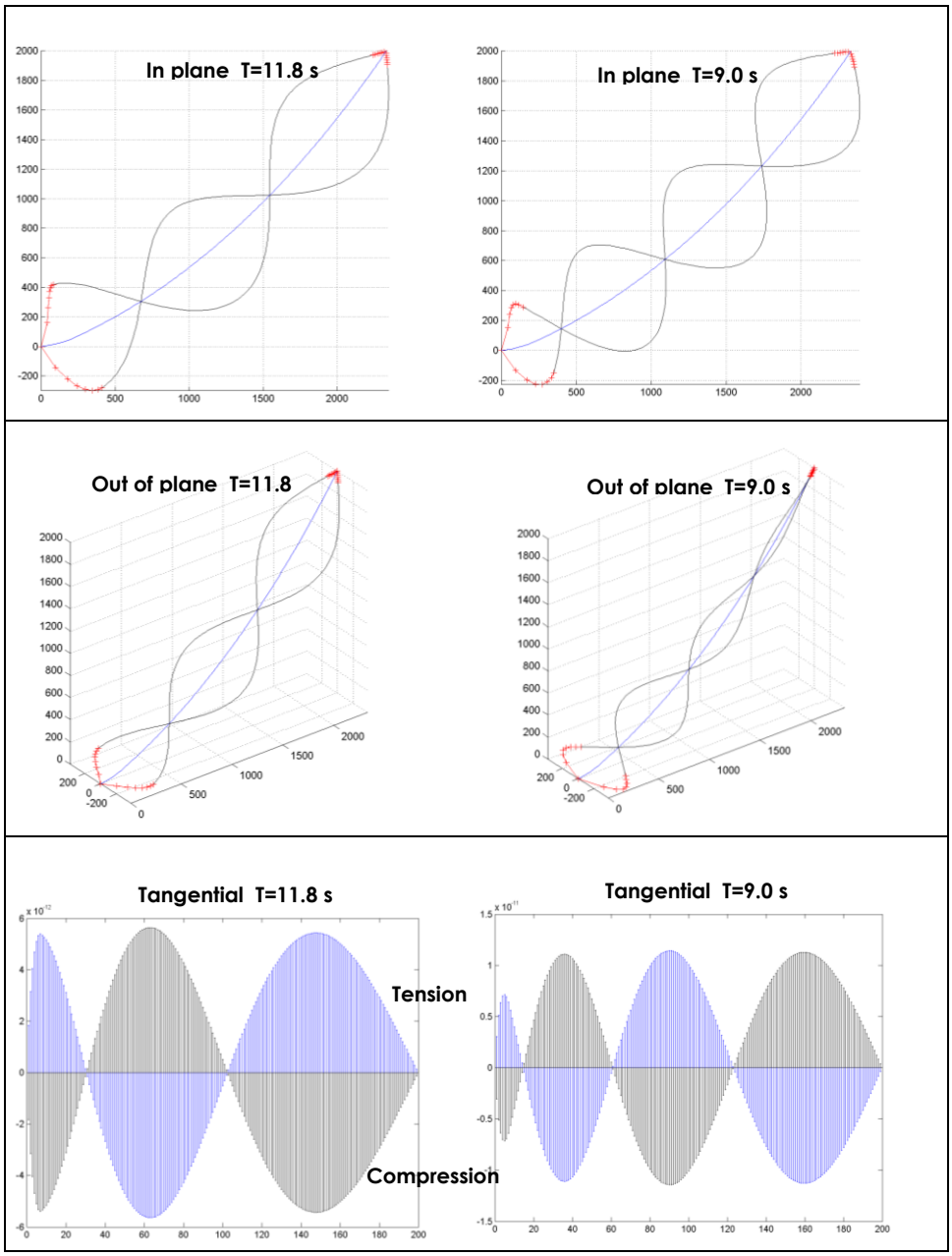

Figure 37 Third and fourth modal shapes for the Steel System in air.

First two modal shapes for this system in the 2nd case are shown in Figure 38.

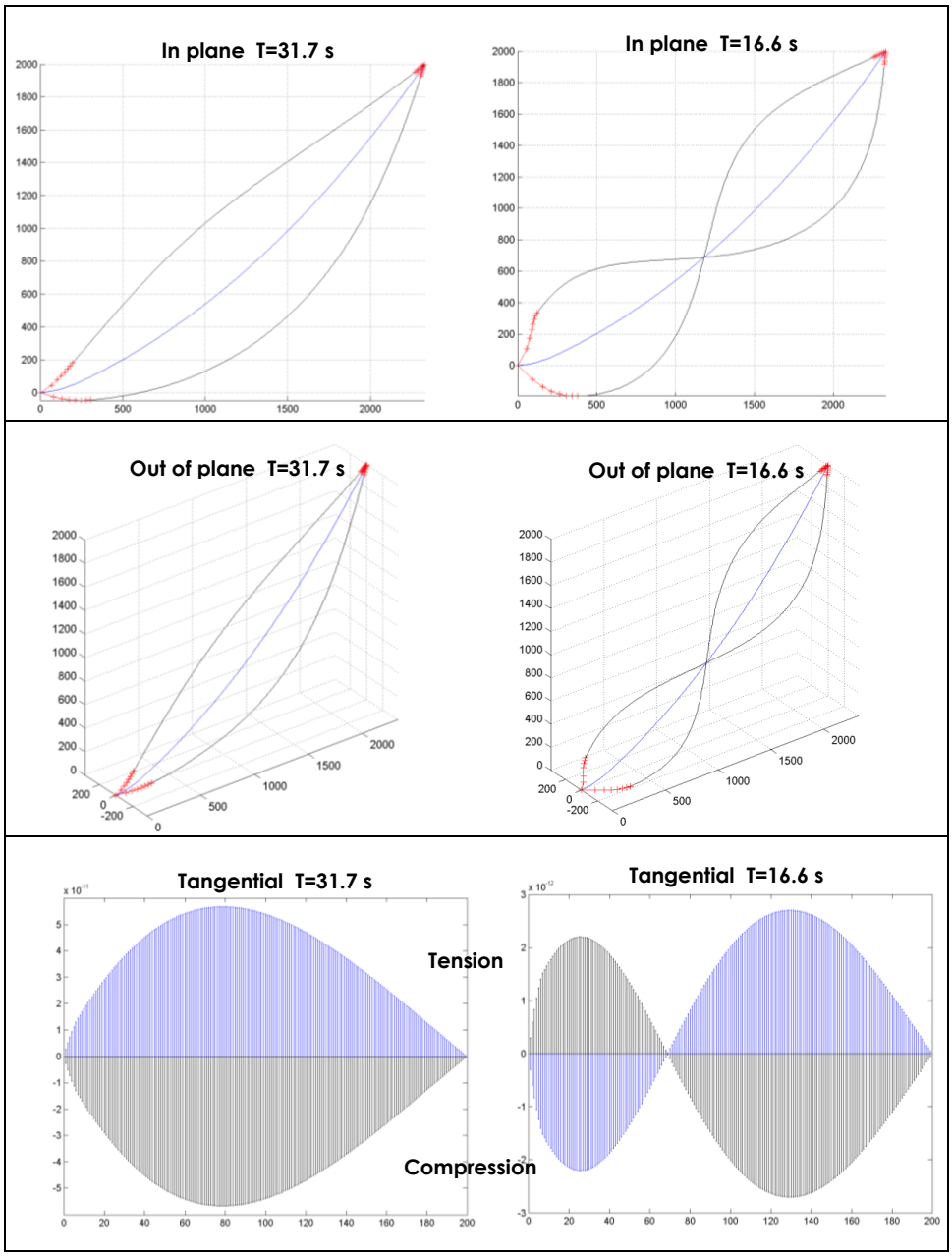

Figure 38 First two modal shapes for the Steel System with submerged weight.

3rd and 4th modal shapes for this system in the 2nd case are shown in Figure 39.

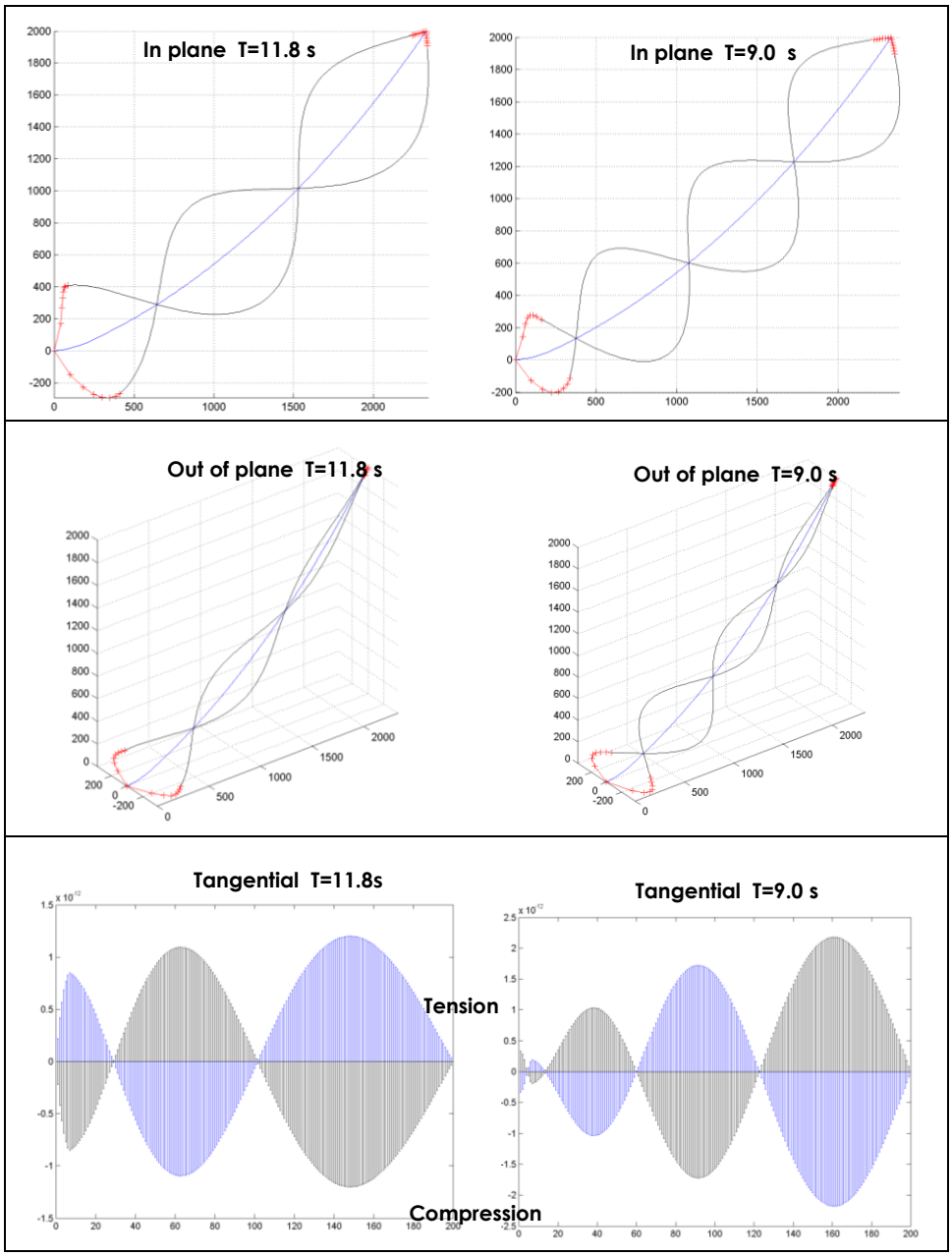

Figure 39 Third and fourth modal shapes for the Steel System with submerged weight.

The first two modal shapes for the 3rd case are shown in Figure 40.

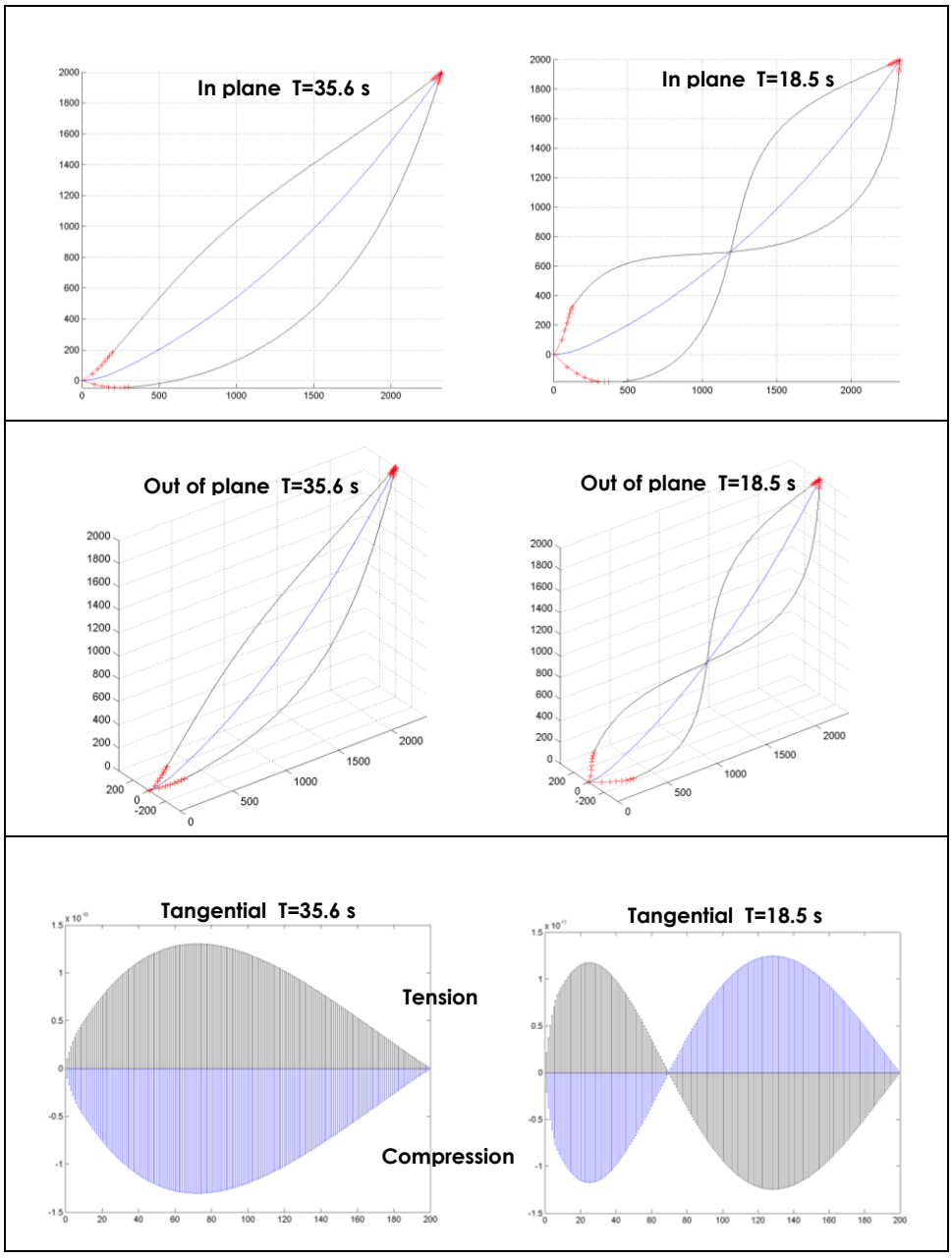

Figure 40 First two modal shapes for the Steel System in water with added mass.

3rd and 4th modal shapes for this system in the 3rd case are shown in Figure 41.

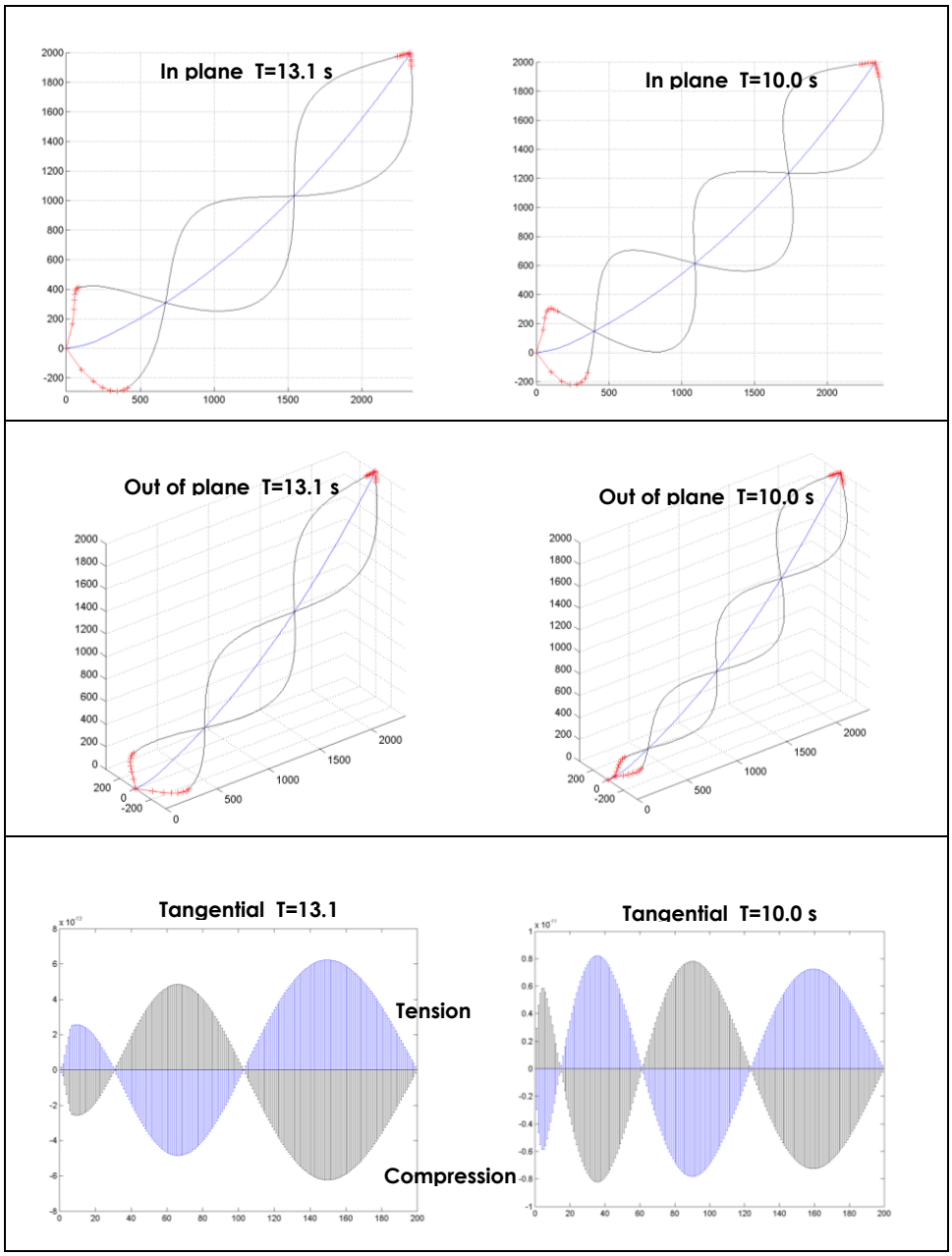

Figure 41 Third and fourth modal shapes for the Steel System in water with added mass.

The first two modal shapes for the 4th case are shown in Figure 42.

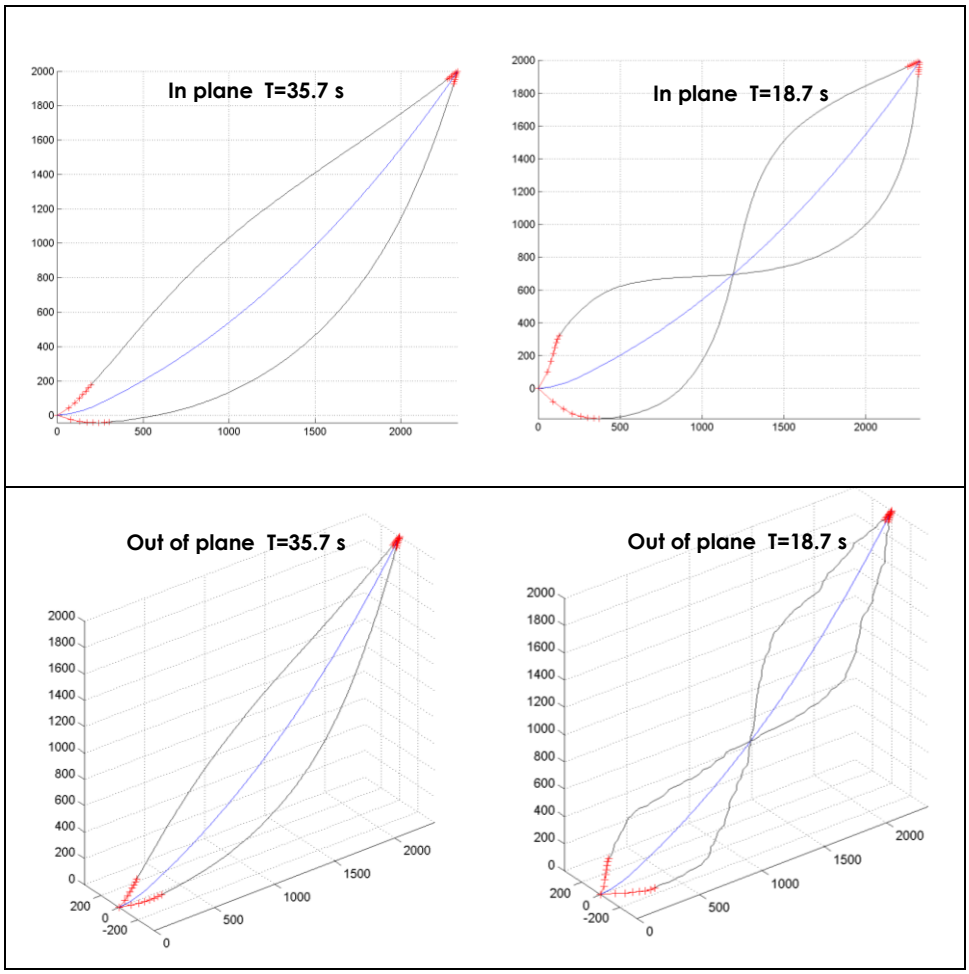

Figure 42 First two modal shapes for the Steel System considering submerged weight, added mass, and damping.

The above shapes correspond to the 0.1 sag level of damping and are scaled

3rd and 4th modal shapes for this system in the 4th case are shown in Figure 43.

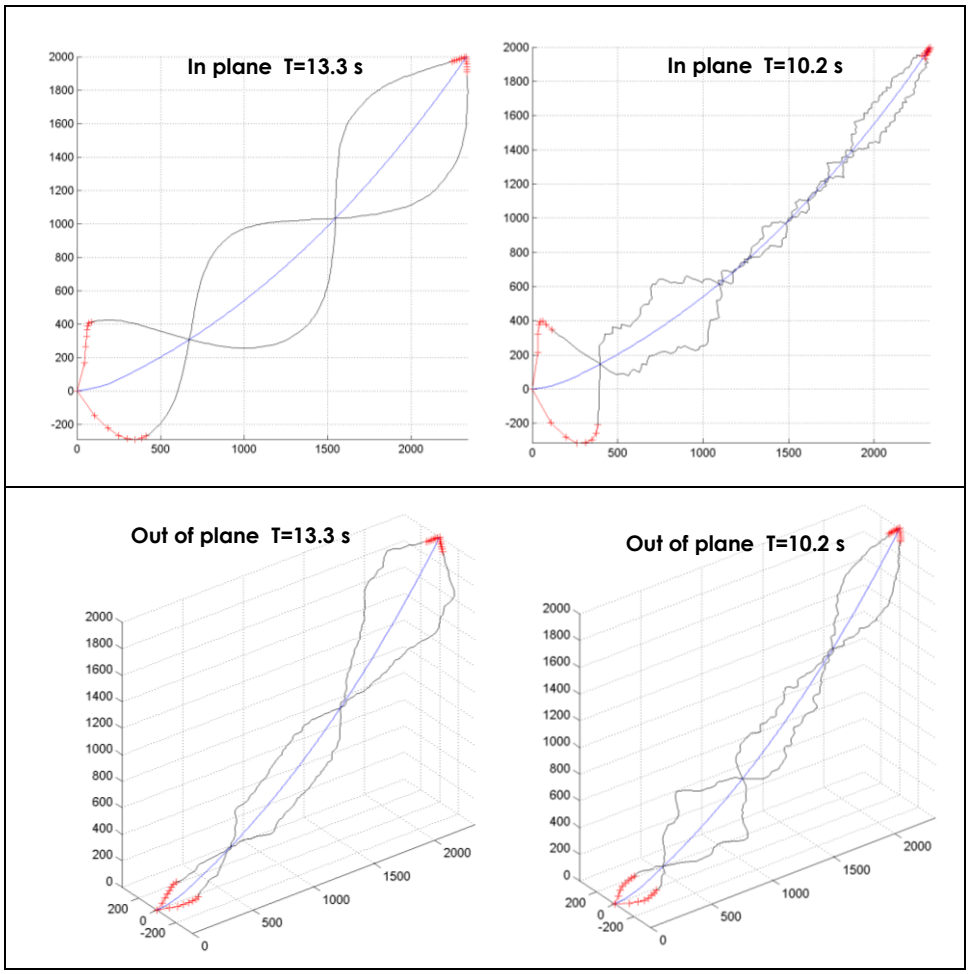

Figure 43 Third and fourth modal shapes for the Steel System, considering submerged weight, added mass, and damping.

The above shapes correspond to the 0.1 sag level of damping and are scaled.

Similarly as in the Steel Rope System, for this Steel System, the last surrounding case referring to the tangential mode was not developed because no tangential components where included in the damping matrix.

Regarding the behavior of the Steel System, in all the surrounding cases, except for the damping case, the in-plane modes were very uniform in the distribution of their shape along the length of cable. This behavior was found in the Steel Rope System as well.

For the out-of-plane modal shapes there is uniformity in the modal shapes for the first and second modes in all the cases, except for those with damping. The modal shapes had more amplitude in the lowest part of the cable, except for the 3rd case, where the submerged weight, added mass and no damping were included, where the higher amplitude was found in the upper part of the cable.

For the tangential modal shapes there is a regularity in each mode, regarding the distribution of the shape along the length of the cable, except for the second case, where the mooring line is modeled with just submerged weight, but no added mass or damping. There is in these tangential modal shapes a correspondence between them and the modal shapes of the in-plane and out-of-plane components for all the cases except for the last case mentioned.

In all the cases the first mode showed always uniformity in its modal shape regardless of the surrounding environment of the mooring line, similarly as the previous Steel Rope System assessed.

There is not a noticeable change in the modal shapes for the in-plane, and out-of-plane components at the point where the chain and steel rope are joined. However a sharp change in slope was found in the tangential mode shapes at the point where the bottom chain is joined to the rope.

5.2.4 Damped natural periods for the Steel System

Different values of damped natural periods were found in the Steel System by following the formulation proposed in chapter four. These natural periods depend on the amount of sag used in the normalization to form the damping matrix. The periods for the same modes for the case where the mooring line is modeled with submerged weight, added mas, and damping are shown in Figure 44.

The increment of damping due to the increment of the value of sag for the normalization of the modal shape can be seen. As in the Steel Rope System the fundamental period is observed to be longer than 20 seconds.

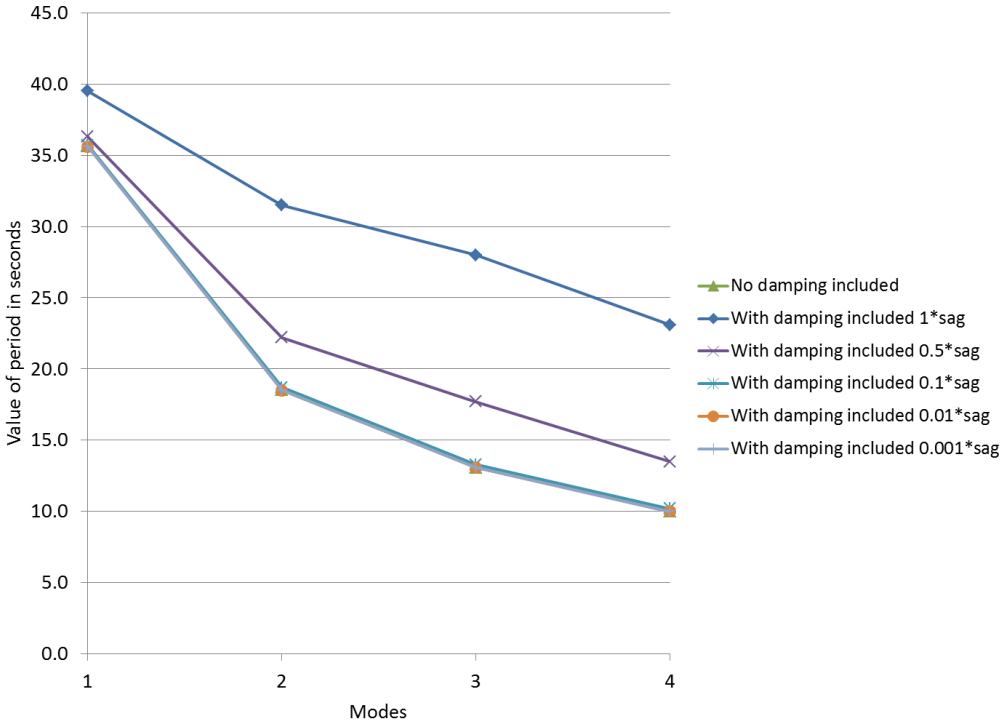

Figure 44 First four damped natural periods for the Steel System.

5.2.5 Behavior of the Polyester System

The first eight natural periods obtained for the Polyester System in each environment are presented in Table 15 for the first three cases which do not involve damping.

Table 15 First eight natural periods for Polyester System.

Case	First eight periods (s)							
	1	2	3	4	5	6	7	8
1) Air	19.9	11.0	7.9	5.7	4.5	3.7	3.3	3.0
2) Weight submerged	12.8	8.5	5.0	3.7	3.4	2.9	2.3	2.1
3) Weight submerged, added mass	22.3	12.3	8.8	6.4	5.0	4.2	3.7	3.3

The natural periods and the damping ratio (ζ) produced by modal shapes, normalized with respect to different values of sag of the cable, are shown in Table 16 for the Polyester System.

Table 16 First four damped natural periods for different values of normalized motion amplitude in Polyester System.

Case	First four periods (s) and damping ratio ζ (%)							
	1	ζ	2	ζ	3	ζ	4	ζ
1 Sag	22.4	9.4	12.3	0.0	9.3	32.3	7.8	57.2
0.5 Sag	22.3	0.0	12.3	0.0	9.0	21.0	7.2	45.8
0.1 Sag	22.3	0.0	12.3	0.0	8.8	0.0	6.5	17.5
0.01 Sag	22.3	0.0	12.3	0.0	8.8	0.0	6.4	0.0
0.001 Sag	22.3	0.0	12.3	0.0	8.8	0.0	6.4	0.0

The first two modal shapes for this system in air are shown in Figure 45.

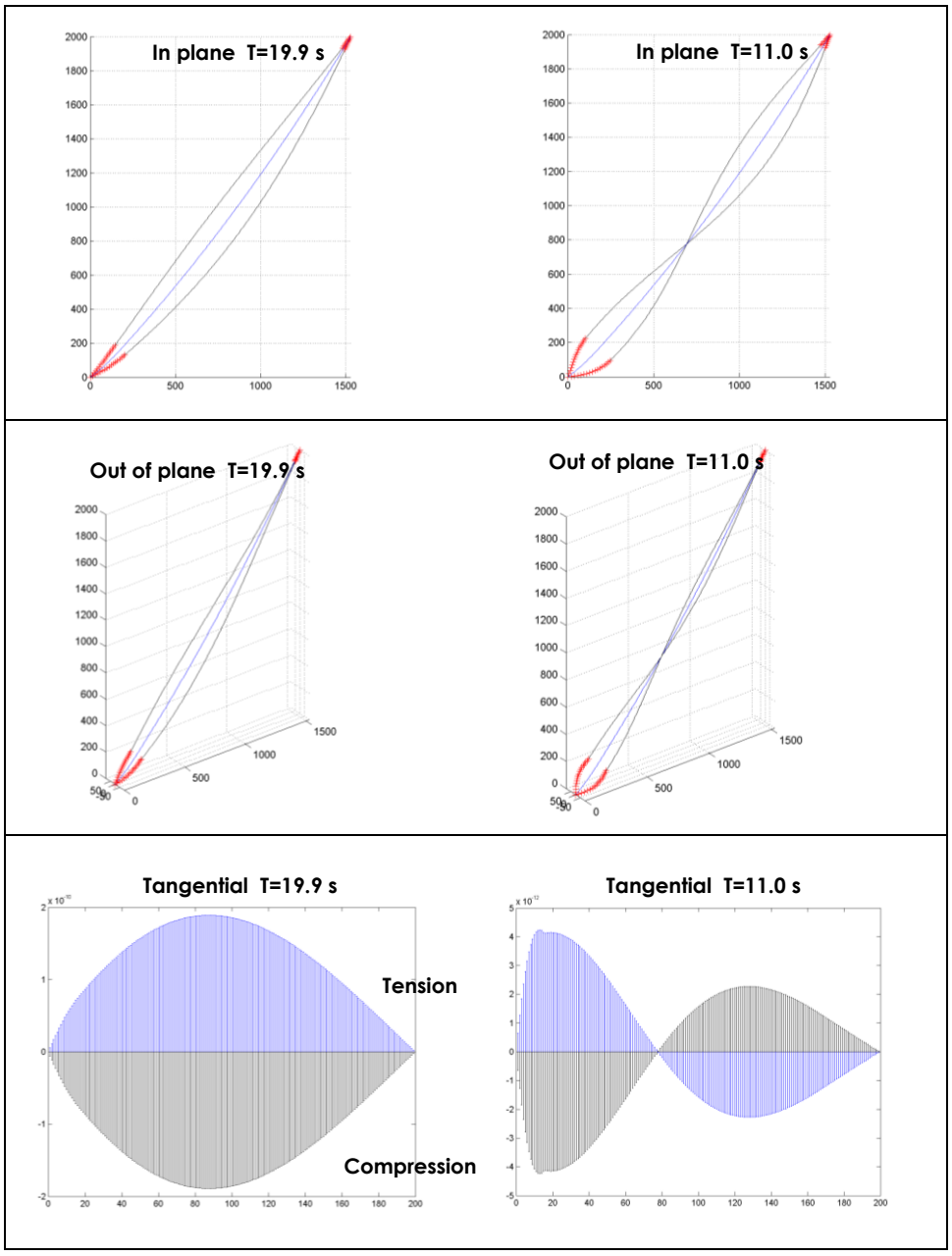

Figure 45 First two modal shapes for the Polyester System in air.

The 3rd and 4th modal shapes for this system in air are shown in Figure 46.

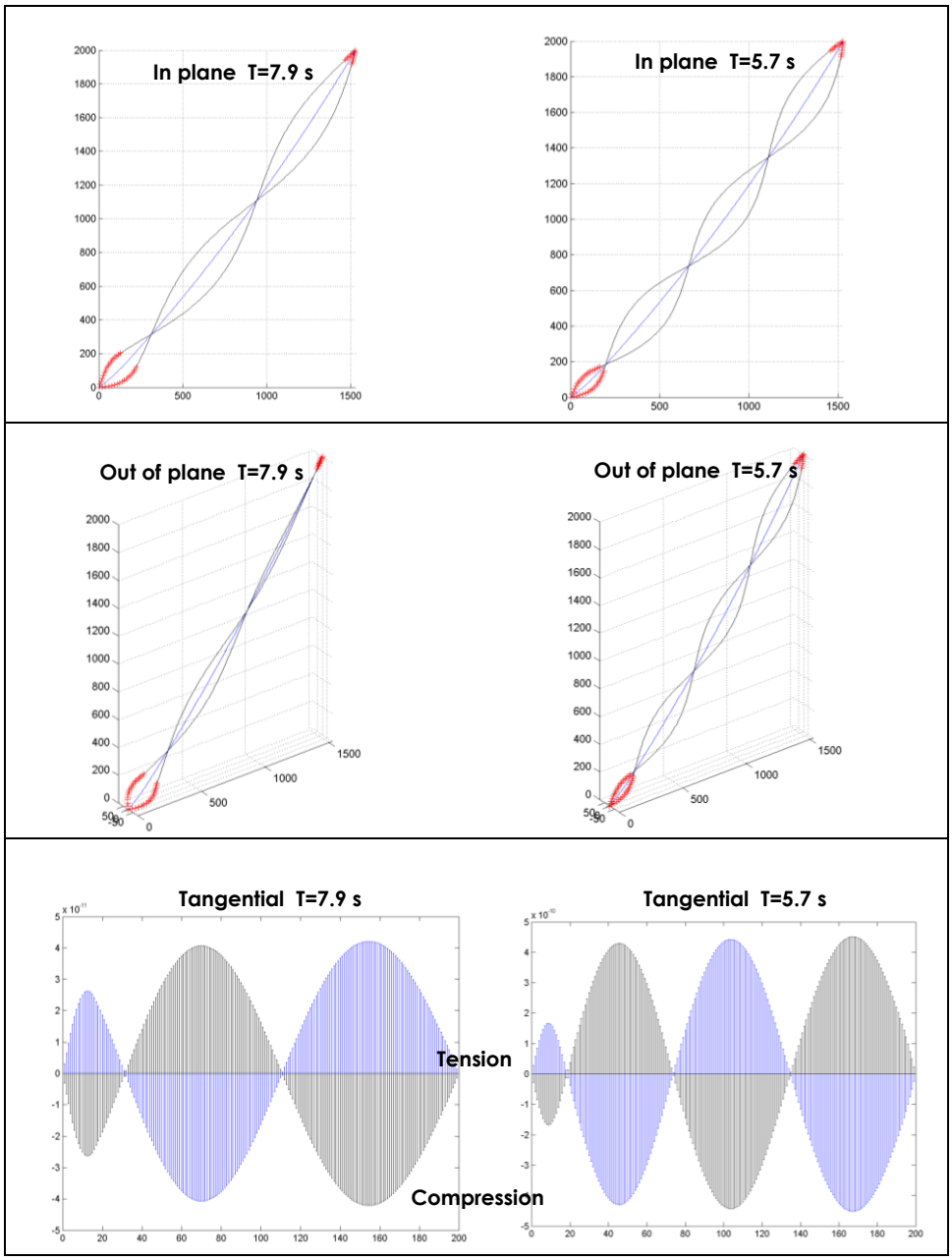

Figure 46 Third and fourth modal shapes for the Polyester System in air.

First two modal shapes for this system in the 2nd case are shown in Figure 47.

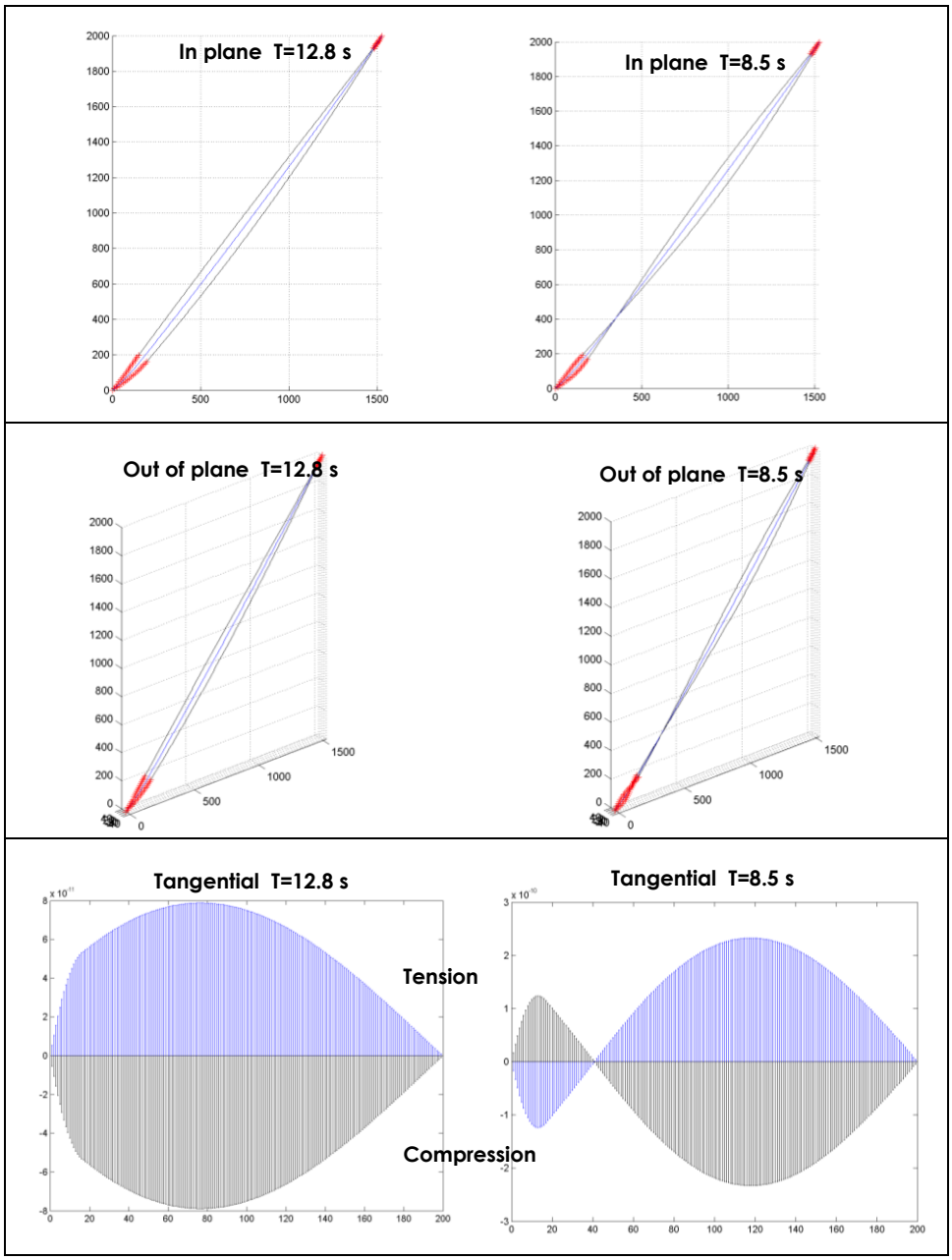

Figure 47 First two modal shapes for the Polyester System with submerged weight.

3rd and 4th modal shapes for this system in the 2nd case are shown in Figure 48.

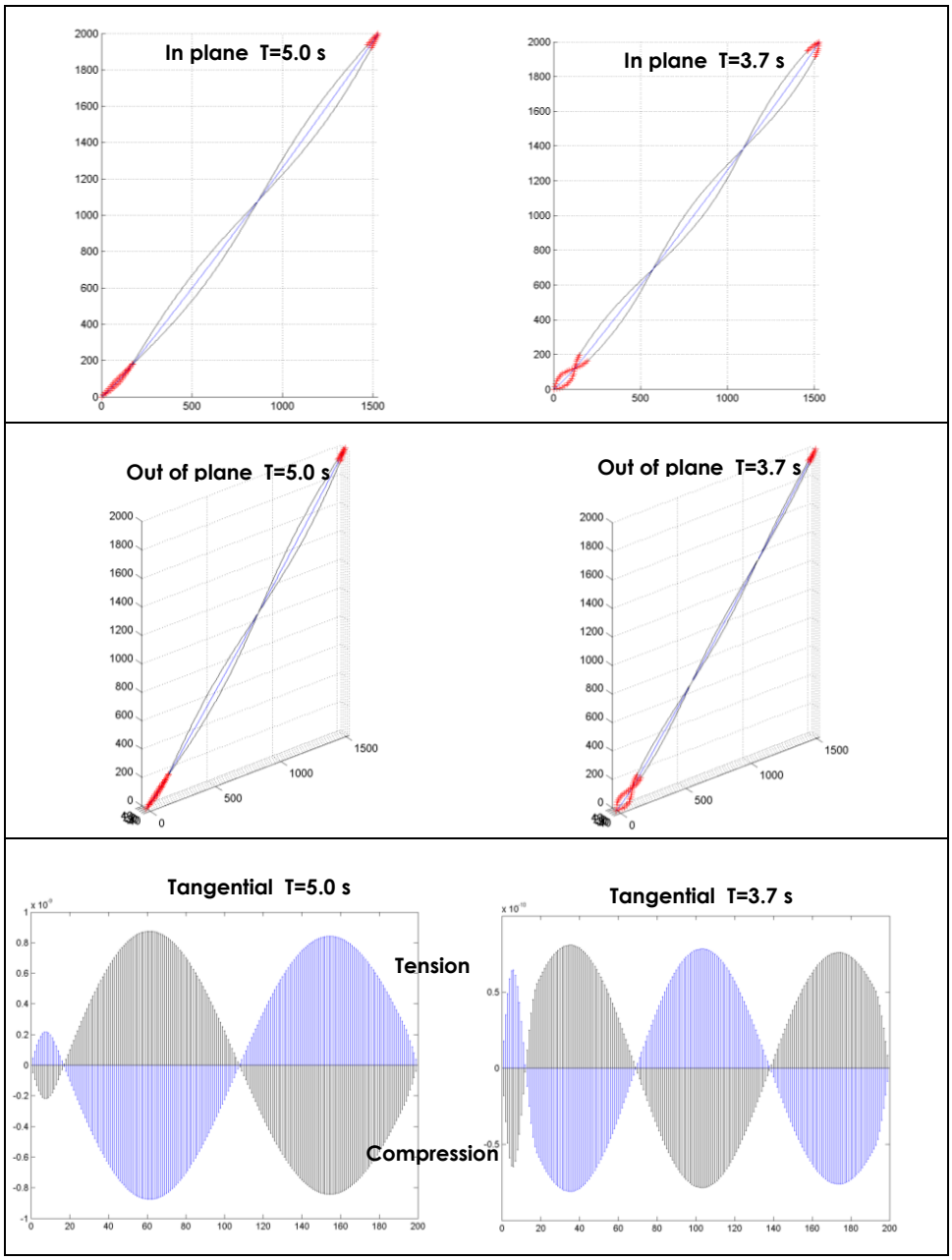

Figure 48 Third and fourth modal shapes for the Polyester System with submerged weight.

The first two modal shapes for the 3rd case are shown in Figure 49.

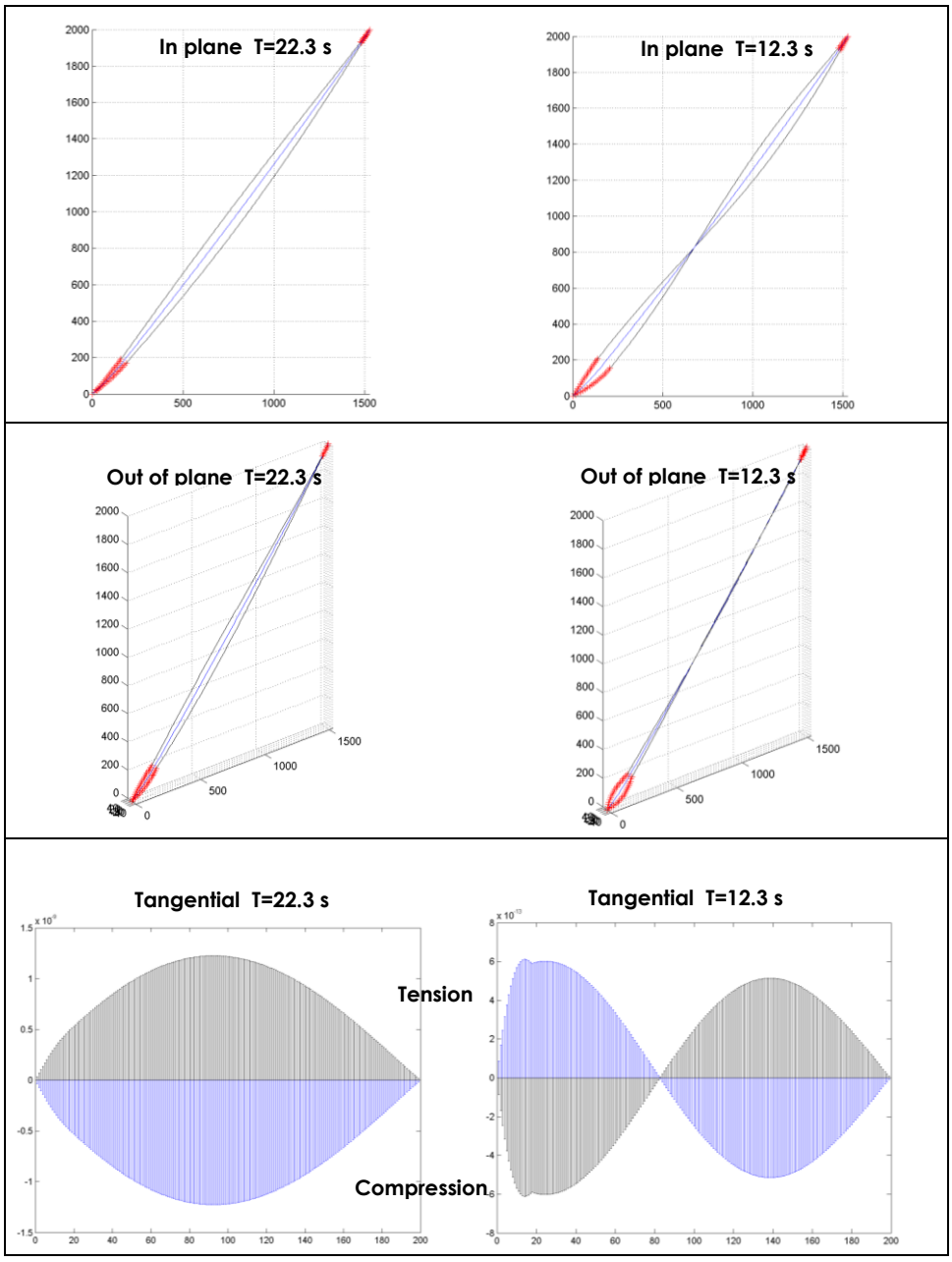

Figure 49 First two modal shapes for the Polyester System in water with added mass.

3rd and 4th modal shapes for this system, in the 3rd case, are shown in Figure 50.

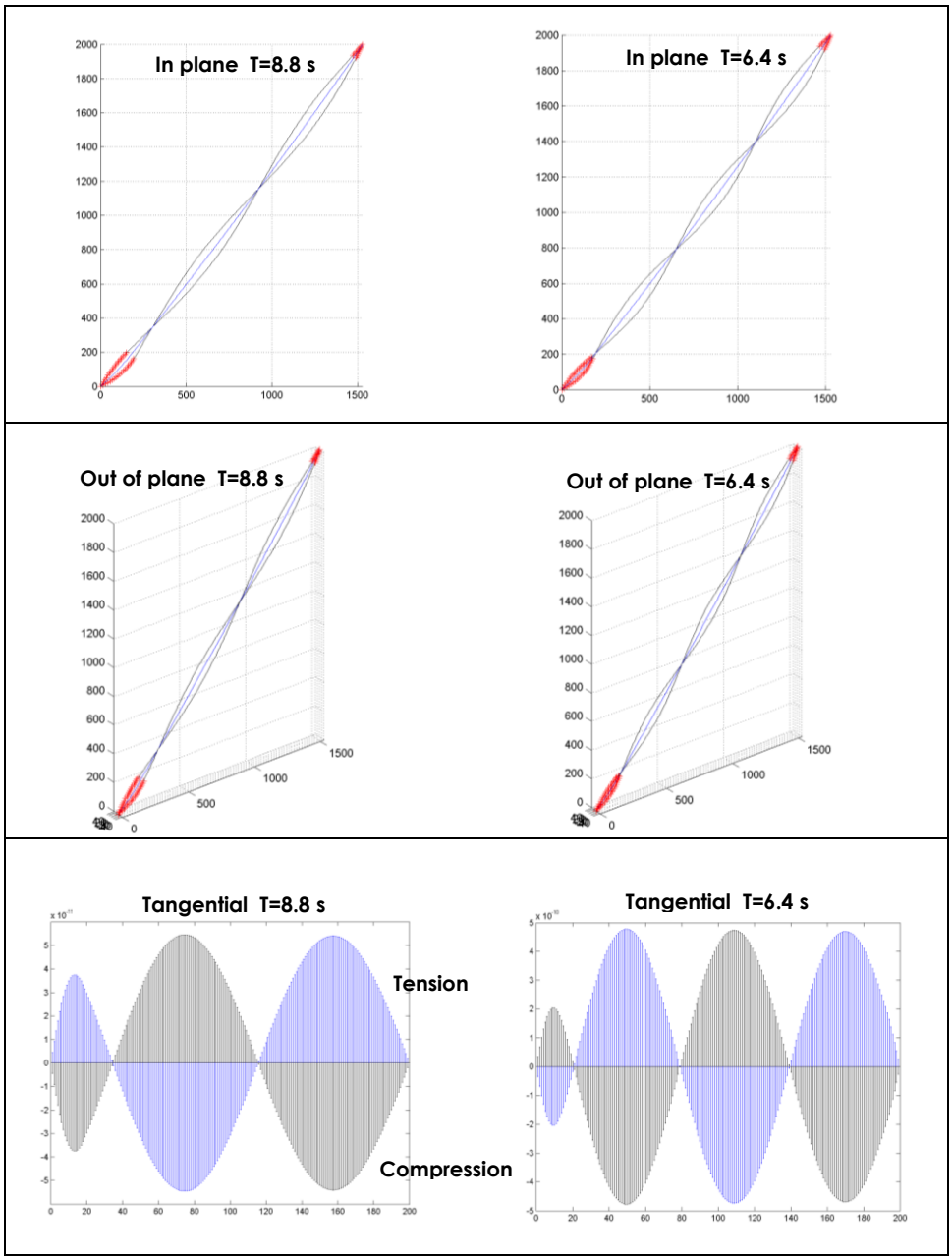

Figure 50 Third and fourth modal shapes for the Polyester System in water with added mass.

The first two modal shapes for the 4th case are shown in Figure 51.

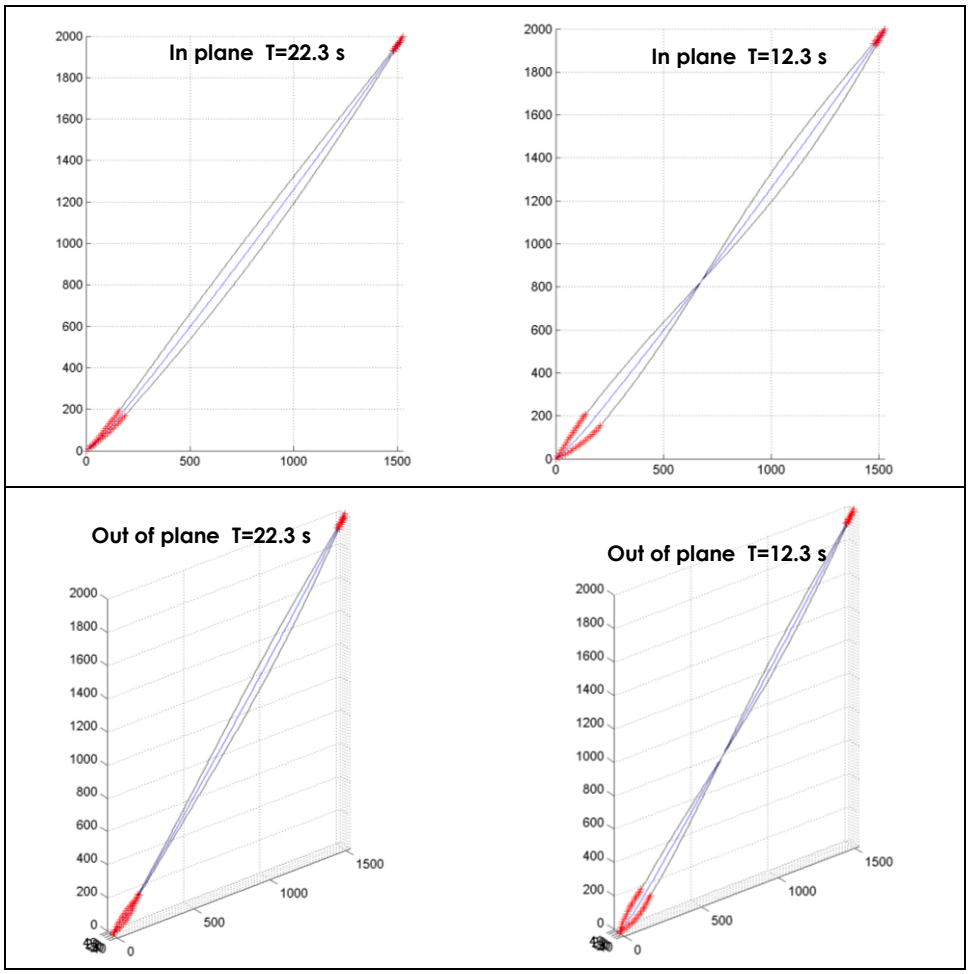

Figure 51 First two modal shapes for the Polyester System considering submerged weight, added mass, and damping.

3rd and 4th modal shapes for this system, in the 4th case, are shown in Figure 52.

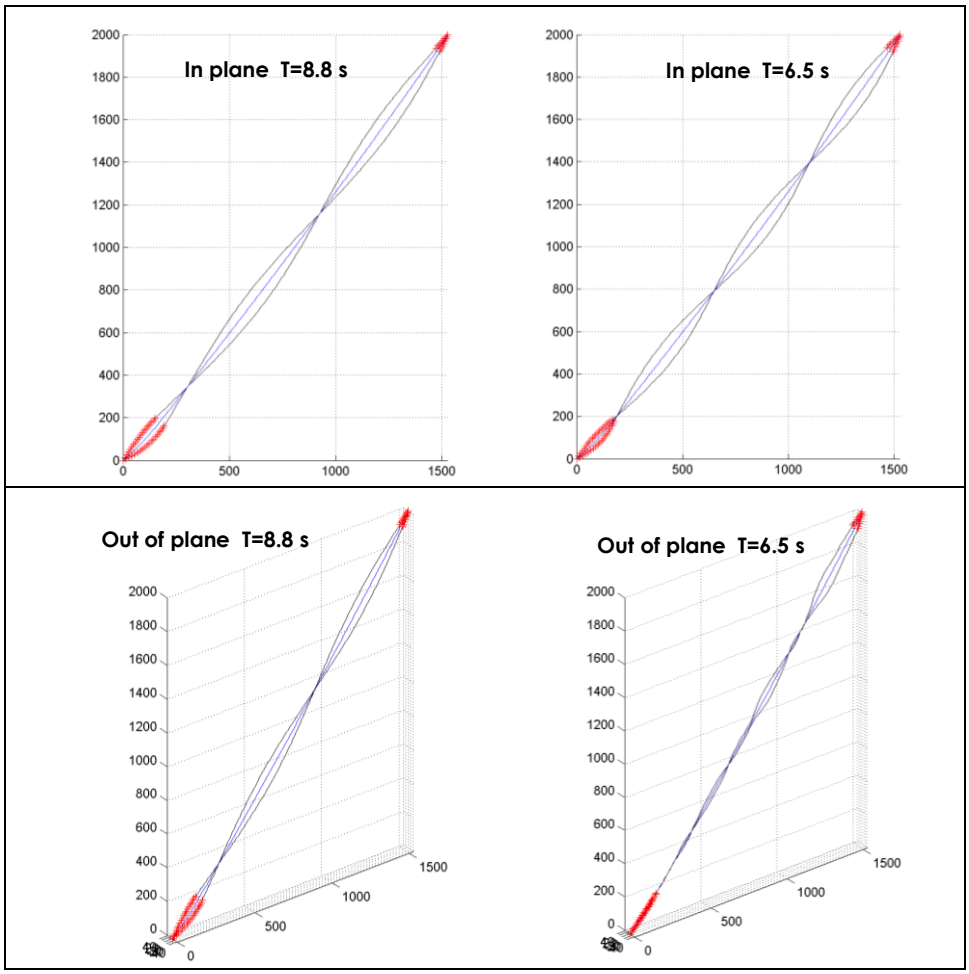

Figure 52 Third and fourth modal shapes for the Polyester System, considering submerged weight, added mass, and damping.

In this system too, the last surrounding case referring to the tangential mode was not developed because no tangential components where included in the damping matrix.

Finally, in the behavior of the Polyester System, the uniformity for the in-plane modes in the distribution of their shape along the length of cable was not found.

Regarding the out-of-plane modal shapes for this system there was not uniformity found, as in some patterns in the Steel System.

For the tangential modal shapes, there is regularity in each mode, related with the number of crossing times of the longitudinal axis. A better correspondence than in the previous systems between the tangential modal shapes and those associated with the out-of-plane component was found.

In all the cases the first mode showed uniformity in the first modal shape, except for the out-of-plane cases with no damping included, where the amplitude is slightly bigger in the lower part of the cable.

There is little change in the modal shapes for the in-plane and out-of-plane shapes at the point where the chain and polyester rope are joined. However, a distinct change in slope is evident in the tangential mode shapes at the point where the lower chain is joined to the polyester rope.

The relatively small magnitude in the sag is noticeable in the modal shapes compared to the modal shapes of the Steel System and the Steel Rope System.

5.2.6 Damped natural periods for the Polyester System

The first four natural periods for the Polyester System in water with and without damping are shown in Figure 53, considering different values of sag normalization to define the damping level.

There is not a contrast between the natural periods including damping and without damping for this example. In all the cases the fundamental period was near to 20 seconds. The natural periods for the higher modes are far from the first natural period.

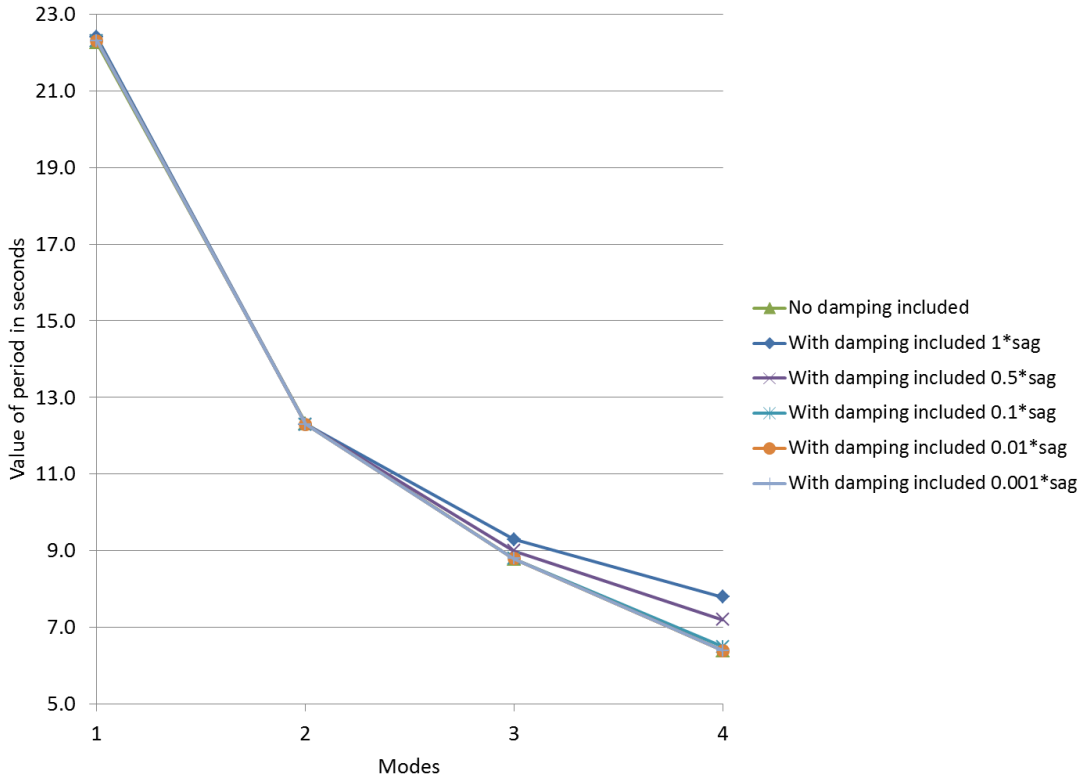

Figure 53 First four damped natural periods for the Polyester System.

5.2.7 Comparison of systems

The fundamental natural period for the four systems is tabulated in Table 17. Here, the different surroundings for each system can be analyzed, except for the case where damping is included.

Table 17 Fundamental natural periods for each system.

System	Surroundings considered	Top tension (kN)	Fundamental period (s)
Steel rope system	Air	3661	27.5
	Water, only submerged weight	2946	27.1
	Water, submerged weight, and added mass	2946	30.5
Steel system	Air	3647	32.1
	Water, only submerged weight	2946	31.7
	Water, submerged weight, and added mass	2946	35.6
Polyester system	Air	3954	19.9
	Water, only submerged weight	2946	12.8
	Water, submerged weight, and added mass	2946	22.3

The fundamental period for each system is shown in Figure 54. In this plot the tendency of each system can be seen for the different surrounding cases, except with damping.

In all the systems the lowest period was for the case with only the submerged weight, followed by the case in air, the case with submerged weight and added mass, and finally the case with damping.

The Steel System offered larger periods than the other two systems for each surrounding case.

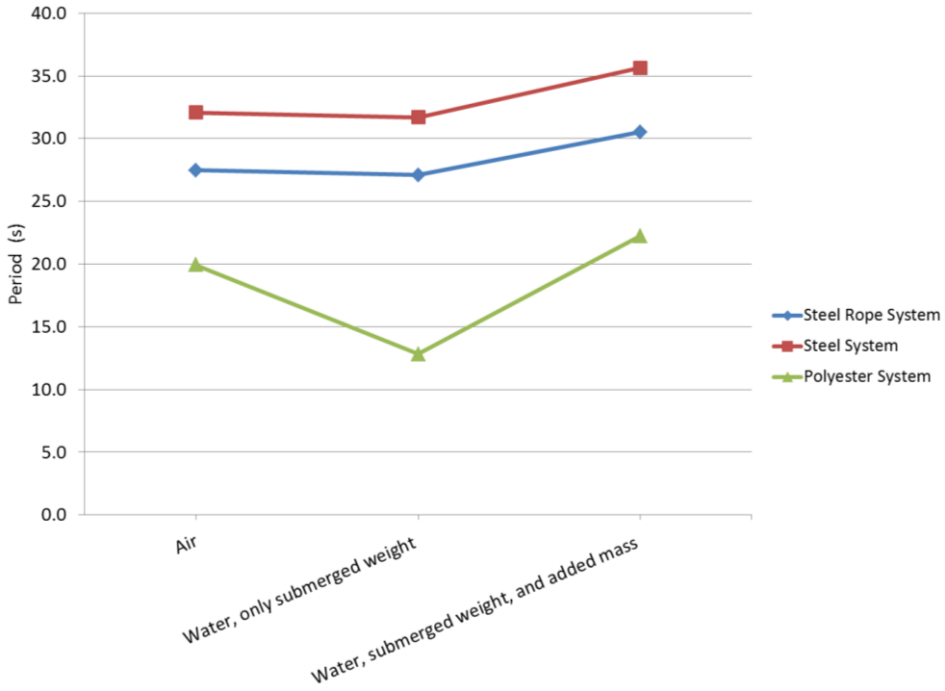

Figure 54 Fundamental periods of free vibration for the three systems for three surrounding environments.

A comparison with different values of natural periods, and damping ratios for the three systems are shown in Table 18. These values of periods and damping ratios were obtained based on modal shapes normalized by the values of amplitude referred in the table.

Table 18 Fundamental damped natural periods and damping ratios for the three systems.

Amplitude	Natural Period (s)		
	Steel Rope System	Steel System	Polyester System
1 Sag	40.3	39.5	22.4
0.5 Sag	35.4	36.3	22.3
0.1 Sag	31.5	35.7	22.3
0.01 Sag	30.6	35.6	22.3
0.001 Sag	30.5	35.6	22.3

Amplitude	Damping Ratio ζ (%)		
	Steel Rope System	Steel System	Polyester System
1 Sag	65.4	43.3	9.4
0.5 Sag	50.8	19.5	0.0
0.1 Sag	25.0	7.5	0.0
0.01 Sag	8.1	0.0	0.0
0.001 Sag	0.0	0.0	0.0

6. SUMMARY AND CONCLUSIONS

The aim of this project was to study the dynamics of specific kinds of mooring lines, focusing on the impact of damping in the modal analysis. The mooring lines proposed to study comprised up to three segments of different materials. These examples were realistic examples of the mooring lines employed in current offshore facilities. The presence of different materials in one mooring line, as in the case of two of the examples proposed, was another important factor to investigate in the modal analysis performed.

The model adopted to perform the modal analysis was based on a variational formulation presented by Chucheepsakul and Srinil (2002). The work-energy produced by the external and internal forces in a submerged cable can be analyzed to define the structural stiffness of the mooring line, and consequently its static configuration is found under specific characteristics.

From this point, the modal analysis can be executed adding a damping matrix in the problem. This damping matrix was assembled based on a statistical linearization of the nonlinear drag force with the associated displacement of each point of the mooring line in water, produced during its motion relative to the initial static deformed configuration.

Besides the case where the damping is included, other cases of study were added in order to contrast different scenarios where the cables could vibrate. These cases where the cable could vibrate were called surrounding environments. The four cases studied were:

1) *Air*. The cable included its weight without buoyancy.
2) *Water, only submerged weight*. The buoyancy is included in the weight of the cable.
3) *Water, submerged weight, and added mass*. Buoyancy and added mass included.
4) *Water, submerged weight, added mass, and damping*. Buoyancy, added mass, and drag damping considered, for different values of motion amplitude relative to the static sag in the cable.

The natural periods of each above termed case were the lowest in the instance number two. In this case the net weight and the effective mass are the lowest. Since there is no added mass, and no damping, this example is related to one as if the mooring line were in air.

The first case, entitled Air, where the cable does not have reduction in its weight because of the buoyancy, and has no added mass or damping, has the second lowest natural period for each one of the systems.

The cases 1 and 2 have the lowest natural periods for each system. This is a part of the verification of the model used. Obtaining lower periods in an air environment makes sense, expecting that the cables will vibrate with higher frequencies than the same cables submerged in water.

Three mooring systems were analyzed. One mooring system was of steel rope, called “Steel Rope System”. The other two of them were realistic designs of deepwater mooring lines: one was called “Steel System” made up with a main insert of steel rope,

and two end segments of chain, and the named "Polyester System" composed by two extreme segments of chain and a main middle segment of polyester.

As expected, the natural periods for each of the three systems increase when drag damping is included. It was observed that there is a correspondence between the value of the amplitude of the motion of the cable and the damping obtained. The larger the amplitude considered in the modal shape, the larger value of damping obtained. From this point it can be concluded that the better understanding of damping in the vibration of mooring lines, and its participation as an important factor in the entire analysis of mooring lines, may improve their design and the safety of offshore facilities where they are installed.

When no damping was included in the modal analysis the in-plane and out-of-plane modal shapes showed a smooth transition between the steel chain and the steel rope or polyester rope. In contrast, the tangential modal shapes for those cases showed noticeable changes in slope at the connection between the bottom chain and the rope, indicative of large gradients in axial displacement related to dynamic tension and compression forces.

When damping was included, the tangential mode shape was not investigated, because only the lateral motion of the cable was considered to be damped by the water.

From the three mooring systems studied, the Steel Rope System is an exercise nearer to an idealization than to a real situation because at the ends of the mooring line it needs to have short lengths of abrasion resistant material in order to be connected to the

anchor and the floating system, nevertheless the example was useful to understand the behavior between the other two mooring systems.

The primary focus was on contrasting the Steel System and the Polyester System. For example, it can be said that the Steel System always showed higher values of natural periods of vibration than the Polyester System for the same cases of study. From the point of view of being farther from the periods of excitation of waves in a common storm, it can be stated that the named Steel System is safer than the Polyester System.

The Polyester System always showed, for all the cases assessed, the lowest values of natural periods. Apart from its first natural period, the rest of the natural periods were the nearest to the periods of excitation produced by waves in prevailing seas. This could lead to more problems of fatigue in these mooring systems than in the Steel System.

The methodology followed was acceptable for adaptation in the representation of different kinds of materials in one mooring line; however, it was not practical enough to represent the exact values of length of the different segments of the line because the initial length of the mooring line is not an explicit input parameter.

Furthermore, the discretization into equal height slices produced finite elements that in the lowest part of any mooring line were longer than in the upper part, especially in cases where the tension is relatively low and there is a large sag in the static deformed configuration.

The addition of the lateral amplitudes of displacement to formulate a damping matrix appears to be a very useful way to reproduce damping in mooring lines produced

by water. Furthermore, the addition of the damping effect on the tangential modal shapes is desirable in order to better understand modal behavior near the transition between materials in the specific case where damping is considered.

Further study to improve the application of this method can be important to obtain more accurate results on this phenomenon. Moreover, the generation of damping including the effects of tangential modes can be important to consider in future studies.

The main internal force present in mooring lines is the axial force. All the analyses developed in this work were performed considering it; however, the inclusion of bending stiffness as an additional factor in the modal analysis of mooring lines is desirable for future works.

REFERENCES

API. (2005). *Design and Analysis of Stationkeeping Systems for Floating Structures.* American Petroleum Institute, Washington, D.C., 39-43.

Burgess, J. J., and Triantafyllou, M. S. (1988). "The elastic frequencies of cables."*Journal of Sound and Vibration, 120*(1), 153-165.

Chucheepsakul, S., and Srinil, N. (2002). "Free vibrations of three-dimensional extensible marine cables with specified top tension via a variational method."*Ocean Engineering, 29*(9), 1067-1096.

Chucheepsakul, S., Srinil, N., and Petchpeart, P. (2003). "A variational approach for three-dimensional model of extensible marine cables with specified top tension."*Applied Mathematical Modelling, 27*(10), 781-803.

DuBuque, G. (2011). *A lumped parameter equilibrium model of a submerged body with mooring lines.* Master of Science Thesis, Univesity of Washington, Seattle.

Grinfogel, L. (1984). *Dynamics of elastic taut inclined cables.* Master of Science Thesis, Massachusetts Institute of Technology, Cambridge.

Irvine, H.M. (1978). "Free vibrations of inclined cables." *Journal of the Structural Division, 104*(2), 343-347.

Irvine, H.M. (1992). *Cable Structures*. Dover Publications, New York, 16-19.

Lanczos, C. (1986). *The Variational Principles of Mechanics*, Dover Publications, New York, 54-60.

Rao, S.S. (2007). *Vibration of Continuous Systems*, Wiley, New York, 676-680.

Rega, G., Srinil, N., and Alaggio, R. (2008). "Experimental and numerical studies of inclined cables: free and parametrically-forced vibrations." *Journal of Theoretical and Applied Mechanics, 46*(3), 621-640.

Tedesco, J.W., McDougal, W.G., & Ross, C.A. (1999). *Structural Dynamics, Theory and Applications*, Addison-Wesley, California, 731-732.

Timoshenko, S.P. (1953). *History of Strength of Materials, With a Brief Account of the History of Theory of Elasticity and Theory of Structure*, McGraw-Hill, New York, 85-86.

Triantafyllou, M.S., and Bliek, A. (1983). *The dynamics of inclined taut and slack marine cables*. Offshore Technology Conference, Houston, 4498, 469-473.

Zhou, X., Yan, S., and Chu, F. (2011). "In-plane free vibrations of an inclined taut cable."*Journal of Vibration and Acoustics, 133*(3), 031001-031001.

Zill, D.G., Cullen, M.R., and Wright, W.S. (2012). *Differential Equations With Boundary-Value Problems*, Brooks/Cole, Boston, 26-28.

APPENDIX A

$$[T] = \begin{bmatrix} T1_j & 0 & T2_j & 0 & T3_j & 0 & 0 & 0 & 00 & 0 & 0 \\ T4_j & T1_j & T5_j & T2_j & T6_j & T3_j & 0 & 0 & 00 & 0 & 0 \\ T7_j & 0 & T8_j & 0 & T9_j & 0 & 0 & 0 & 00 & 0 & 0 \\ T10_j & T7_j & T11_j & T8_j & T12_j & T9_j & 0 & 0 & 00 & 0 & 0 \\ T13_j & 0 & 0 & 0 & T14_j & 0 & 0 & 0 & 00 & 0 & 0 \\ T15_j & T13_j & 0 & 0 & T16_j & T14_j & 0 & 0 & 00 & 0 & 0 \\ 0 & 0 & 0 & 0 & 0 & 0 & T1_{j+1} & 0 & T2_{j+1} & 0 & T3_{j+1} & 0 \\ 0 & 0 & 0 & 0 & 0 & 0 & T4_{j+1} & T1_{j+1} & T5_{j+1} & T2_{j+1} & T6_{j+1} & T3_{j+1} \\ 0 & 0 & 0 & 0 & 0 & 0 & T7_{j+1} & 0 & T8_{j+1} & 0 & T9_{j+1} & 0 \\ 0 & 0 & 0 & 0 & 0 & 0 & T10_{j+1} & T7_{j+1} & T11_{j+1} & T8_{j+1} & T12_{j+1} & T9_{j+1} \\ 0 & 0 & 0 & 0 & 0 & 0 & T13_{j+1} & 0 & 0 & 0 & T14_{j+1} & 0 \\ 0 & 0 & 0 & 0 & 0 & 0 & T15_{j+1} & T13_{j+1} & 0 & 0 & T16_{j+1} & T14_{j+1} \end{bmatrix}$$

In the above transformation matrix the subscrips *j* and *j*+1 refers to the initial and end node of each finite element. From that matrix each term is developed below.

$T1 = cos\emptyset\ cos\theta$

$T2 = -sin\theta$

$T3 = -sin\emptyset\ cos\theta$

$T4 = -cos\emptyset\ sin\theta\ (\theta') - sin\emptyset\ cos\theta\ (\emptyset')$

$T5 = -cos\theta\ (\theta')$

$T6 = sin\emptyset\ sin\theta\ (\theta') - cos\emptyset\ cos\theta\ (\emptyset')$

$T7 = cos\emptyset\ sin\theta$

$T8 = cos\theta$

$T9 = -sin\emptyset\ sin\theta$

$T10 = cos\emptyset\ cos\theta\ (\theta') - sin\emptyset\ sin\theta\ (\emptyset')$

$T11 = -sin\theta\ (\theta')$

$T12 = -sin\emptyset\ cos\theta(\theta') - cos\emptyset\ sin\theta(\emptyset')$

$$T13 = sin\theta$$

$$T14 = cos\theta$$

$$T15 = cos\emptyset\ (\emptyset')$$

$$T16 = -sin\emptyset\ (\emptyset')$$

$$\theta = tan^{-1}\left(\frac{y_0'}{x_0'}\right)$$

$$\emptyset = tan^{-1}\left(\frac{1}{\sqrt{x_0'^2 + y_0'^2}}\right)$$

$$\theta' = \left(\frac{x_0'y_0'' - y_0'x_0''}{x_0'^2 + y_0'^2}\right)$$

$$\emptyset' = \frac{-(x_0'y_0'' - y_0'x_0'')}{(1 + x_0'^2 + y_0'^2)\sqrt{x_0'^2 + y_0'^2}}$$